Calculations in Modified Gauge Theory

Testing Some Ideas From QCD in a Toy Model

by

Evan Cameron Thomas

B.Sc., The University of Washington, 2007
M.Sc., The University of British Columbia, 2011

A THESIS SUBMITTED IN PARTIAL FULFILLMENT OF
THE REQUIREMENTS FOR THE DEGREE OF

DOCTOR OF PHILOSOPHY

in

The Faculty of Graduate and Postdoctoral Studies

(Physics)

THE UNIVERSITY OF BRITISH COLUMBIA

(Vancouver)

December 2017

Abstract

We use a deformed "center-stablised" gauge theory, which can be brought into a weak coupling regime while remaining confined and gapped, as a toy model to study some ideas from real QCD. The deformed model has the correct nontrivial θ-dependence and degeneracy of topological sectors conjectured for QCD, and is, apparently, smoothly connected to the strongly coupled undeformed Yang-Mills, so that we can perhaps expect to get some qualitative insights into QCD. We demonstrate the presence of a nondispersive contact term in the topological susceptibility, which contributes with the opposite sign to normal dispersive contributions coming from physical propagating degrees of freedom. We further show that, despite the system being completely gapped with no massless physical degrees of freedom, the system has a Casimir-like, power scaling, dependence on boundaries, in contrast with the naive expectation that a system with only massive degrees of freedom should have a weak (exponentially small) dependence on long distance effects. This behaviour suggests the possibility for a solution for the cosmological dark energy problem coming from the strongly coupled QCD sector on a manifold with a boundary, which would have the correct sign and be of the correct order of magnitude. Next, we investigate the interaction between point-like topological charges (monopoles) and extended sheet-like topological defects (domain walls) in attempt to explain some recent lattice QCD results suggesting that extended topological objects are more important to understanding the relevant field configurations in QCD than the instantons traditionally expected. Finally, we derive the existence of excited metastable vacuum states and calculate their decay rate to the true ground state of the theory, comparing with the expected results discussed years ago in proper QCD. The presence of metastable vacuum states with a nonzero effective θ parameter, like those present in the deformed model, could explain $\mathcal{P}$ and $\mathcal{CP}$ violation in heavy ion collisions observed on an event by event basis, which seem to average away over many events.

Lay Summary

We investigate a toy model related to the true theory for the strong nuclear interaction which binds nuclear matter. The toy model is much easier to work with, but preserves many important aspects of the true theory, especially related to the vacuum structure. We use this simplified model to study some ideas in the true theory, in which there are no obvious ways to perform the relevant calculations. Our computations provide some insight into a particular dependence of the bulk energy density on the size of the system, the structure of the type of configurations relevant in the theory, and some old questions about semi-stable vacuum states. These results could help explain the origins for cosmological dark energy, some recent results in a different lattice approximation which differ from conventional wisdom, and some odd observations in heavy ion collisions.

Preface

Chapter 2 is primarily a review of the deformed "center-stabilised" gauge theory model discussed by Lawrence Yaffe and Mithat Ünsal in [85], and as such, aside from a few corrections and expanded discussions, does not represent any original work attributable to myself. Chapter 3 is adapted from work titled "Topological Susceptibility and Contact Term in QCD: A Toy Model" published in Physical Review D 85:044039 [80]. The content in Chapter 4 is published as "Casimir Scaling in Gauge Theories with a Gap: Deformed QCD As a Toy Model" in Physical Review D 86:065029 [79]. Chapter 5 is published as "Long Range Order in Gauge Theories: Deformed QCD As a Toy Model" in Physical Review D 87:085027 [81]. Chapter 6 was the result of a project in collaboration with another student, Amit Bhoonah, with whom I worked on the numerical simulations presented, and is published as "Metastable vacuum decay and θ dependence in gauge theory. Deformed QCD as a toy model." in Nuclear Physics B 890:30 [7]. I did the bulk of the writing for that paper, and actually removed the short section Amit wrote in the text of Chapter 6, since it was not particularly relevant for this presentation, such that the text presented here represents my writing. In all four of these works my supervisor, Ariel Zhitnitsky, suggested the fundamental ideas and wrote many of the parts about historical context and relation to other theories and models scattered throughout.

Table of Contents

List of Figures

Chapter 1

Introduction

Gauge theories, the class of Quantum Field Theories (QFTs) exhibiting generalised versions of the gauge symmetry from electrodynamics, have been extremely successful in describing the fundamental forces (excepting gravity) via vector boson mediated particle interactions. Quantum Electrodynamics (QED) has been relatively easy to work with, being weakly coupled and amenable to perturbation theory at all accessible scales, and has matched experiment extremely well. By contrast, Quantum Chromodynamics (QCD), the theory for the strong nuclear force, is strongly coupled (highly nonlinear) at low temperature. The coupling runs down at higher temperature, but unfortunately the system undergoes a phase transition (crossover) from "confined" hadronic matter to a "deconfined" quark gluon plasma state before the coupling is small in a perturbative sense. This means that, while there is a weak coupling regime, the perturbative calculations we can do at weak coupling cannot tell us much about the confined phase. As a result, people have looked for other ways to approach QCD, including: phenomenological models that attempt to write down informed guesses for an effective theory; lattice models that discretise space and attempt to calculate correlators by brute force Monte-Carlo simulation of the path integral; and AdS/CFT calculations that produce weakly coupled dual gravity theories to QCD-like strongly coupled field theories.

Each of the approaches mentioned above has its shortcomings. Phenomenological approaches can be difficult to get any predictive power from, since they are not necessarily describing any behaviour accurately outside the observed phenomena they are based on. Lattice QCD is extremely numerically expensive, requiring significant time on expensive supercomputers to do realistic calculations. It can also be quite difficult to get any kind of physical intuition about the reasons for effects seen on the lattice. AdS/CFT does not have a known direct dual to QCD, so instead makes some arguments in supersymmetric models and/or gauge models with different gauge groups than the SU(3) describing real QCD.

Hopefully, despite not having a perfect calculational tool, using multiple desperate approaches will allow us to form an increasingly good picture of

the behaviour of real QCD as we see similar effects in different approximations. As such, we investigate a different approximation to those listed above, the so called "center-stablised" or "deformed" gauge theory developed by Lawrence Yaffe and Mithat Ünsal [85], and apply it to carry out some calculations. The model is built by taking a normal gauge theory, with Yang-Mills Lagrangian, and adding an extra term (deformation) to the Lagrangian acting as a potential penalty for the order parameter for the deconfinement phase transition. This means, by suitable choice of parameters, we can enforce a confined phase to arbitrarily large temperature (and so arbitrarily small coupling). Thus, we can work in a model which is weakly coupled, so amenable to perturbation theory and semiclassical treatment, but describes a confined system which is, apparently, smoothly connected to the real strongly coupled system without a phase transition between the two.

We begin, in Chapter 2, by reviewing the relevant aspects of the model, showing the two dual descriptions, as a Coulomb gas of topological monopoles and as a coupled sine-Gordon model, for the low energy effective theory at weak coupling. In Chapter 3, we discuss the topological susceptibility, a key element in the resolution of the $U(1)_A$ problem in QCD, and demonstrate the presence of a nondispersive "contact" term in both dual descriptions of the low energy effective theory. The contact term has the opposite sign to the contribution from any physical propagating degrees of freedom as is necessary to satisfy the Ward Identity, which requires a cancellation with the contribution coming from the physical fields. Previously, there was no consistent method for deriving the contact term in a four dimensional gauge theory. Instead, Witten inserted this term directly by hand [93] and Veneziano added an extra "ghost" field that leads to a contact term when integrated out [90, 91], but in this model the contact term arises naturally. [80]

Next, we show, in Chapter 4, that a zero mode analysis of the monopole configurations describing the Coulomb gas description gives a Casimir-like power scaling for the bulk energy density, as described by the topological susceptibility, rather than the naive expectation for a gapped system with no massless physical. If only physical degrees of freedom contribute, their dispersion relations dictate an exponential suppression of any bulk dependence on the boundary. In contrast, the deformed model has a nondispersive We further argue that, if it persists in undeformed QCD at strong coupling, such a Casimir scaling could lead to a solution for the cosmological dark energy naturally following from QCD on a bounded manifold, without the need for new fields or new physics. [79]

In Chapter 5, we address some recent lattice QCD results suggesting that the topological defects, relevant in gauge configurations that saturate the path integrals, are extended objects looking like interleaved sheets of opposite topological charge, rather than the point-like instantons people have traditionally discussed. A class of domain wall objects that appear in the deformed model have similar properties, being (classically) topologically stable with sheets of opposite topological charge interleaved. We consider their interaction with point-like monopoles and explain a possible dynamical reason for the absence of point-like objects in relevant configurations. [81]

Finally, in Chapter 6, we demonstrate the presence of metastable vacuum states (with energy higher than the true vacuum) in the deformed model and calculate the decay rate from the metastable states to the true vacuum. We also discuss how the presence of such metastable states can, if similar states exist in undeformed strongly coupled QCD, lead to $\mathcal{P}$ and $\mathcal{CP}$ effects that have apparently been observed in some heavy ion collisions. [7]

Chapter 2

Description of the Model

In this chapter we discuss the "center-stabilised" deformed Yang-Mills developed in [85] and references therein, before moving on to a discussion of the topological properties of this theory in Chapter 3, and some applications in Chapters 4, 5, and 6. In the deformed theory an extra term is put into the Lagrangian in order to prevent the center symmetry breaking that characterises the QCD phase transition between "confined" hadronic matter and "deconfined" quark-gluon plasma. The extra term is a penalty for states in which the order parameter for such a transition develops an expectation value. Thus, we have a theory which remains confined at high temperature in a weak coupling regime, and for which it is claimed [85] that there does not exist an order parameter to differentiate the low temperature (non-Abelian) confined regime from the high temperature (Abelian) confined regime. This means we can do some simple semiclassical calculations in a confined theory that, as we shall discuss, retains some interesting properties of, and is smoothly connected to, undeformed Yang-Mills. For some other extensions of this model related to inclusion of adjoint fermions, extensions to general gauge groups, and so on, see[60–62] and references therein. We follow [85] in deriving the relevant parts of the theory.

2.1 Formulation of the Theory

We start with pure Yang-Mills (gluodynamics) with gauge group $SU(N)$ on the manifold $\mathbb{R}^3 \times S^1$ with the standard action

$$S^{YM} = \int_{\mathbb{R}^3 \times S^1} d^4x \, \frac{1}{2g^2} \mathrm{tr} \left[F_{\mu\nu}^2(x) \right], \tag{2.1}$$

and add to it a deformation action,

$$\Delta S \equiv \int_{\mathbb{R}^3} d^3x \, \frac{1}{L^3} P \left[\Omega(\mathbf{x}) \right], \tag{2.2}$$

built out of the Wilson loop (Polyakov loop) wrapping the compact dimension,

$$\Omega(\mathbf{x}) \equiv \mathcal{P}\left[e^{i\oint dx_4\ A_4(\mathbf{x},x_4)}\right]. \tag{2.3}$$

The "double-trace" deformation potential $P[\Omega]$ respects the symmetries of the original theory and is built to stabilise the phase with unbroken center symmetry. It is defined by

$$P[\Omega] \equiv \sum_{n=1}^{\lfloor N/2\rfloor} a_n \left|\mathrm{tr}\left[\Omega^n\right]\right|^2. \tag{2.4}$$

Here $\lfloor N/2\rfloor$ denotes the integer part of $N/2$ and $\{a_n\}$ is a set of suitably large positive coefficients.

The centre of the gauge group is the subgroup of elements which commute with all elements of the full group, is isomorphic to $\mathbb{Z}_N$ for the gauge group $SU(N)$, and is the symmetry corresponding to the confinement deconfinement phase transition. The first term of $P[\Omega]$, proportional to $\left|\mathrm{tr}\left[\Omega\right]\right|^2$ (with a sufficiently large positive coefficient), will prevent breaking of the center symmetry from $\mathbb{Z}_N$ to $\mathbb{Z}_1$ with order parameter $\langle\mathrm{tr}\left[\Omega\right]\rangle$, but will not prevent $\mathrm{tr}\left[\Omega^2\right]$ from developing a vacuum expectation value so that it will not prevent the center symmetry breaking from $\mathbb{Z}_N$ to $\mathbb{Z}_2$ with order parameter $\langle\mathrm{tr}\left[\Omega^2\right]\rangle$. The term proportional to $\left|\mathrm{tr}\left[\Omega^2\right]\right|^2$ however does prevent such a symmetry breaking. Likewise, for each other subset $\mathbb{Z}_p$ of $\mathbb{Z}_N$ (with $N \mod p = 0$), there needs to be a corresponding term, proportional to $\left|\mathrm{tr}\left[\Omega^p\right]\right|^2$, in the deformation potential. This is the reason for including terms up to $\left|\mathrm{tr}\left[\Omega^{\lfloor N/2\rfloor}\right]\right|^2$. Note that for real life QCD the gauge group is $SU(3)$ and so in that case only one term would be necessary,

$$P[\Omega] = a\left|\mathrm{tr}\left[\Omega\right]\right|^2. \tag{2.5}$$

In undeformed pure gluodynamics the effective potential for the Wilson loop, whose expectation value acts as an order parameter, is minimised for Ω an element of $\mathbb{Z}_N$, which corresponds to a deconfined phase. The deformation potential (2.4) with sufficiently large $\{a_n\}$ however changes the effective potential for the Wilson line so that it is minimised instead by configurations in which $\mathrm{tr}\left[\Omega^n\right] = 0$, which in turn implies that the eigenvalues of Ω are uniformly distributed around the unit circle. Thus, the set of eigenvalues is invariant under the $\mathbb{Z}_N$ transformations, which multiply each eigenvalue by $e^{2\pi ik/N}$ (rotate the unit circle by k/N). The center symmetry is then unbroken by construction. The coefficients, $\{a_n\}$, can be suitably chosen

such that the deformation potential, $P[\Omega]$, forces unbroken symmetry at any compactification scales [85], but for our purposes we are only interested in small compactifications ($L \ll \Lambda^{-1}$ where L is the length of the compactified dimension, interpreted as an inverse temperature, and Λ is the QCD scale). The idea here is to go to weak coupling for mathematical control but to look at low-energy behaviour at that scale since we are interested in vacuum behaviour. At small compactification, the gauge coupling at the compactification scale is small so that we can work in a perturbative regime and explicitly evaluate the potential for the Wilson loop due to Quantum fluctuations as in [32, 85]. The one-loop potential is

$$V[\Omega] = \int_{\mathbb{R}^3} d^3x \frac{1}{L^4} \mathcal{V}[\Omega(x)], \tag{2.6}$$

with

$$\mathcal{V}[\Omega] = -\frac{2}{\pi^2} \sum_{n=1}^{\infty} \frac{1}{n^4} \left|\mathrm{tr}\left[\Omega^n\right]\right|^2. \tag{2.7}$$

The undeformed potential for the Wilson loop (2.7) is minimised when Ω is an element of the center, $\mathbb{Z}_N$, so that $\Omega = e^{2\pi i k/N}$. The deformation potential (2.4) must therefore overcome this one-loop potential and force Ω to not choose one particular element of $\mathbb{Z}_N$. We must choose the coefficients $\{a_n\}$ to be larger than $2/\left(\pi^2 n^4\right)$. A simple choice is $a_n = 4/\left(\pi^2 n^4\right)$. With this choice, the full one-loop effective potential for the Wilson loop is minimised for $\mathrm{tr}\left[\Omega^n\right] = 0$ for all $n \neq 0 \bmod N$, indicating unbroken center symmetry.

2.2 Infrared Description

As mentioned in the previous section, we are interested in the regime in which the compactification size is small, $L \ll \Lambda^{-1}$, and so the gauge coupling is small at the compactification scale, $g^2(1/L) \ll 1$. So, in our deformed theory, the combined effective potential for the Wilson loop is the sum of (2.7) and (2.4), which is minimised by field configurations with

$$\Omega = \mathrm{Diag}\left(1, e^{2\pi i/N}, e^{4\pi i/N}, \ldots, e^{2\pi i(N-1)/N}\right), \tag{2.8}$$

up to conjugation by an arbitrary element of $SU(N)$. The configuration (2.8) can be thought of as braking the gauge symmetry down to its maximal Abelian subgroup, $SU(N) \to U(1)^{N-1}$. In the gauge in which Ω is diagonal, the modes of the diagonal components of the gauge field with zero

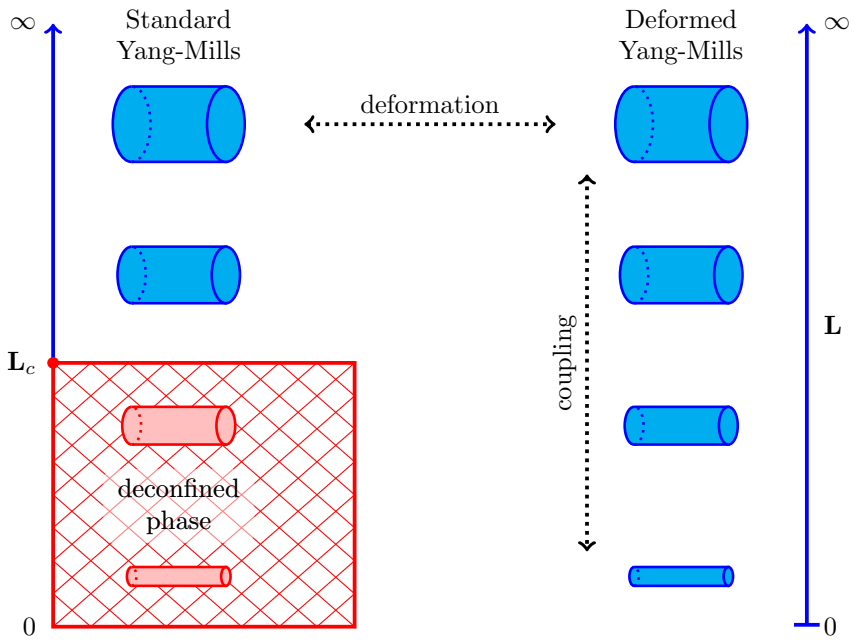

Figure 2.1: Diagram depicting the deformation removing the phase transition to a deconfined phase at weak coupling. It is based on a similar diagram from [85].

momentum along the compactified dimension describe the $U(1)^{N-1}$ photons. Modes of the diagonal gauge field with non-zero momentum in the compactified dimension form a Kaluza-Klein tower and receive masses that are integer multiples of $2\pi/L$ and become large for small L. The remaining off-diagonal components of the gauge field form a Kaluza-Klein tower of charged W-bosons which receive masses that are integer multiples of $2\pi/NL$. Then the lightest W-boson mass, $m_W \equiv 2\pi/NL$, describes the scale below which the dynamics are effectively Abelian.

As described in [85], the proper infrared description of the theory is a dilute gas of N types of monopoles, characterised by their magnetic charges, which are proportional to the simple roots and affine root of the Lie algebra for the gauge group $U(1)^N$. Although the symmetry breaking is $SU(N) \to U(1)^{N-1}$, it is simpler to work with $U(1)^N$ and, as we will see, the extra degree of freedom will completely decouple from the dynamics.

The extended root system is given by the simple roots,

$$\begin{array}{rcccl} \alpha_1 & = & (1,-1,0,\ldots,0) & = & \hat{e}_1-\hat{e}_2, \\ \alpha_2 & = & (0,1,-1,\ldots,0) & = & \hat{e}_2-\hat{e}_3, \\ & \vdots & & & \\ \alpha_{N-1} & = & (0,\ldots,0,1,-1) & = & \hat{e}_{N-1}-\hat{e}_N, \end{array} \tag{2.9}$$

and the affine root,

$$\alpha_N \;=\; (-1,0,\ldots,0,1) \;=\; \hat{e}_N-\hat{e}_1.$$

We denote this root system by Δ_{aff} and note that the roots obey the inner product relation

$$\alpha_a\cdot\alpha_b = 2\delta_{a,b}-\delta_{a,b+1}-\delta_{a,b-1}. \tag{2.10}$$

For a fundamental monopole with magnetic charge $\alpha_a\in\Delta_{\text{aff}}$, the topological charge is given by

$$Q=\int_{\mathbb{R}^3\times S^1} d^4x\;\frac{1}{16\pi^2}\text{tr}\left[F_{\mu\nu}\tilde{F}^{\mu\nu}\right]=\pm\frac{1}{N}, \tag{2.11}$$

and the Yang-Mills action is given by

$$\begin{aligned} S_{YM} &= \int_{\mathbb{R}^3\times S^1} d^4x\;\frac{1}{2g^2}\text{tr}\left[F_{\mu\nu}^2\right] \\ &= \left|\int_{\mathbb{R}^3\times S^1} d^4x\;\frac{1}{2g^2}\text{tr}\left[F_{\mu\nu}\tilde{F}^{\mu\nu}\right]\right| = \frac{8\pi^2}{g^2}\left|Q\right|. \end{aligned} \tag{2.12}$$

The second equivalence hold because the classical monopole solutions are self dual [32],

$$F_{\mu\nu}=\tilde{F}_{\mu\nu}.$$

For an antimonopole with magnetic charge $-\alpha_a$, the Yang-Mills action is the same (2.12) and the topological charge changes sign, $Q=-1/N$.

So the infrared description, at distances larger than the compactification length L, is given by a three dimensional dilute monopole gas with N types of monopoles (and so N types of anti-monopoles) interacting by a species dependent Coulomb potential with interactions defined by the inner product (2.10),

$$\begin{aligned} V_{a,b}(\mathbf{r}) &= L\left(\frac{2\pi}{g}\right)^2\frac{(\pm\alpha_a)\cdot(\pm\alpha_b)}{4\pi\left|\mathbf{r}\right|} \\ &= \pm L\left(\frac{2\pi}{g}\right)^2\frac{2\delta_{a,b}-\delta_{a,b-1}-\delta_{a,b+1}}{4\pi\left|\mathbf{r}\right|}, \end{aligned} \tag{2.13}$$

where the overall sign is plus for a monopole-monopole or antimonopole-antimonopole interaction and minus for a monopole-antimonopole interaction. For a given monopole configuration with $n^{(a)}$ monopoles and $\bar{n}^{(a)}$ antimonopoles of types $a = 1, \ldots, N$, at positions $\mathbf{r}_k^{(a)}, k = 1, \ldots, n^a$ and $\bar{\mathbf{r}}_k^{(a)}, k = 1, \ldots, \bar{n}^a$ respectively, the three dimensional $U(1)^N$ magnetic field is given by

$$\mathbf{B}(\mathbf{x}) = \sum_{a=1}^{N} \frac{2\pi}{g} \alpha_a \left[\sum_{k=1}^{n^{(a)}} \frac{\mathbf{x} - \mathbf{r}_k^{(a)}}{4\pi \left| \mathbf{x} - \mathbf{r}_k^{(a)} \right|^3} - \sum_{l=1}^{\bar{n}^{(a)}} \frac{\mathbf{x} - \bar{\mathbf{r}}_l^{(a)}}{4\pi \left| \mathbf{x} - \bar{\mathbf{r}}_l^{(a)} \right|^3} \right]. \tag{2.14}$$

Letting

$$\begin{aligned} M^{(a)} &= n^{(a)} + \bar{n}^{(a)}, \\ \mathbf{r}_k^{(a)} &= \begin{cases} \mathbf{r}_k^{(a)} & \text{for} \quad k \leq n^{(a)} \\ \bar{\mathbf{r}}_{k-n^{(a)}}^{(a)} & \text{for} \quad k > n^{(a)} \end{cases}, \\ Q_k^{(a)} &= \begin{cases} +1 & \text{for} \quad k \leq n^{(a)} \\ -1 & \text{for} \quad k > n^{(a)} \end{cases}, \end{aligned} \tag{2.15}$$

we can write (2.14) in a more compact form,

$$\mathbf{B}(\mathbf{x}) = \sum_{a=1}^{N} \frac{2\pi}{g} \alpha_a \left[\sum_{k=1}^{M^{(a)}} Q_k^{(a)} \frac{\mathbf{x} - \mathbf{r}_k^{(a)}}{4\pi \left| \mathbf{x} - \mathbf{r}_k^{(a)} \right|^3} \right]. \tag{2.16}$$

The action for such a monopole configuration is a combination of the monopole self-energies and the Coulomb interaction potential energies for each pair of monopoles,

$$S_{\mathrm{MG}} = S_{\mathrm{self}} \sum_{a=1}^{N} M^{(a)} + S_{\mathrm{int}}, \tag{2.17}$$

where

$$S_{\mathrm{int}} = \frac{2\pi^2 L}{g^2} \sum_{a,b=1}^{N} \alpha_a \cdot \alpha_b \left[\sum_{k=1}^{M^{(a)}} \sum_{l=1}^{M^{(b)}} Q_k^{(a)} Q_l^{(b)} G\left(\mathbf{r}_k^{(a)} - \mathbf{r}_l^{(b)} \right) \right] \tag{2.18}$$

and

$$G(\mathbf{r}) \equiv \frac{1}{4\pi \left| \mathbf{r} \right|}. \tag{2.19}$$

The canonical partition function is then given, as usual, by a sum over all possible monopole configurations with a statistical weight e^{-S},

$$\mathcal{Z} = \int \prod_{a=1}^{N} d\mu^{(a)} \; e^{-S_{\mathrm{int}}}, \tag{2.20}$$

with measure

$$d\mu^{(a)} = \sum_{n^{(a)}=0}^{\infty} \frac{(\zeta/2)^{n^{(a)}}}{n^{(a)}!} \sum_{\bar{n}^{(a)}=0}^{\infty} \frac{(\zeta/2)^{\bar{n}^{(a)}}}{\bar{n}^{(a)}!} \int_{\mathbb{R}^3} \prod_{k=1}^{n^{(a)}} d\mathbf{r}_k^{(a)} \int_{\mathbb{R}^3} \prod_{l=1}^{\bar{n}^{(a)}} d\bar{\mathbf{r}}_k^{(a)}. \quad (2.21)$$

The monopole fugacity, ζ, describes the density of monopoles and is given by,

$$\zeta \equiv C\, e^{-S_{\text{self}}} = A m_W^3 \left(g^2 N\right)^{-2} e^{-\Delta S} e^{-8\pi^2/N g^2(m_W)}, \quad (2.22)$$

where the C factor is the one-loop functional determinant in the monopole background as described in the appendix of [85].

Next we show explicitly that the above monopole partition function (2.20) is equivalent to a sine-Gordon partition function which describes the proper θ-dependence for the QCD vacuum.

2.3 Monopole Sine-Gordon Equivalence

The sine-Gordon partition function for this model describes a three dimensional N-component real scalar field theory, given by

$$\mathcal{Z} = \int \prod_{a=1}^{N} \mathcal{D}\sigma_a\, e^{-S_{\text{dual}}[\boldsymbol{\sigma}]}, \quad (2.23)$$

with

$$S_{\text{dual}} = \int_{\mathbb{R}^3} d^3x \left[\frac{1}{2L} \left(\frac{g}{2\pi}\right)^2 (\nabla \boldsymbol{\sigma})^2 - \zeta \sum_{a=1}^{N} \cos(\alpha_a \cdot \boldsymbol{\sigma}) \right]. \quad (2.24)$$

Considering the cosine term,

$$\begin{aligned} \exp\left[\zeta \int_{\mathbb{R}^3} d^3x \sum_{a=0}^{N} \cos(\alpha_a \cdot \boldsymbol{\sigma})\right] &= \prod_{a=1}^{N} \exp\left[\zeta \int_{\mathbb{R}^3} d^3x\, \cos(\alpha_a \cdot \boldsymbol{\sigma})\right] \\ &= \prod_{a=1}^{N} \exp\left[\frac{\zeta}{2} \int_{\mathbb{R}^3} d^3x\, \left(e^{i\alpha_a \cdot \boldsymbol{\sigma}} + e^{-i\alpha_a \cdot \boldsymbol{\sigma}}\right)\right], \end{aligned} \quad (2.25)$$

we can apply the power series representation for the exponential, $e^x = \sum x^n/n!$, and get

$$\prod_{a=1}^{N} \left\{ \sum_{M^{(a)}=0}^{\infty} \frac{(\zeta/2)^{M^{(a)}}}{M^{(a)}!} \prod_{m=0}^{M^{(a)}} \left[\int_{\mathbb{R}^3} d^3x_m \left(e^{i\alpha_a \cdot \boldsymbol{\sigma}(x_m)} + e^{-i\alpha_a \cdot \boldsymbol{\sigma}(x_m)} \right) \right] \right\}. \quad (2.26)$$

We then make use of the binomial theorem,

$$(x+y)^n = \sum_{k=0}^{n} \left(\begin{array}{c} n \\ k \end{array} \right) x^{n-k} y^k \text{ with } \left(\begin{array}{c} n \\ k \end{array} \right) = \frac{n!}{(n-k)!k!}, \tag{2.27}$$

and arrive at,

$$\prod_{a=1}^{N} \sum_{M^{(a)}=0}^{\infty} \left\{ \sum_{m=0}^{M^{(a)}} \frac{(\zeta/2)^{M^{(a)}}}{m!(M^{(a)}-m)!} \left[\prod_{k=1}^{M^{(a)}} \int_{\mathbb{R}^3} d^3x_k \right] \right\} \exp\left[i \sum_{k=1}^{M^{(a)}} Q_k^{(a)} \alpha_a \cdot \boldsymbol{\sigma}_k \right]$$
$$= \left[\prod_{a=1}^{N} \int d\mu^{(a)} \right] \exp\left[i \sum_{a=0}^{N} \sum_{k=0}^{M^{(a)}} Q_k^{(a)} \alpha_a \cdot \boldsymbol{\sigma}(x_k) \right], \tag{2.28}$$

where $d\mu^{(a)}$ is given in (2.21). Thus, inserting (2.28) into the sine-Gordon partition function (2.23), we have

$$\mathcal{Z} = \int \prod_{a=1}^{N} \left[\mathcal{D}\sigma_a \, d\mu^{(a)} \right] \exp\left[-\beta \int_{\mathbb{R}^3} d^3x \, \mathcal{L} \right]$$
$$\mathcal{L} = \frac{1}{2} (\nabla \boldsymbol{\sigma})^2 - \frac{i}{\beta} \sum_{a=1}^{N} \sum_{k=1}^{M^{(a)}} Q_k^{(a)} \delta(\mathbf{x}_k^{(a)} - \mathbf{x}) \alpha_a \cdot \boldsymbol{\sigma}(\mathbf{x}), \tag{2.29}$$

where

$$\beta \equiv \frac{1}{L} \left(\frac{g}{2\pi} \right)^2. \tag{2.30}$$

Treating the last term in the exponent as a source term,

$$J(\mathbf{x}) \equiv \frac{-i}{\beta} \sum_{a=1}^{N} \sum_{k=1}^{M^{(a)}} Q_k^{(a)} \delta(\mathbf{x}_k^{(a)} - \mathbf{x}) \alpha_a, \tag{2.31}$$

and completing the square with the shift $\sigma(\mathbf{x}) \to \sigma(\mathbf{x}) + \int d^3y \, G(\mathbf{x}-\mathbf{y}) J(\mathbf{y})$, we have,

$$\mathcal{Z} = \mathcal{Z}_0 \int \left[\prod_{a=0}^{N} d\mu^{(a)} \right] \exp\left\{ \frac{\beta}{2} \int_{\mathbb{R}^3} d^3x \int_{\mathbb{R}^3} d^3y \, [J(\mathbf{x}) G(\mathbf{x}-\mathbf{y}) J(\mathbf{y})] \right\}, \tag{2.32}$$

in which $\mathcal{Z}_0$ is the functional determinant

$$\mathcal{Z}_0 \equiv \int \left[\prod_{a=0}^{N} \mathcal{D}\sigma_a \right] \exp\left[\frac{-\beta}{2} \int_{\mathbb{R}^3} d^3x \, (\nabla \boldsymbol{\sigma})^2 \right]. \tag{2.33}$$

The above determinant does not contain any of the relevant physics and is just a constant prefactor that will drop out of any calculation of operator expectation values in the monopole ensemble. Finally, inserting the expression for the source (2.31), the partition function becomes,

$$\mathcal{Z} = \mathcal{Z}_0 \int \left[\prod_{a=0}^{N} d\mu^{(a)}\right] \times \exp\left[\frac{-2\pi^2 L}{g^2} \sum_{a,b=1}^{N} \sum_{k=1}^{M^{(a)}} \sum_{l=0}^{M^{(b)}} \alpha_a \cdot \alpha_b \, Q_k^{(a)} Q_l^{(b)} G(\mathbf{x}_k^{(a)} - \mathbf{x}_l^{(b)})\right], \quad (2.34)$$

which is the partition function for the monopole gas from (2.20).

Next, including a θ-parameter in the Yang-Mills action,

$$S_{\rm YM} \to S_{\rm YM} + i\theta \int_{\mathbb{R}^3 \times S^1} \frac{1}{16\pi^2} \mathrm{tr}\left[F_{\mu\nu}\tilde{F}^{\mu\nu}\right], \quad (2.35)$$

with $\tilde{F}^{\mu\nu} \equiv \epsilon^{\mu\nu\rho\sigma} F_{\rho\sigma}$, multiplies each monopole fugacity by $e^{i\theta/N}$ and anti-monopole fugacity by $e^{-i\theta/N}$. In the dual sine-Gordon theory this inclusion is equivalent to shifting the cosine term so that [1]

$$S_{\rm dual} \to \int_{\mathbb{R}^3} \left[\frac{1}{2L}\left(\frac{g}{2\pi}\right)^2 (\nabla \boldsymbol{\sigma})^2 - \zeta \sum_{a=1}^{N} \cos\left(\alpha_a \cdot \boldsymbol{\sigma} + \frac{\theta}{N}\right)\right]. \quad (2.36)$$

The θ parameter enters the effective Lagrangian (2.36) as θ/N which is the direct consequence of the fractional topological charges of the monopoles (2.11). Nevertheless, the theory is still 2π periodic. This 2π periodicity of the theory is restored not due to the 2π periodicity of Lagrangian (2.36). Rather, it is restored as a result of summation over all branches of the theory when the levels cross at $\theta = \pi(mod\ 2\pi)$ and one branch replaces another and becomes the lowest energy state. Indeed, the ground state energy density is determined by minimisation of the effective potential (2.36) when summation $\sum_{l=0}^{N-1}$ over all branches is assumed in the definition of the canonical partition function (2.20). It is given by

$$E_{min}(\theta) = -\lim_{V\to\infty} \frac{1}{VL} \ln\left\{\sum_{l=0}^{N-1} \exp\left[V\zeta N \cos\left(\frac{\theta + 2\pi\, l}{N}\right)\right]\right\}, \quad (2.37)$$

[1] We note in passing that there is a typo in [85] in sine-Gordon representation which is corrected here. Also, it has been stated (incorrectly) in [85] that the sine-Gordon Lagrangian is 2π periodic as a result of a symmetry. This statement is incorrect, as the claimed symmetry is not in fact a symmetry of the theory, such that θ parameter enters the Lagrangian as θ/N as it should. To check this insert $\boldsymbol{\sigma} = 0$ and notice that the θ-dependence is explicitly different after the transformation suggested in [85].

where V is 3d volume of the system. (2.37) shows that in the limit $V \to \infty$ cusp singularities occur at the values at $\theta = \pi \ (mod\ 2\pi)$ where the lowest energy vacuum state switches from one analytic branch to another. The first derivative of the vacuum energy, which is proportional to the topological density condensate, is two-valued at these points. This means that whenever $\theta = \pi \ (mod\ 2\pi)$ we stay with two degenerate vacua in the thermodynamic limit. If, on the other hand, the thermodynamic limit is performed for a fixed value of θ, any information on other states is completely lost in (2.37). Correspondingly, the 2π periodicity in θ is also lost in infinite volume formulae. We miss the chance to know about additional states when we work in the infinite volume limit from the very beginning. As a result, usual $V = \infty$ formulae become blind to the very existence of a whole set of different vacua, which is in fact responsible for restoration of the 2π periodicity in θ. The model under consideration explicitly supports this pattern in deformed QCD where all computations are under complete theoretical control.

Such a pattern is known to emerge in many four dimensional supersymmetric models, and also gluodynamics in the limit $N = \infty$. It has been further argued [34] that the same pattern also emerges in four dimensional gluodynamics at any finite N. We follow, in fact, the technique from [34] to arrive at (2.37) in analysing the θ periodicity of the theory. The same pattern emerges in holographic description of QCD [96] at $N = \infty$ as well.

Finally, considering the expectation value

$$\begin{aligned}\langle e^{\pm i\alpha_b\cdot\boldsymbol{\sigma}(\mathbf{y})}\rangle &= \frac{1}{\mathcal{Z}}\int\left[\prod_{a=1}^{N}\mathcal{D}\sigma_a\, d\mu^{(a)}\right]\times \\ &\qquad \exp\left\{-\beta\int_{\mathbb{R}^3} d^3x\left[\frac{1}{2}\left(\nabla\boldsymbol{\sigma}\right)^2 + J\cdot\boldsymbol{\sigma} \mp \frac{i}{\beta}\delta(x-y)\alpha_b\cdot\boldsymbol{\sigma}\right]\right\} \\ &= \frac{\mathcal{Z}_0}{\mathcal{Z}}\int\left[\prod_{a=0}^{N} d\mu^{(a)}\right] e^{-S_{\rm MG}}\exp\left[\pm\frac{4\pi^2 L}{g^2}\sum_{a=1}^{N}\sum_{k=1}^{M^{(a)}} Q_k^{(a)}\alpha_a\cdot\alpha_b G(x_k^{(a)}-y)\right],\end{aligned} \tag{2.38}$$

we note that the operator $e^{i\alpha_a\cdot\boldsymbol{\sigma}(\mathbf{x})}$ is the creation operator for a monopole of type a at $\mathbf{x}$, i.e.

$$\mathcal{M}_a(\mathbf{x}) = e^{i\alpha_a\cdot\boldsymbol{\sigma}(\mathbf{x})}. \tag{2.39}$$

Likewise, the operator for an antimonopole is $\bar{\mathcal{M}}_a(\mathbf{x}) = e^{-i\alpha_a\cdot\boldsymbol{\sigma}(\mathbf{x})}$. The expectation values of these operators in fact determine the ground state of the theory.

2.4 Mass Gap

The cosine potential in the sine-Gordon action (2.24) gives rise to a mass term for the dual scalar fields. Expanding the potential around the minimum $\boldsymbol{\sigma} = 0$ up to quadratic order and rescaling $\boldsymbol{\sigma} \to L(2\pi)^2/g^2\boldsymbol{\sigma}$ to put the kinetic term into canonical form, and gives (up to a constant term)

$$V(\boldsymbol{\sigma}) \cong \frac{1}{2} m_\sigma^2 \sum_{a=1}^{N} (\sigma_{a+1} - \sigma_i)^2, \tag{2.40}$$

with

$$m_\sigma^2 \equiv L\zeta \left(\frac{2\pi}{g}\right)^2. \tag{2.41}$$

The above mass term is diagonalised by the discrete Fourier transform

$$\tilde{\sigma}_b \equiv \frac{1}{\sqrt{N}} \sum_{a=0}^{N} e^{\frac{-2\pi i a b}{N}} \sigma_a, \tag{2.42}$$

becoming

$$V(\boldsymbol{\sigma}) \cong \frac{1}{2} \sum_{a=1}^{N} m_a^2 \left|\tilde{\sigma}_a\right|^2, \tag{2.43}$$

where $m_a = m_\sigma \sin(\pi a/N)$. So the only scalar field which remains massless is the Nth field, which is the field associated with the affine root. Inserting the discrete Fourier transform (2.42) into the full cosine potential however shows that the Nth field drops out of the cosine potential completely, so although it remains massless, it completely decouples from the theory and does not interact with the other components at all.

Chapter 3

Topological Susceptibility and Contact Term

This chapter reproduces the work presented in [80]. We explicitly demonstrate the presence of a contact term in the topological susceptibility for the deformed gauge theory. It contributes with a sign opposite the contributions from physical propagating degrees of freedom such that the relevant Ward identities are satisfied.

3.1 The Contact Term and Degeneracy of Topological Sectors

In this section we present an overview of the nature of the contact term which is not related to any physical degrees of freedom . We explain how we know about its mere existence because of requirements imposed by the anomalous Ward Identities, which require its presence. We also give a simple two dimensional example explaining how this term emerges in gauge theories. The nature of this "weird" contribution is entirely determined by the topological properties of the model rather than the physical propagating degrees of freedom of the system. Thus, we will find similar behaviour in theories with similar topological properties irrespective of the particularities of the theories. Such calculations cannot be carried out at present in undeformed QCD, but can in the simplified deformed model we consider. As such, because this model exhibits a similar topological structure to what we expect for proper undeformed QCD, we have some hope that calculations, which can be performed here, can provide some useful insight.

3.1.1 The Contact Term

We start with definition of the topological susceptibility χ which is the main ingredient of the resolution of the $U(1)_A$ problem in QCD [90, 91, 93], see also [42, 54, 64]. The necessity for the contact term in topological

susceptibility χ can be explained in few lines as follows. We define the topological susceptibility χ in the standard way:

$$\chi(\theta=0) = \left.\frac{\partial^2 E_{\rm vac}(\theta)}{\partial\theta^2}\right|_{\theta=0} = \lim_{k\to 0}\int {\rm d}^4x e^{ikx}\langle T\{q(x),q(0)\}\rangle, \tag{3.1}$$

where θ is the conventional θ parameter which enters the Lagrangian along with topological density operator $q(x)$, see precise definitions below. The most important feature of the topological susceptibility χ, for our present discussion, is that it does not vanish in spite of the fact that $q = \partial_\mu K^\mu$ is total divergence. Furthermore, any physical state of mass m_G, momentum $k \to 0$ and coupling $\langle 0|q|G\rangle = c_G$ contributes to the dispersive portion of the topological susceptibility with negative sign [2]

$$\begin{aligned}\chi_{\rm dispersive} &\sim \lim_{k\to 0}\int {\rm d}^4x e^{ikx}\langle T\{q(x),q(0)\}\rangle \\ &\sim \lim_{k\to 0}\frac{\langle 0|q|G\rangle\langle G|q|0\rangle}{-k^2-m_G^2} \simeq -\frac{|c_G|^2}{m_G^2} \leq 0, \end{aligned}\tag{3.2}$$

while the resolution of the $U(1)_A$ problem, which would provide a physical mass for the η' meson, requires a positive sign for the topological susceptibility (3.3), see the original reference [90] for a thorough discussion,

$$\chi_{\rm non-dispersive} = \lim_{k\to 0}\int {\rm d}^4x e^{ikx}\langle T\{q(x),q(0)\}\rangle > 0\,. \tag{3.3}$$

Therefore, there must be a contact contribution to χ, which is not related to any propagating physical degrees of freedom, and it must have the "wrong" sign, by which we mean opposite to any term originating from physical propagators, in order to saturate the topological susceptibility (3.3). In the framework [93] the contact term with the "wrong" sign has been simply postulated, while in refs.[90, 91] the Veneziano ghost had been introduced to saturate the required property (3.3). This Veneziano ghost field is simply an unphysical degree of freedom with the "wrong" sign in the kinetic term such that it generates the same contact term when integrated out. It should be emphasised that these two descriptions are equivalent and simply two separate ways of describing the same physics and that in these two pictures, the claim that the "contact" term does not come from physical propagating degrees of freedom is manifest.

[2] We use the Euclidean notations where path integral computations are normally performed.

It should be mentioned here that the "wrong" sign in topological susceptibility (3.3) is not the only manifestation of this "weird" unphysical degree of freedom. In fact, one can argue that the well known mismatch between Bekenstein-Hawking entropy and the entropy of entanglement for gauge fields is due to the same gauge configurations which saturate the contact term in the topological susceptibility in QCD as discussed in [101]. In both cases the extra term with a "wrong" sign is due to distinct topological sectors in gauge theories. This extra term is non-dispersive in nature, can not restored from the conventional spectral function through dispersion relations, and is not associated with any physical propagating degrees of freedom.

3.1.2 Topological Susceptibility and Contact Term in 2D QED

The goal here is to give some insights on the nature of the contact term using a simple exactly solvable two dimensional QED_2 [48]. We follow [100, 101] to discuss all essential elements related to the contact term.

We start by considering two dimensional photodynamics (QED formulated without fermions) which is naively a trivial theory as it does not have any physical propagating degrees of freedom. However, we shall argue that this (naively trivial) two dimensional photodynamics nevertheless has a contact term which is related to the existence of different topological sectors in the theory. Thus, the presence of degenerate topological sectors in the system, which we call the "degeneracy" for short[3] , is the source for this contact term which is not related to any physical propagating degrees of freedom.

The topological susceptibility χ in this model is defined as follows

$$\chi \equiv \frac{e^2}{4\pi^2} \lim_{k\to 0} \int \mathrm{d}^2x e^{ikx} \langle TE(x)E(0)\rangle \,, \tag{3.4}$$

[3]Not to be confused with conventional term "degeneracy" when two or more physically distinct states are present in the system. In the context of this paper, the "degeneracy" references the existence of winding states $|n\rangle$ constructed as follows: $\mathcal{T}|n\rangle = |n+1\rangle$. In this formula the operator $\mathcal{T}$ is the large gauge transformation operator which commutes with the Hamiltonian $[\mathcal{T}, H] = 0$, implying the "degeneracy" of the winding states $|n\rangle$. The physical vacuum state is *unique* and constructed as a superposition of $|n\rangle$ states. In path integral approach the presence of N different sectors in the system is reflected by summation over $k \in \mathbb{Z}$ in (3.12), (3.13), and (3.14).

where $q = \frac{e}{2\pi}E$ is the topological charge density operator and

$$\int \mathrm{d}^2x\ q(x) = \frac{e}{2\pi}\int \mathrm{d}^2x\ E(x) = k \tag{3.5}$$

is the integer valued topological charge in the 2d $U(1)$ gauge theory, $E(x) = \partial_1 A_2 - \partial_2 A_1$ is the field strength. The expression for the topological susceptibility in 2d Schwinger QED model when the fermions are included into the system is known exactly [67, 68]

$$\chi_{QED} = \frac{e^2}{4\pi^2}\int \mathrm{d}^2x \left[\delta^2(x) - \frac{e^2}{2\pi^2}K_0(\mu|x|)\right], \tag{3.6}$$

where $\mu^2 = e^2/\pi$ is the mass of the single physical state in this model, and $K_0(\mu|x|)$ is the modified Bessel function of order 0, which is the Green's function of this massive particle. The expression for χ for pure photodynamics is given by (3.6) with coupling $e = 0$ in the brackets [4] which corresponds to the de-coupling from matter field ψ, i.e.

$$\chi_{E\&M} = \frac{e^2}{4\pi^2}\int \mathrm{d}^2x \left[\delta^2(x)\right] = \frac{e^2}{4\pi^2}. \tag{3.7}$$

The crucial observation here is as follows: any physical state contributes to χ with negative sign

$$\chi_{dispersive} \sim \lim_{k\to 0}\sum_n \frac{\langle 0|\frac{e}{2\pi}E|n\rangle\langle n|\frac{e}{2\pi}E|0\rangle}{-k^2 - m_n^2} < 0, \tag{3.8}$$

in accordance with the general formula (3.2) in four dimensions discussed previously. In particular, the term proportional $-K_0(\mu|x|)$ with negative sign in equation (3.6) results from the only physical field of mass μ. However, there is also a contact term $\int \mathrm{d}^2x \left[\delta^2(x)\right]$ in (3.6) and (3.7) which contributes to the topological susceptibility χ with the *opposite sign*, and which can not be identified according to (3.8) with any contribution from any physical asymptotic state. In the two-dimensional theory without a fermion (photodynamics), there are no asymptotic states since there are no possible polarisation states, and so it is clear that the contact term (3.7) is not related to any physical propagating degree of freedom. Likewise, with a fermion included, there is one physical degree of freedom, yet we see also the additional "contact" contribution in (3.6).

[4] the factor $\frac{e^2}{4\pi^2}$ in front of (3.6) does not vanish in this limit as it is due to our definition (3.4) rather than result of dynamics

This term has fundamentally different, non-dispersive nature. In fact it is ultimately related to different topological sectors of the theory and the degeneracy of the ground state as we shortly review below. Without this contribution it would be impossible to satisfy the Ward Identity because the physical propagating degrees of freedom can only contribute with sign $(-)$ to the correlation function as (3.8) suggests, while the Ward Identity requires $\chi_{QED}(m=0)=0$ in the chiral limit $m=0$. One can explicitly check that Ward Identity is indeed automatically satisfied only as a result of exact cancellation between conventional dispersive term with sign $(-)$ and non-dispersive term (3.7) with sign $(+)$,

$$\chi_{QED} = \frac{e^2}{4\pi^2}\int \mathrm{d}^2x \left[\delta^2(x) - \frac{e^2}{2\pi^2}K_0(\mu|x|)\right] \\ = \frac{e^2}{4\pi^2}\left[1 - \frac{e^2}{\pi}\frac{1}{\mu^2}\right] = \frac{e^2}{4\pi^2}\left[1-1\right] = 0. \quad (3.9)$$

Therefore, contact term actually plays a crucial role in maintaining the consistency of the theory, because the Ward Identity can not be satisfied without it. While the exact formula (3.6) is known, it does not hint at the kind of physics responsible for the contact term with the "wrong sign", mainly what sort of field configurations should saturate the contact term. Below, we provide some insights on this matter.

3.1.3 The Contact Term from Summation Over Topological Sectors

The goal here is to demonstrate that the contact term in the exact formulae (3.6) and (3.7) is a result of the summation over different topological k sectors in the $2d$ pure $U(1)$ gauge theory. The relevant "instanton-like" configurations are defined on a two dimensional Euclidean torus with total area V as follows [67, 68],

$$A_\mu^{(k)} = -\frac{\pi k}{eV}\epsilon_{\mu\nu}x^\nu, \quad eE^{(k)} = \frac{2\pi k}{V}, \quad (3.10)$$

such that the action of this classical configuration is

$$\frac{1}{2}\int d^2x E^2 = \frac{2\pi^2 k^2}{e^2 V}. \quad (3.11)$$

This configuration corresponds to the topological charge k as defined by (3.5). The next step is to compute the topological susceptibility for the

theory defined by the following partition function

$$\mathcal{Z} = \sum_{k\in\mathbb{Z}} \int \mathcal{D}A e^{-\frac{1}{2}\int d^2x E^2}. \tag{3.12}$$

All integrals in this partition function are Gaussian and can be easily evaluated. The result is determined essentially by the classical configurations (3.10) and (3.11) since real propagating degrees of freedom are not present in the system of pure $U(1)$ gauge field theory in two dimensions. We are interested in computing χ defined by equation (3.4). In the path integral approach it can be represented as follows,

$$\chi_{E\&M} = \frac{e^2}{4\pi^2\mathcal{Z}} \sum_{k\in\mathbb{Z}} \int \mathcal{D}A \int \mathrm{d}^2x E(x)E(0) e^{-\frac{1}{2}\int d^2x E^2}. \tag{3.13}$$

This Gaussian integral can be easily evaluated and the result is as follows [100, 101],

$$\chi_{E\&M} = \frac{e^2}{4\pi^2} \cdot V \cdot \frac{\sum\limits_{k\in\mathbb{Z}} \frac{4\pi^2k^2}{e^2V^2} \exp(-\frac{2\pi^2k^2}{e^2V})}{\sum\limits_{k\in\mathbb{Z}} \exp(-\frac{2\pi^2k^2}{e^2V})}. \tag{3.14}$$

In the large volume limit $V \to \infty$ one can evaluate the sums entering (3.14) by replacing $\sum_{k\in\mathbb{Z}} \to \int dk$, and the leading term in equation (3.14) takes the form

$$\chi_{E\&M} = \frac{e^2}{4\pi^2} \cdot V \cdot \frac{4\pi^2}{e^2V^2} \cdot \frac{e^2V}{4\pi^2} = \frac{e^2}{4\pi^2}. \tag{3.15}$$

A few comments are in order. First, the obtained expression for the topological susceptibility (3.15) is finite in the limit $V \to \infty$, coincides with the contact term from exact computations (3.6), (3.7) performed for the $2d$ Schwinger model, and has the "wrong" sign in comparison with any physical contributions (3.8). Second, the topological sectors with very large $k \sim \sqrt{e^2V}$ saturate the series (3.14). As we can see from the computations presented above, the final result (3.15) is sensitive to the boundaries, infrared regularisation, and many other aspects which are normally ignored when a theory from the very beginning is formulated in infinite space with conventional assumption about trivial behaviour at infinity. Lastly, the contribution (3.15) does not vanish in a trivial model with no propagating degrees of freedom present in the system. This term is entirely determined by the behaviour at the boundary, which is conveniently represented by

the classical topological configurations (3.10) describing different topological sectors (3.5), and accounts for the degeneracy of the ground state. In this way, large distance physics enter despite the lack of physical long distance degrees of freedom. Furthermore, we know that this term must be present in the theory when the dynamical quarks are introduced into the system. Indeed, it plays a crucial role in this case as it saturates the Ward Identity as (3.9) shows.

We conclude this section by noting that the contact term in the framework of [48] can be computed in terms of the Kogut-Susskind ghost by replacing the standard path integral procedure of summation over different topological sectors above as follows. The topological density $q = \frac{e}{2\pi}E$ in $2d$ QED is given by $\frac{e}{2\pi}E = (\frac{e}{2\pi})\frac{\sqrt{\pi}}{e}\left(\Box\hat{\phi} - \Box\phi_1\right)$ where $\hat{\phi}$ is the physical massive field of the model and ϕ_1 is the ghost [48]. The relevant correlation function in coordinate space which enters the expression for the topological susceptibility (3.4) can be explicitly computed using the ghost as follows

$$\begin{aligned}\chi_{QED}(x) &\equiv \left\langle T\frac{e}{2\pi}E(x), \frac{e}{2\pi}E(0)\right\rangle \\ &= \left(\frac{e}{2\pi}\right)^2 \frac{\pi}{e^2}\int \frac{\mathrm{d}^2p}{(2\pi)^2}p^4 e^{-ipx}\left[-\frac{1}{p^2+\mu^2}+\frac{1}{p^2}\right] \\ &= \left(\frac{e}{2\pi}\right)^2\left[\delta^2(x) - \frac{e^2}{2\pi^2}K_0(\mu|x|)\right] \quad (3.16)\end{aligned}$$

where we used the known expressions for the Green's functions. The obtained expression precisely reproduces the exact result (3.6) as claimed. In the limit $e \to 0$ when the fermion matter field decouples from gauge degrees of freedom we reproduce the contact term (3.7), (3.15) which was previously derived as a result of summation over different topological sectors of the theory. The non-dispersive contribution manifests itself in this description in terms of the unphysical ghost scalar field which provides the required "wrong" sign for the contact term. These two different descriptions are analogous to the same two computations in four dimensions mentioned in Section 3.1.1, with and without the Veneziano ghost, and again we emphasise the equivalence of the two. In the picture wherein the contact term is saturated by a ghost field we see again how the contact term is not related to physical propagating degrees of freedom.

3.2 Topological Susceptibility in the Deformed QCD

Next we consider the topological susceptibility in the deformed theory discussed in the previous chapter in both the monopole and sine-Gordon formalisms. We define the topological density $q(\mathbf{x})$ and topological charge Q by

$$Q \equiv \frac{1}{16\pi^2}\int_{\mathbb{R}^3\times S^1} d^4x \ \mathrm{tr}\left[F_{\mu\nu}\tilde{F}^{\mu\nu}\right] = L\int_{\mathbb{R}^3} d^3x \ \left[q(\mathbf{x})\right] \tag{3.17}$$

and as in (3.1) the topological susceptibility χ is given by

$$\chi = L\lim_{\mathbf{k}\to 0}\int d^3x \ e^{i\mathbf{k}\cdot\mathbf{x}}\left\langle q(\mathbf{x})q(0)\right\rangle . \tag{3.18}$$

First, in next subsection we compute the topological susceptibility directly, using the monopole gas representation. As the next step, we reproduce our results using sine Gordon representation of the theory. Finally, we compute the topological susceptibility with a single massless quark introduced into the system. Essentially, the goal here is to discuss the same physics related to the nondispersive contact term and topological sectors in the deformed model for QCD, in close analogy to our discussions in 2d QED in Section 3.1.

3.2.1 Topological Susceptibility in the Monopole Picture

In order to compute the functional form of the topological susceptibility in the monopole theory we consider the topological density,

$$\begin{aligned} q(\mathbf{x}) &= \frac{1}{16\pi^2}\mathrm{tr}\left[F_{\mu\nu}\tilde{F}^{\mu\nu}\right] = \frac{-1}{8\pi^2}\epsilon^{ijk4}\sum_{a=1}^{N}F_{jk}^{(a)}F_{i4}^{(a)} \\ &= \frac{g}{4\pi^2}\sum_{a=1}^{N}\left\langle A_4^{(a)}\right\rangle\left[\nabla\cdot\mathbf{B}^{(a)}(\mathbf{x})\right], \end{aligned} \tag{3.19}$$

where the $U(1)^N$ magnetic field, $B^i = \epsilon^{ijk4}F_{jk}/2g$ is given by

$$\mathbf{B}^{(a)}(\mathbf{x}) = \frac{2\pi}{g}\alpha_a\left[\sum_{k=1}^{n^{(a)}}\frac{\mathbf{x}-\mathbf{r}_k^{(a)}}{4\pi\left|\mathbf{x}-\mathbf{r}_k^{(a)}\right|^3} - \sum_{k=1}^{n^{(a)}}\frac{\mathbf{x}-\mathbf{r}_k^{(a)}}{4\pi\left|\mathbf{x}-\mathbf{r}_k^{(a)}\right|^3}\right], \tag{3.20}$$

and $\left\langle A_4^{(a)} \right\rangle$ is just the expectation value of the diagonal gauge fields in the compact direction,

$$\left\langle A_4^{(a)} \right\rangle = \frac{2\pi}{NL}\mu^a. \tag{3.21}$$

The above μ^a are the fundamental weights for the $SU(N)$ algebra and are defined by

$$\mu^a \cdot \alpha_b \equiv \frac{1}{2}\delta_b^a \alpha_b^2 = \delta_b^a. \tag{3.22}$$

Inserting the magnetic field for the monopole ensemble into the topological density expression (3.19) and applying Gauss's theorem to the result, we arrive at

$$\begin{aligned} q(\mathbf{x}) &= \sum_{a=1}^{N} \frac{1}{LN} \left[\sum_{k=1}^{n^{(a)}} \delta(\mathbf{r}_k^{(a)} - \mathbf{x}) - \sum_{l=1}^{\bar{n}^{(a)}} \delta(\bar{\mathbf{r}}_l^{(a)} - \mathbf{x}) \right] \\ &= \frac{1}{LN} \sum_{a=1}^{N} \sum_{k=1}^{M^{(a)}} Q_k^{(a)} \delta(\mathbf{r}_k^{(a)} - \mathbf{x}), \end{aligned} \tag{3.23}$$

which obviously gives the proper topological charge for a single monopole or antimonopole, $Q = \pm 1/N$. The topological density operator $q(\mathbf{x})$ has dimension four as it should.

The expectation value $\langle q(\mathbf{x})q(0)\rangle$ is the topological density operator (3.23) evaluated at each point inserted in the partition function (2.20),

$$\begin{aligned} \langle qq \rangle &= \frac{1}{\mathcal{Z}} \int \prod_{a=1}^{N} d\mu^{(a)} \; [q(\mathbf{x})q(0)]\, e^{-S_{\rm int}} \\ &= \frac{1}{\mathcal{Z}N^2L^2} \int \prod_{a=1}^{N} d\mu^{(a)} \sum_{a,b=1}^{N} \sum_{k=1}^{M^{(a)}} \sum_{l=1}^{M^{(b)}} \left[Q_k^{(a)} Q_l^{(b)} \delta(\mathbf{r}_k^{(a)} - \mathbf{x}) \delta(\mathbf{r}_l^{(b)}) \right] e^{-S_{\rm int}} \\ &= \frac{1}{\mathcal{Z}N^2L^2} \int d\mu \sum_m \sum_n \left[Q_m Q_n \; \delta(\mathbf{r}_m - \mathbf{x}) \delta(\mathbf{r}_n) \right] e^{-S_{\rm int}} \\ &= \frac{1}{\mathcal{Z}N^2L^2} \int d\mu \left\{ \delta(\mathbf{x}) \sum_m \delta(\mathbf{r}_m) e^{-S_{\rm int}} + \right. \\ &\qquad \left. \sum_m \sum_{n \neq m} \left[Q_m Q_n \; \delta(\mathbf{r}_m - \mathbf{x}) \delta(\mathbf{r}_n) \right] e^{-S_{\rm int}} \right\} \\ &= \frac{\zeta}{NL^2} \left\{ \delta(\mathbf{x}) - \mathcal{O}(\zeta) \right\}, \end{aligned} \tag{3.24}$$

where we have condensed the indices to just m and n which run over each monopole in the ensemble. In the above expression, the double sum of delta functions gives a set of terms in which each pair of monopoles in the ensemble are moved to the points $\mathbf{x}$ and 0 and computes the partition function given that arrangement. The monopole gas experiences Debye screening so that the field due to any static charge falls off exponentially with characteristic length m_σ^{-1}. The number density $\mathcal{N}$ of monopoles is given by the monopole fugacity, $\sim \zeta$, so that the average number of monopoles in a "Debye volume" is given by

$$\mathcal{N} \equiv m_\sigma^{-3}\zeta = \left(\frac{g}{2\pi}\right)^3 \frac{1}{\sqrt{L^3\zeta}} \gg 1. \tag{3.25}$$

The last inequality holds since the monopole fugacity is exponentially suppressed, $\zeta \sim e^{-1/g^2}$, and in fact we can view (3.25) as a constraint on the validity of our approximation. The statement here is that inserting or removing a particular monopole will not drastically affect the monopole ensemble as a result of condition (3.25), so that we can compute expectations of operators in the original ensemble without considering the back-reaction on the ensemble itself. Then, because removing any given monopole does not significantly change the ensemble, we can treat the delta functions in the third line of (3.24) as simply creation operators. The second term in (3.24), which is a dispersive term, reduces to the form $\langle M^\dagger M\rangle$ since it is only non-zero for monopole-antimonopole pairs of the same type. The factor overall factor of ζ and additional factor in $\mathcal{O}(\zeta)$ in formula (3.24) appears because each monopole we remove from the ensemble leaves a factor of $\zeta/N^{(a)}$ in the monopole measure, and there are $N^{(a)}$ such terms for each type of monopole so that we are left with just a factor of ζ.

The computed non-dispersive contribution (3.24) to the topological susceptibility in the deformed gauge model has exactly the same structure we observed in two dimensional QED discussed in Section 3.1. In particular, it is expressed in terms of a $\delta(\mathbf{x})$ function, and it has the "wrong sign" similar to (3.7). Furthermore, this contribution is not related to any physical propagating degrees of freedom, but rather, it is determined by degenerate topological sectors of the theory. The corresponding "degeneracy" is formulated in terms of monopoles which essentially describe the tunnelling transitions between those "degenerate" sectors, see Section 3.2.3 for more comments on the physical meaning of the formula. If we neglect a small term $\mathcal{O}(\zeta)$ in formula (3.24) we arrive to the following final expression for

the topological susceptibility in deformed gauge theory without quarks

$$\chi_{YM} = \frac{\zeta}{NL^2}\int d^4x\,[\delta(\mathbf{x})] = \frac{\zeta}{NL}. \tag{3.26}$$

It has dimension four as it should. This expression is a direct analog of equation (3.7) derived for two dimensional QED. The same formula (3.26) can be computed also in the dual sine-Gordon theory by differentiation of the ground state energy density (2.37) with respect to the θ as general expression (3.1) states

$$\chi_{YM}(\theta=0) = \left.\frac{\partial^2 E_{\min}(\theta)}{\partial\theta^2}\right|_{\theta=0} = \frac{\zeta}{NL}, \qquad E_{\min}(\theta=0) = -\frac{N\zeta}{L}. \tag{3.27}$$

Agreement between the two computations can be considered as a consistency check of our approach in the weakly coupled regime. One can explicitly see that the general relation $\chi_{YM} \sim E_{\min}(\theta=0)/N^2$ holds for the deformed model as a result of θ/N dependence in equation (2.36). Real strongly coupled QCD is that the vacuum energy scales as N^2 in QCD rather than, apparently, $\sim N$ in (3.27). To rectify these two, note that the domain of validity for this model is defined by $LN\Lambda \ll 1$, as discussed in [85], so that $L \sim 1/N$.

3.2.2 Topological Susceptibility in the Presence of the Light Quarks

Our goal here is to introduce a single massless quark ψ into the system to see how the topological susceptibility changes in this case. We anticipate that the emerging structure should be very similar to (3.6) as the topological susceptibility must vanish in the presence of massless quark in the system: $\chi_{QCD}(m_q=0)=0$ as the direct consequence of the Ward Identities discussed in Section 3.1.

The low energy description of the system in confined phase with a single quark is accomplished by introducing the η' meson. As usual, the η' would be conventional massless Goldstone boson if the chiral anomaly is ignored. In the dual sine-Gordon theory the η' field appears exclusively in combination with the θ parameter as $\theta \to \theta - \eta'$. As it is well known, this is the direct result of the transformation properties of the path integral measure under

the chiral transformations $\psi \to \exp(i\gamma_5 \frac{\eta'}{2})\psi$. Therefore we have,

$$\begin{aligned}
\mathcal{Z} &= \int \prod_{a=0}^{N} \mathcal{D}\sigma_a \mathcal{D}\eta' \exp\{-S_\sigma - S_{\eta'} - S_{int}\} \qquad (3.28)\\
S_\sigma &= \int_{\mathbb{R}^3} d^3x \cdot \frac{1}{2L}\left(\frac{g}{2\pi}\right)^2 (\nabla \boldsymbol{\sigma})^2\\
S_{\eta'} &= \int_{\mathbb{R}^3} d^3x \cdot \frac{c}{2}\left(\nabla \eta'\right)^2\\
S_{int} &= -\int_{\mathbb{R}^3} d^3x \cdot \zeta \sum_{a=1}^{N} \cos\left(\alpha_a \cdot \boldsymbol{\sigma} + \frac{\theta - \eta'}{N}\right),
\end{aligned}$$

where coefficient c determines the normalisation of the η' field and has dimension one. This coefficient, in principle, can be computed in this model, but such a computation is beyond the scope of the present work and not particularly illuminating. In four dimensional QCD the coefficient c is expressed in terms of standard notations as $(c/L) \to f_{\eta'}^2$. In terms of these parameters the η' mass is given by

$$m_{\eta'}^2 = \frac{\zeta}{cN}. \qquad (3.29)$$

Since η' shows up in the Yang-Mills Lagrangian as $\eta' F\tilde{F}$, we can compute our requisite expectation, $\langle F\tilde{F}, F\tilde{F}\rangle$, by functional differentiation with respect to η',

$$\langle q(\mathbf{x})q(\mathbf{y})\rangle = \frac{1}{\mathcal{Z}} \frac{i\,\delta}{\delta\eta'(x)} \frac{i\,\delta}{\delta\eta'(y)} \mathcal{Z}\Big|_{\theta=0}. \qquad (3.30)$$

Thus we have,

$$\begin{aligned}
\langle q(\mathbf{x})q(\mathbf{y})\rangle &= \frac{1}{\mathcal{Z}} \frac{\delta}{\delta\eta'(y)} \int \mathcal{D}\boldsymbol{\sigma}\mathcal{D}\eta' \left[\frac{-\zeta}{NL^2} \int_{\mathbb{R}^3} d^3r_1\, \delta(\mathbf{r}_1 - \mathbf{x}) \sum_{a=1}^{N} \frac{\eta'(\mathbf{r}_1)}{N}\right] e^{-S}\\
&= \frac{1}{\mathcal{Z}} \int \mathcal{D}\boldsymbol{\sigma}\mathcal{D}\eta' \left[\frac{\zeta}{NL^2} \int d^3r_1\, \delta(\mathbf{r}_1 - \mathbf{x})\delta(\mathbf{r}_1 - \mathbf{y})\right] e^{-S}\\
&- \frac{1}{\mathcal{Z}} \int \mathcal{D}\boldsymbol{\sigma}\mathcal{D}\eta' \left[\frac{\zeta^2}{NL^2} \int d^3r_1 \int d^3r_2\, \delta(\mathbf{r}_1 - \mathbf{x})\delta(\mathbf{r}_2 - \mathbf{y})\times \right.\\
&\qquad \left. \sum_{a,b=1}^{N} \frac{\eta'(\mathbf{r}_1)}{N} \frac{\eta'(\mathbf{r}_2)}{N}\right] e^{-S}\\
&= \frac{\zeta}{NL^2}\left[\delta(\mathbf{x} - \mathbf{y}) - \frac{\zeta}{N}\langle \eta'(\mathbf{x})\eta'(\mathbf{y})\rangle\right]. \qquad (3.31)
\end{aligned}$$

The first term in (3.31) is precisely non-dispersive contact term with the "wrong sign" that we computed previously in pure gauge theory using two different methods, see (3.26) and (3.27). The second term represents the conventional dispersive contribution of the physical η' state [5]. One can compute it by redefining $\eta' \to \eta'/\sqrt{c}$ field to bring its kinetic term $S_{\eta'}$ to the canonical form. In the lowest order approximation it is reduced to the conventional Green's function of the free massive η' scalar field with mass determined by (3.29), such that

$$\chi_{QCD} = \int d^4x \langle q(\mathbf{x})q(\mathbf{y})\rangle = \frac{\zeta}{NL}\int d^3x \left[\delta(\mathbf{x}) - m^2_{\eta'}\frac{e^{-m_{\eta'}r}}{4\pi r}\right] = 0, \quad (3.32)$$

where we represented the canonical η' propagator in terms of its free Green's function in three dimensions.

The structure of this equation follows precisely the same pattern we observed in analysis of two dimensional QED, see (3.6). Indeed, it contains the non-dispersive term due to the degeneracy of the topological sectors of the theory. This contact term (which is not related to any physical propagating degrees of freedom) has been computed using monopoles describing the transitions between these topological sectors (3.26). The second term emerges as a result of insertion of the massless quark into the system. It enters χ_{QCD} precisely in such a way that the Ward Identity $\chi_{QCD}(m_q = 0) = 0$ is automatically satisfied as a result of cancellation between the two terms in close analogy with the two dimensional case (3.9). We should also mention that very similar structure emerges in real strongly coupled QCD in the framework wherein the contact term is saturated by the Veneziano ghost. This structure has been confirmed by QCD lattice studies, see [102, 104] for some details and references to original lattice results.

[5] This additional interactions due to the η' exchange may in fact be used as a probe to study the relevant topological charges present in the system. It was precisely the idea behind the proposal, see relatively recent papers [56, 99] and earlier references therein, that θ/N behaviour unambiguously implies that the relevant vacuum fluctuations must have fractional topological charges $1/N$. In the present weakly coupled regime these ideas have a precise realisation as the basic vacuum fluctuations are indeed the fractionally charged monopoles (3.23). The results of [56, 99] are in fact much more generic as they are not based on a weakness of the interaction or semiclassical expansion, but rather, on generic features of the η' system which are unambiguously fixed by the Ward Identity. In the approach advocated in [56, 99] one can not study the dynamics of fractionally charged constituents in contrast with the present paper where the dynamics is completely fixed and governed by (3.28). However, the fact that the constituents carry fractional topological charge $1/N$ can be recovered in the approach [56, 99] because the color-singlet η' field enters the effective Lagrangian in a unique way and serves as a perfect probe of the relevant topological charges of the constituents in the system.

3.2.3 Interpretation

The results derived in previous sections were formulated in Euclidean space using conventional Euclidean path integral approach. Our goal here is to give a physical interpretation of these results in physical terms formulated in Minkowski space time. First of all, the $\delta(\mathbf{x})$ function which appear in the expression for topological susceptibility (3.26) should, in fact, be understood as total divergence,

$$\chi \sim \int \delta(\mathbf{x})\, \mathrm{d}^3x = \int \mathrm{d}^3x\ \partial_\mu \left(\frac{x^\mu}{4\pi x^3} \right) = \oint_{S_2} \mathrm{d}\Sigma_\mu \left(\frac{x^\mu}{4\pi x^3} \right). \tag{3.33}$$

Indeed, the starting point to derive χ was the topological density operator (3.23) which is expressed in terms of $\delta(\mathbf{x} - \mathbf{x_i})$ functions, but in fact represents the topologically nontrivial boundary conditions determined by the behaviour at a distant surface S_2 as (3.33) states. The representation (3.33) explicitly shows that we are not dealing with ultraviolet (UV) properties of the problem wherein our approximation breaks down. Our treatment of the problem is perfectly justified as $\delta(\mathbf{x} - \mathbf{x_i})$ functions actually represent the far infrared (IR) part of physics rather than UV physics. This explains why our description is valid for $x \gg L$ in spite of presence of the apparently UV singular elements such as the $\delta(\mathbf{x} - \mathbf{x_i})$ functions which appear in the equations in sections 3.2.1 and 3.2.2.

Our next comment is about the interpretation of the classical monopole gas from chapter 2. The monopoles in our framework are not real particles, they are pseudo-particles which live in Euclidean space and describe the physical tunnelling processes between different winding states $|n\rangle$ and $|n+1\rangle$. The grand canonical partition function written in terms of the classical Coulomb gas (2.34) is simply a convenient way to describe this physics of tunnelling. In particular, the monopole fugacity ζ together with factor L^{-1} should be understood as number of tunnelling events per unit time per unit volume

$$\left(\frac{\mathcal{N} \text{ of tunnelling events}}{VL} \right) = \frac{N\zeta}{L}, \tag{3.34}$$

where extra factor N in (3.34) accounts for N different types of monopoles present in the system. The expression (3.34) is precisely the contact term, up to factor $1/N^2$ computed in (3.26). It is not a coincidence that number of tunnelling events per unit time per unit volume precisely concurs with the absolute value of the energy density of the system (3.27), since the energy density (3.27) in our model is saturated by the topological fluctuations which are not related to any physical propagating degrees of freedom. We

emphasise that while this energy density is not related to any fluctuations of real physical particles, this energy, nevertheless, is still real physical observable parameter, though it can not be defined in terms of conventional Dayson T-product. Instead, it is defined in terms of the Wick's T-product, see Appendix of [101] on a number of subtleties with definition of the energy.

Finally, the characteristic Debye screening length which appears in the Coulomb gas representation in chapter 2

$$r_D \equiv m_\sigma^{-1} = \frac{g}{2\pi\sqrt{L\zeta}} \gg L \tag{3.35}$$

should be interpreted as a typical distance in physical $3d$ space in which the tunnelling event is felt by other fields present in the system. The tunnelling interpretation also explains the "wrong" sign in residues of the correlation function (3.26) as we describe the tunnelling in terms of the Euclidean objects interpolating between physically equivalent topological sectors $|n\rangle$ rather than the tunnelling of conventional physical degree of freedom between distinct vacuum states in condensed matter physics.

3.3 Comments

The main results of this chapter can be formulated as follows. We studied a number of different ingredients related to θ dependence, the non-dispersive contribution in topological susceptibility with the "wrong sign", topological sectors in gauge theories, and related subjects using a simple "deformed QCD". This model is a weakly coupled gauge theory, which however has all the relevant essential elements allowing us to study difficult and nontrivial questions which are known to be present in real strongly coupled QCD. Essentially we tested the ideas related to the $U(1)_A$ problem formulated long ago in [42, 54, 64, 90, 91, 93] in a theoretically controllable manner using the deformed gauge theory as a toy model. One can explicitly see how all the crucial elements work. Here we compute the contact term in the topological susceptibility, (3.24) or (3.31), directly, reproducing conjectured results by Witten [93], who put in the contact term by hand, and Veneziano [90, 91], who put in some auxiliary ghost fields that saturate the contact term when integrated out. See [106] for more details about the use of auxiliary fields in this context.

As this model is a weakly coupled gauge theory, one can try to formulate (and answer) many other questions which are normally the prerogative of numerical Monte Carlo simulations. One such question is the study

of scaling properties of the contact term. We can address what happens to the contact term when the Minkowski space-time $R_{3,1}$ gets slightly deformed. For example, what happens when infinite Minkowski space-time $R_{3,1}$ is replaced by a large, but finite size torus? Or, what happens when the Minkowski space-time $R_{3,1}$ is replaced by FRW metric characterised by the dimensional parameter $R \sim H^{-1}$ describing the size of horizon (H being the Hubble constant)? A naive expectation based on common sense suggests that any physical observable in QCD must not be sensitive to very large distances $\sim \exp(-\Lambda_{\rm QCD} R)$ as QCD has a mass gap $\sim \Lambda_{\rm QCD}$. Such a naive expectation seems to formally follows from the dispersion relations similar to (3.2), which dictate that a sensitivity to very large distances must be exponentially suppressed with a mass gap present in the system, and there are not any physical massless states in the spectrum. However, as we discussed, along with conventional dispersive contribution (3.2) in the system, there is also the non-dispersive contribution (3.3) which emerges as a result of topologically nontrivial sectors in four dimensional QCD. This contact term may lead to a power-like corrections $R^{-1} + \mathcal{O}(R^{-2})$ rather than exponential-like $\sim \exp(-\Lambda_{\rm QCD} R)$ because the dispersion relations do not dictate the scaling properties of this term. In fact, this term in the deformed model in infinite Minkowski space has been explicitly computed in this chapter and it is given by (3.26), (3.32). As our model is a weakly coupled gauge theory, one can, in principle, compute the correction to the formulae (3.26), (3.32) due to the finite size of the system [79]. In other words, one can then try to compute the corrections to the monopole fugacity ζ when the model is formulated in a finite manifold determined by size R. This is the content of the next chapter.

Chapter 4

Casimir Scaling and Dark Energy

This chapter reproduces the work presented in [79]. We show that the deformed model exhibits a power-like Casimir scaling with the size of the manifold it is placed on, rather than the exponential scaling one might expect for a gapped theory.

4.1 Motivation

The main motivation for the study presented in this chapter is a suggestion on the dynamical Dark Energy (DE) model which is entirely rooted in the strongly coupled QCD, without any new fields and/or coupling constants [88, 89, 100, 101]. The key element of the proposal [88, 89, 100, 101] is based on paradigm that the relevant energy which enters the Einstein equations is in fact the difference $\Delta E \equiv E - E_{\rm Mink}$ between the energies of a system in a non-trivial background and Minkowski space-time geometry, similar to the well known Casimir effect when the observed energy is a difference between the energy computed for a system with conducting boundaries (positioned at finite distance $\mathbb{L}$) and infinite Minkowski space[6]. This paradigm is based on the conjecture that gravity, as described by the Einstein equations, is a low-energy effective interaction which, as such, should not be sensitive to the microscopic degrees of freedom in the system but to some effective scale. Thus, the energy density that enters the semiclassical Einstein equations should not be the "bare" energy as computed in QFT, and indeed we know it cannot be, but rather a "renormalised" energy density. We propose the renormalisation scheme given above which sets the vacuum energy to zero in

[6]Here and in what follows we use term "Casimir effect" to emphasise the power like sensitivity to large distances irrespective of their nature. A crucial distinct feature which characterises the system we are interested in is the presence of dimensional parameter $\mathbb{L} \sim H^{-1}$ (where H is a Hubble constant) in the system which discriminates it from infinitely large and flat Minkowski space-time.

Minkowski space wherein the Einstein equations are automatically satisfied as the Ricci tensor identically vanishes.

The above prescription is in fact the standard subtraction procedure that is normally used for the description of horizon thermodynamics [6, 35] as well as in a course of computations of different Green's function in a curved background by subtracting infinities originating in the flat space [8]. In the present context such a definition $\Delta E \equiv (E - E_{\rm Mink})$ for the vacuum energy was first advocated in 1967 by Zeldovich [97] who argued that $\rho_{\rm vac} \sim G m_p^6$ with m_p being the proton's mass. Subsequently, such a definition for the relevant effective energy $\Delta E \equiv (E - E_{\rm Mink})$ which enters the Einstein equations has been advocated from different perspectives in a number of papers, see, for example, the relatively recent works [45, 46, 50, 52, 59, 69, 78, 98] and references therein.

We study the scaling behavior of ΔE when the background deviates slightly from Minkowski space. The difference ΔE must obviously vanish when any deviations (parametrised by Hubble constant or inverse size of the visible universe, $H \sim \mathbb{L}^{-1}$) go to zero as this corresponds to the transition to infinite flat Minkowski space. A naive expectation based on common sense suggests that $\Delta E \sim \exp(-\Lambda_{\rm QCD}/H) \sim \exp(-10^{41})$ as QCD has a mass gap $\sim \Lambda_{\rm QCD} \sim 100$ MeV, and therefore, ΔE must not be very sensitive to size of our universe $\mathbb{L} \sim H^{-1}$. Such a naive expectation formally follows from the dispersion relations which dictate that a sensitivity to very large distances must be exponentially suppressed when the mass gap is present in the system[7].

However, as emphasised in [100, 101] in strongly coupled gauge theories along with conventional dispersive contribution there exists a non-dispersive contribution, not related to any physical propagating degrees of freedom. This non-dispersive (contact) term generally emerges as a result of topologically nontrivial sectors in four dimensional QCD. The variation of this contact term with variation of the background may lead to a power like scaling $\Delta E \sim H + \mathcal{O}(H)^2$ rather than to an exponential like $\Delta E \sim \exp(-\Lambda_{\rm QCD}/H)$ since its contribution is not determined by some gapped dispersion relations. If true, the difference between two metrics (FLRW and Minkowski) would lead to an estimate

$$\Delta E \sim \frac{\Lambda_{\rm QCD}^3}{\mathbb{L}} \sim (10^{-3}{\rm eV})^4, \; 1/\mathbb{L} \sim H \sim 10^{-33}{\rm eV} \tag{4.1}$$

[7]The Casimir effect due to the massless $E\&M$ field obvious shows such power dependence $\Delta E = -\frac{\pi^2}{720\mathbb{L}^4}$. Similar computations for a massive scalar particle with mass m leads to an exponentially suppressed result $\Delta E \sim \exp(-m\mathbb{L})$ as expected, see e.g.[57].

which is amazingly close to the observed dark energy value today. It is interesting to note that expression (4.1) reduces to Zeldovich's formula $\rho_{\rm vac} \sim G m_p^6$ if one replaces $\Lambda_{QCD} \to m_p$ and $H \to G\Lambda_{QCD}^3$. The last step follows from the solution of the Friedman equation

$$H^2 = \frac{8\pi G}{3}\left(\rho_{DE} + \rho_M\right), \quad \rho_{DE} \sim H\Lambda_{\rm QCD}^3 \tag{4.2}$$

when the dark energy component dominates the matter component, $\rho_{DE} \gg \rho_M$. In this case the evolution of the universe approaches a de-Sitter state with constant expansion rate $H \sim G\Lambda_{QCD}^3$ as follows from (4.2).

A comprehensive phenomenological analysis of this model has been recently performed in [12], see also [65, 71] where comparisons with current observational data including SnIa, BAO, CMB, BBN have been presented. The conclusion was that this model is consistent with all presently available data. The main goal here is not comparison of this model with observations; we refer the reader to [12] on this matter. Rather, the purpose of this chapter is to attempt to get some deep theoretical insights behind the Casimir type behaviour (4.1) in a gapped theory such as QCD.

Another motivation to study the Casimir like behaviour in QCD is a proposal [102, 104] that the $\mathcal{P}$ odd correlations observed at RHIC and LHC is in fact another manifestation of long range order advocated in this work. Furthermore, an apparently universal thermal spectrum observed in all high energy collisions when the statistical thermalisation could never be reached in the systems, might be also related to the same contact term, not related to any physical propagating degrees of freedom, see [102, 104] and references therein for the details.

There are a number of arguments supporting the power like behaviour $\Delta E \sim H + \mathcal{O}(H)^2$ in gauge theories, see Section 4.3 where we present some general arguments suggesting the Casimir like corrections in gauge theories with nontrivial topological structure. However, it is always desirable and very instructive to see how the general arguments work in some simplified settings.

First, one can examine the exactly solvable two dimensional QED. Despite this model containing only a single physical massive field, still one can explicitly compute $\Delta E \sim \mathbb{L}^{-1}$ which is in drastic contrast with the naively expected exponential suppression, $\Delta E \sim e^{-\mathbb{L}}$ [86].

Another piece of support for this power-like behaviour is an explicit computation in a simple case of a Rindler space-time in four dimensional QCD [55, 100, 102]. These computations explicitly show that the power like behaviour emerges in four dimensional gauge systems in spite of the

fact that the physical spectrum is gapped. Thus, a power-like behaviour is not a specific feature of two dimensional physics. Accounting for the non-trivial topological sectors in QCD in Rindler space was accomplished in [55, 100, 102] using unphysical auxiliary field, the so-called Veneziano ghost, which encodes the same "contact term" described in the previous chapter. As discussed, the inclusion of different topological sectors was instead introduced by an unphysical ghost field which saturates the "contact term".

Finally, power like behaviour $\Delta E \sim L^{-1}$ is also supported by recent lattice results [36]. The approach advocated in [36] is based on the physical Coulomb gauge wherein nontrivial topological structure of the gauge fields is represented by the so-called Gribov copies. The power like correction $\sim L^{-1}$ had been also noticed, though in quite different context, in [74] where numerical computations were performed using the so-called instanton liquid model.

While a number of supporting arguments presented above suggest the Casimir-type power law scaling $\Delta E \sim H + \mathcal{O}(H)^2$ in strongly coupled QCD, a simple explanation for this behaviour is still lacking. Indeed, skeptics would argue that two dimensional example [86] is a special case, while in four dimensions everything could be very different. A similar skepticism can also be expressed with the ghost based computations [55, 100, 102] as the entire treatment of the problem is based on an auxiliary ghost field which does not belong to the physical Hilbert space and has been inserted by hand. Finally, the numerical computations [36, 74] can not provide a simple physical picture explaining the nature of the phenomenon as the entire effect is hidden in numerics.

This is precisely the goal for the present study: to consider the energy dependence on the boundary conditions this simplified ("deformed") version of QCD which, on one hand, is a weakly coupled gauge theory wherein computations can be performed in theoretically controllable manner. On other hand, this deformation preserves all the relevant elements of strongly coupled QCD such as confinement, degeneracy of topological sectors, non-trivial θ dependence, presence of non-dispersive contribution to topological susceptibility, and other crucial aspects, for this phenomenon to emerge.

4.2 Casimir-Type Behaviour in Deformed QCD

Up to this point the theory was formulated on $\mathbb{R}^3 \times S^1$ with small compactification size L for compact time coordinate S^1 and infinitely large space

$\mathbb{R}^3$ describing three other dimensions. Here however, we are actually interested in behaviour of the system when a space with large dimensions $\mathbb{R}^3$ receives some small modifications, for example the theory is defined in a ball $\mathbb{R}^3 \to \mathbb{B}^3$ with $\mathbb{L}$ being a very large size of the compact dimension of the sphere $\mathbb{S}^2$ which is a boundary of the ball $\mathbb{B}^3$. Such a modification can be thought as a simplest way to model and test the sensitivity of our theory to arbitrary large distances such as size of our visible universe determined by the Hubble constant $H/\Lambda_{\rm QCD} \sim 10^{-41}$. We want to know how the topological susceptibility of the system which describes the θ dependent portion of the vacuum energy $E_{\rm vac}(\theta = 0)$ changes with slight variation of that large size of the system. We assume that $\mathbb{L} \sim H^{-1} \sim 10$ Gpc is much larger than any other scales of the problem. Essentially we want to see whether our deformed model with a mass gap m_σ predicts an exponential scaling typical for a free massive particle

$$\Delta E(\mathbb{L}) \equiv \left[E(\mathbb{B}^3) - E(\mathbb{R}^3)\right] \sim \exp(-m_\sigma \mathbb{L}) \tag{4.3}$$

or demonstrates a Casimir type behaviour

$$\Delta E(\mathbb{L}) \equiv \left[E(\mathbb{B}^3) - E(\mathbb{R}^3)\right] \sim \frac{1}{\mathbb{L}} + \mathcal{O}\left(\frac{1}{\mathbb{L}}\right)^2 . \tag{4.4}$$

If we did not have a non-dispersive contribution in our system, we would immediately predict the behaviour (4.3) as the only available option for a gapped theory in close analogy with conventional Casimir computations for a massive particle $\Delta E(\mathbb{L}) \sim \exp(-m\mathbb{L})$, see for example the review paper [57]. However, our system is more interesting as it exhibits a non-dispersive term resulting from degeneracy of topological sectors in gauge theory as discussed in the previous chapter. This contact term, being unrelated to any physical degrees of freedom, may provide different scaling properties since conventional dispersion relations do not dictate its behaviour at very large distances. As we shall argue, the deformed gauge model indeed exhibits the Casimir type behaviour (4.4) in a drastic departure from the conventional viewpoint represented by equation (4.3). As we reviewed in the previous section we interpret a tiny deviation of the θ-dependent vacuum energy $E_{\rm vac}$ in expanding universe (in comparison with Minkowski space-time) as a main source of the observed dark energy. The Casimir type behaviour (4.4) plays a key role in possibility of such an identification.

We start our discussion in Section 4.2.1 with conventional 4d instanton computations [77] in which infrared regularisation for some gauge modes is required and achieved by putting the system into a sphere with finite radius

$\mathbb{L}$. It allows us to compute power like corrections to the standard instanton density [77]. However, the corresponding corrections being computed for a fixed instanton size ρ can not be interpreted as a physically observable quantity because the integral ($\int d\rho$) over large size instantons diverges for this system when semiclassical approximation for large ρ breaks down. Nevertheless, this example explicitly shows when and why a Casimir type correction (to conventional formula computed in infinite $\mathbb{R}^4$ space) emerges.

Next, we compute a similar correction for the deformed model in Section 4.2.2 wherein a Casimir type correction also appears, resulting from the same physics related to topological sectors of the theory. In contrast with the previous case, the correction computed in this system is physically "observable" quantity as it represents the vacuum energy of the system. Indeed, the tunnelling transitions in this case are described by weakly coupled monopoles, such that semiclassical computations of the vacuum energy (3.34),(6.1) expressed in terms of the density ζ of pseudo-particles are fully justified. The size of pseudo-particles (fractionally charged monopoles) which describe the tunnelling events in this model is fixed by construction [80, 85] so there is no divergence as seen in the instanton case.

We conclude in Section 4.4 with a few final comments.

4.2.1 Casimir-Type Corrections for 4D Instantons

Our goal here is to study a power like correction to the instanton density described in the classic paper [77]. As such, we adopt 't Hooft's notation, and in particular, use the same background-dependent gauge $C_4 = \mathcal{D}_\mu A_\mu^{\mathrm{a\ qu}}$, which drastically simplifies all computations. Essentially, the problem is reduced to analysis of the normalisation factors for finite number of zero modes (8 for $SU(2)$ gauge group) in this gauge wherein the system is defined in a sphere with large but finite radius radius $\mathbb{L}$. Essentially we follow the construction described in section XI of [77]. The corresponding normalisation factor explicitly enters the expression for the instanton density as it accompanies the integration over collective variables. The contribution from non-zero modes does not exhibit such corrections as we argue in Section 4.2.3. We now concentrate on the zero modes and power like corrections which accompany the normalisation factors if the system is defined on a large but finite space $\mathbb{B}^4_{\mathbb{L}}$ (four dimensional interior of a ball of radius $\mathbb{L}$) rather than an infinite space $\mathbb{R}^4$.

We start with four translational zero modes which have the form

$$A_\mu^{\mathrm{a\ qu}}(\nu) \sim \eta_{a\mu\nu}(1+r^2)^{-2}, \quad \nu = 1, ..., 4 \tag{4.5}$$

where we use 't Hooft's notations for $\eta_{a\mu\nu}$ symbols and dimensionless coordinate $r^2 = x_\mu^2$ measured in units of $\rho = 1$. Computing the corresponding correction factor due to the translation zero modes $\kappa_{\rm tr.}$, we have

$$\kappa_{\rm tr.} \equiv \frac{\int_0^{\mathbb{L}} d^4x [A_\mu^{\rm a\ qu}(\nu)]^2}{\int_0^{\infty} d^4x [A_\mu^{\rm a\ qu}(\nu)]^2} \simeq \left[1 - \frac{3}{\mathbb{L}^4} + \mathcal{O}(\frac{1}{\mathbb{L}^6})\right]. \tag{4.6}$$

The corresponding correction factor to the instanton density has power like correction as anticipated. As a result of additional rotational symmetry one should expect, in general, $\mathbb{L}^{-2}$ corrections, while translation zero modes lead to a much smaller correction $\sim \mathbb{L}^{-4}$ as equation (4.6) shows. As such, it will be neglected in what follows. Dilation and global gauge rotations lead to $\sim \mathbb{L}^{-2}$ as we discuss below.

For the dilation zero mode

$$A_\mu^{\rm a\ qu} \sim \eta_{a\mu\nu} x^\nu (1 + r^2)^{-2} \tag{4.7}$$

a similar formula reads

$$\kappa_{\rm dil.} \equiv \frac{\int_0^{\mathbb{L}} d^4x [A_\mu^{\rm a\ qu}(\nu)]^2}{\int_0^{\infty} d^4x [A_\mu^{\rm a\ qu}(\nu)]^2} \simeq \left[1 - \frac{3}{\mathbb{L}^2} + \mathcal{O}(\frac{1}{\mathbb{L}^4})\right], \tag{4.8}$$

such that the correction to the instanton density is proportional to $\sqrt{\kappa_{\rm dil.}} \simeq (1 - \frac{3}{2\mathbb{L}^2})$.

Computing the corresponding contribution due to three zero modes related to global gauge rotations requires much more refined analysis as explained in [77]. This is due to the specific features of the background dependent gauge $C_4 = \mathcal{D}_\mu A_\mu^{\rm a\ qu}$ when the corresponding three modes are pure gauge artifact. As shown in [77] the corresponding contribution is finite, but very sensitive to the infrared regularisation determined by the size R of large sphere. The corresponding contribution to the instanton density is $\sim (\lambda_4 V)^{3/2}$ where V is the four volume, while $\lambda_4 \sim V^{-1}$ is defined as follows

$$\begin{aligned} \lambda_4 &= \frac{\int_V d^4x [\psi_\mu^a(b)]^2}{\int_V d^4x [\psi^a(b)]^2}, \quad b = 1, 2, 3, \\ \psi^a(b) &= \eta_{a\mu\nu} \bar{\eta}_{b\mu\lambda} \frac{x^\nu x^\lambda}{(1 + x^2)}, \\ \psi_\mu^a(b) &= \mathcal{D}_\mu \psi^a(b) = \eta_{a\lambda\mu} \bar{\eta}_{b\lambda\nu} \frac{x^\nu}{(1 + x^2)^2}. \end{aligned} \tag{4.9}$$

The corresponding power like corrections can be computed in a similar manner to the other zero modes, except that we must retain the regularisation

since the denominator above diverges as $\sim V$. So we have the two correction factors

$$\kappa_{num.} \equiv \frac{\int_0^{\mathbb{L}} d^4x[\psi_\mu^a(b)]^2}{\int_0^{\infty} d^4x[\psi_\mu^a(b)]^2} \simeq \left[1 - \frac{3}{\mathbb{L}^2} + \mathcal{O}(\frac{1}{\mathbb{L}^4})\right],$$

and

$$\kappa_{den.} \equiv \frac{V(R)}{V(\mathbb{L})} \frac{\int_0^{\mathbb{L}} d^4x[\psi^a(b)]^2}{\int_0^{R} d^4x[\psi^a(b)]^2} \simeq \left[1 - \frac{4}{\mathbb{L}^2} + \mathcal{O}(\frac{1}{\mathbb{L}^4})\right].$$

The fraction, $V(R)/V(\mathbb{L})$, is the correction to V in the instanton density factor, and is included here so that we can take the regularisation $R \to \infty$. The combined gauge rotation correction factor is then

$$\kappa_{\text{rot.}} \equiv \frac{\kappa_{num.}}{\kappa_{den.}} \simeq \left[1 + \frac{1}{\mathbb{L}^2} + \mathcal{O}(\frac{1}{\mathbb{L}^4})\right], \tag{4.10}$$

such that the correction to the instanton density is proportional to $(\kappa_{\text{rot.}})^{3/2} \simeq (1 + \frac{3}{2\mathbb{L}^2})$. Accidentally, for $SU(2)$ gauge group the leading $\mathbb{L}^{-2}$ correction from the dilation (4.8) and global gauge rotations (4.10) exactly cancel each other. This accidental cancellation does not hold for general $SU(N)$ gauge group when power of $\kappa_{\text{rot.}}$ enters the instanton density with a different power.

We remark here that the technique used in [77] is essentially a variational approach wherein the boundary conditions are implemented implicitly rather than explicitly. It allows us to use all the zero modes (4.5),(4.7),(4.9) as well as standard classical instanton solution in the original form defined on $\mathbb{R}^4$ in which the conformal invariance is a symmetry of the system. So in this approach, neither the instanton itself, nor its zero modes (4.5),(4.7),(4.9) are solutions of the equation of motions which vanish at the boundary. This approach has been tested in many follow up papers, and we adopt it in the present work using the same technique in the next section. We also point out that the conformal invariance is explicitly broken in the one instanton sector by the size of the instanton ρ, such that corrections take the form $(\frac{\rho^2}{\mathbb{L}^2})^n$. It is restored by the integration $\int d\rho$. However, in this paper we are interested in by the computation in one instanton sector only when dimensional parameter ρ is explicitly present in the system, and is small and fixed, as it is in the deformed model discussed in chapters 2 and 3.

The important message here is that such kind of power correction do appear in general. The source of these corrections is a long range tail of zero modes. We can not derive a definite conclusion from these computations because the integral over large size instantons ($\int d\rho$) diverges and the semi-classical approximation breaks down. However, the same problem studied

in the deformed gauge theory model considered in Section 4.2.2 does not suffer from such deficiencies as semiclassical computations are under complete theoretical control. Thus, a Casimir like correction to the monopole fugacity ζ in this model is explicitly translated to the correction to the vacuum energy density and topological susceptibility (4.17), supporting (4.4) and in huge contrast with naive expectation (4.3). It is important to note that the source of the corrections in the deformed model is the same as in the undeformed QCD considered here, and that source is the long range tails of the zero modes, which lead to large distance sensitivity. The only difference is that the role of the instanton size ρ in computations above in the one instanton sector is played by the inverse monopole mass m_W^{-1} in the next section. Because it is a true scale of the problem however, m_W^{-1} is not integrated over as ρ is.

4.2.2 Casimir-Type Corrections for 3D Monopoles

We now turn to the deformed gauge theory described in chapters 2 and 3 wherein the low-energy behaviour is given by a $U(1)^N$ Coulomb gas of monopoles in Euclidean $\mathbb{R}^3$. Basically, we want to understand the dependence of the monopole fugacity, ζ, which comes out of the measure transformation to collective coordinates, on the size of the system, $\mathbb{L}$. In this case, as in the previous section, we consider the interior of a sphere of large but finite radius $\mathbb{L}$. There are four zero-modes present in this system: three translations since the monopoles are in $\mathbb{R}^3$, no dilations since the monopole size is fixed by the symmetry-breaking scale in this model m_W, and one gauge rotation since the gauge group for a given monopole is $U(1)$. As in [77], we work in a regular gauge to remain sensitive to the large distance physics. The monopole solution in the "hedgehog" regular gauge is given by

$$\begin{aligned} v_\mu^a(x) &= \epsilon_{\mu\nu a}\frac{x^\nu}{|x|^2}\left[1-\frac{m_W|x|}{\sinh(m_W|x|)}\right], \\ \phi^a(x) &= \frac{x^a}{|x|^2}\left[m_W|x|\coth(m_W|x|)-1\right], \end{aligned} \tag{4.11}$$

where we adapted notations from [19, 21] treating the monopole measure in supersymmetric Yang-Mills theory. In formula (4.11) v_μ^a denotes the three spacial gauge fields for the classical solution, and ϕ^a the gauge field in the compact time direction (the "Higgs" field in this model) when all fields can be combined in a single 4d field v_m.

We then want to compute the correction factors for the collective coordinate measure coming from these four zero modes when the system is defined

in a large but finite sphere. We closely follow 't Hooft's treatment [77] presented in the previous section 4.2.1. We start by considering the translation modes defined by the spacial derivative of the classical monopole solution (4.11) with respect to the collective coordinate position

$$Z_m^a(\nu) = -\partial_\nu v_m^a(x-z) + \mathcal{D}_m v_\nu^a = v_{m\nu}^a \tag{4.12}$$

where the minus sign is because $\partial/\partial z = -\partial/\partial x$ since z only enters as $x-z$, and $v_{m\nu}^a$ is the field strength since the covariant derivative is $\mathcal{D}_m = \partial_m - i\,[v_m, *]$. The second term on the right hand side of (4.12) is necessary to keep $Z_m^a(\nu)$ in the background gauge, see [19, 21] for more details.[8] This leads us to the following expression for correction factor due to the translation zero modes

$$\kappa_{\text{tr.}} \equiv \frac{\int_0^{\mathbb{L}} d^4x [Z_m^a(\nu)]^2}{\int_0^{\infty} d^4x [Z_m^a(\nu)]^2} \simeq \left[1 - \frac{1}{m_W \mathbb{L}} + \mathcal{O}(\frac{1}{\mathbb{L}^2})\right] \tag{4.13}$$

Next we consider the gauge rotation zero-mode. As in the previous section, the contribution to the collective coordinate measure, and so the monopole fugacity, is $\sim (\lambda V)^{\frac{1}{2}}$ where V is the three-volume and λ is given by

$$\begin{aligned} \lambda &= \frac{\int_V d^3x \left[B_\mu^a\right]^2}{\int_V d^3x [\phi^a]^2} \\ B_\mu^a &= \frac{1}{2}\epsilon_{\mu\nu\rho}\partial_\nu v_\rho^a = \mathcal{D}_\mu \phi^a. \end{aligned} \tag{4.14}$$

Again, the denominator diverges as $\sim V$ and we look at the two correction factors

$$\kappa_{\text{num.}} \equiv \frac{\int_0^{\mathbb{L}} d^3x [B_\mu^a]^2}{\int_0^{\infty} d^3x [B_\mu^a]^2} \simeq \left[1 - \frac{1}{m_W \mathbb{L}} + \mathcal{O}(\frac{1}{\mathbb{L}^2})\right],$$

and

$$\kappa_{\text{den.}} \equiv \frac{V(R)}{V(\mathbb{L})} \frac{\int_0^{\mathbb{L}} d^3x [\phi^a]^2}{\int_0^{R} d^3x [\phi^a]^2} \simeq \left[1 - \frac{3}{m_W \mathbb{L}} + \mathcal{O}(\frac{1}{\mathbb{L}^2})\right].$$

The total correction factor for the gauge rotation mode is then

$$\kappa_{\text{rot.}} \equiv \frac{\kappa_{\text{num.}}}{\kappa_{\text{den.}}} \simeq \left[1 + \frac{2}{m_W \mathbb{L}} + \mathcal{O}(\frac{1}{\mathbb{L}^2})\right], \tag{4.15}$$

[8] There is also a more extended (and careful) discussion of both the derivation of the "hedgehog" solution, (4.11), and this gauge transformation that must added to the simple derivatives with respect to the zero mode collective coordinates in order to satisfy the gauge condition, presented in Chapter 4 of [72].

and therefore the total correction to the monopole fugacity from the (4.14) is $\sqrt{\kappa_{\text{rot.}}} \simeq (1 + \frac{1}{\mathbb{L}})$. Assembling the total correction to the fugacity,

$$\kappa_{\text{tr.}}^{3/2}\kappa_{\text{rot.}}^{1/2} \simeq \left[1 - \frac{1}{2m_W\mathbb{L}} + \mathcal{O}(\frac{1}{\mathbb{L}^2})\right]. \tag{4.16}$$

Thus, the deformed gauge theory, when put on a manifold with a boundary, receives some corrections to the monopole fugacity compared to Minkowski space that are power-like in the manifold size. The correction (4.16) to the monopole fugacity leads immediately to the same correction to the topological susceptibility and so the background energy density since, as we saw in the previous chapter,

$$\begin{aligned} E_{\text{YM}}(\theta) &= -\frac{N_c\zeta}{L}\cos\left(\frac{\theta}{N_c}\right), \\ \chi_{YM}(\theta = 0) &= \left.\frac{\partial^2 E_{\text{YM}}(\theta)}{\partial\theta^2}\right|_{\theta=0} = \frac{\zeta}{N_c L}. \end{aligned} \tag{4.17}$$

Here we considered only the lowest branch from (2.37) at $\theta = 0$ for simplicity. To be more precise,

$$\zeta(\mathbb{L}) = \zeta \cdot \left[1 - \frac{1}{2m_W\mathbb{L}} + \mathcal{O}(\frac{1}{\mathbb{L}^2})\right], \tag{4.18}$$

where ζ is the monopole fugacity which enters the relation (4.17) computed in infinite Minkowski space. We emphasise that the energy density changes in the bulk of space-time, not only in the vicinity of the boundaries, similar to the Casimir effect when the bulk energy density changes as a result of merely presence of the boundary. To reiterate, the deformed model, despite the presence of a mass gap, displays a surprising Casimir-like sensitivity to large distance boundaries, such that the energy density differs from the Minkowski space value by $\Delta E \sim \frac{1}{m_W\mathbb{L}}$. Again, this is in contrast to the naive expectation based on analysing the physical degrees of freedom, $\Delta E \sim e^{-m\mathbb{L}}$ with $m \sim m_\sigma$ being the lowest mass scale of the problem (4.3).

4.2.3 Non-Zero Mode Contributions

Computations of the Casimir corrections presented in the previous section were based on an analysis of the zero modes when the corresponding normalisation factor explicitly enters the instanton/monopole density. Now, we want to present some arguments suggesting that corrections due to the non-zero mode contributions can be neglected, and, therefore, cannot cancel the

zero modes contribution. Indeed, the computation of non-zero mode contribution is reduced to an analysis of the phase shifts in the scattering matrix which can not change the normalisation of the wave function itself. The only changes that occur are phase shifts. Furthermore, an absolute normalisation is dropped from the final formula for the instanton/monopole density when the ratio of the eigenvalues is considered. This argument is consistent with observation that non-zero mode contribution depends on matter context of the theory as it varies when massive scalar of spinor fields in different representations are part of the consideration. At the same time, the Casimir type corrections computed above are exclusively due to the gauge portion of the theory, not its matter context. Indeed, these Casimir corrections were derived in pure gluodynamics. So, it is difficult to imagine how a Casimir correction to a non-zero mode contribution (even if it is nonzero) might cancel a Casimir type correction originating from an analysis of gauge zero modes.

We also comment that the correction $\mathbb{L}^{-1}$ occurs as a manifestation of a slow power like decay of the zero modes in the background of a topologically nontrivial gauge configuration. It should be contrasted with conventional behaviour of zero modes with a mass gap present in the system from the very beginning (for example, the well studied problem of a double well potential). In former case, the zero modes decay according to a power law leading to the Casimir type correction, while in the later case, the zero modes are well localised configurations which decay exponentially fast at large distances and can not be sensitive to large distance physics. The mass gap is present for all physical degrees of freedom in both models. However, in the former case the mass gap emerges as a result of the same instanton/monopole dynamics, while in the later a mass gap was present in the system from the very beginning and it was not associated with any instanton/monopole dynamics. QCD obviously belongs to the former case, and we therefore expect this effect will persist in real strongly coupled QCD.

Next, our computations of the Casimir correction to the instanton/ monopole density are based on assumption of the dilute gas approximation. This is enforced in Section 4.2.1 by a finite instanton size ρ which is kept fixed and small. On other hand, the semiclassical approximation in Section 4.2.2 is automatically justified due to the parametrically small fugacity ζ, and total neutrality in this system is automatically achieved as long as the size of the system $\mathbb{L}$ is much larger than the Debye screening length m_σ^{-1}, see (3.25). In other words, we assume $\mathbb{L} \gg m_\sigma^{-1}$ such that neutrality of the system is automatically satisfied with exponential accuracy. The finite size of the manifold does not spoil this neutrality if condition $\mathbb{L} \gg m_\sigma^{-1}$ is satisfied.

Furthermore, the computation of the monopole's fugacity ζ and corresponding corrections (4.18) can be performed without taking into account of the interaction of a monopole with other particles from the system as it would correspond to higher order corrections in density expansion $\sim \zeta^2$. This is precisely the procedure which was followed in the original computations by Polyakov in [58] and in the deformed model in [85] at weak coupling.

Also, we emphasise that in the variational approach developed in [77] neither the classical solution nor the corresponding zero modes vanish at the boundary of a finite size manifold. The constraints related to the finite size $\mathbb{L}$ of the manifolds are accounted for implicitly rather than explicitly in this approach. In particular, one should not explicitly cut off the classical action of the configuration as a result of finite size $\mathbb{L}$ in which the instanton/monopole is defined as this contribution is implicitly taken into account by the variational approach. However, even if we use an explicit cutoff for classical solution it still cannot cancel the zero mode corrections as these terms have different behaviour in N. The correction to the classical solution would be one and the same for any N, while corrections due to zero modes depend on N as the correction (4.15) counts number of gauge rotations for $SU(N)$ gauge theory.

Finally, it is quite possible that we overlooked some other possible corrections (for example, some corrections due to the boundaries which may occur in the vicinity of these boundaries). We emphasise that our main result is not the computation of a specific coefficient in front of the correction to fugacity in equation (4.18). Rather, our main point is that these types of corrections do occur in a system with a gap, and it is very difficult to imagine that some boundary corrections might mysteriously cancel these computed bulk corrections. Therefore, we next present some arguments and examples suggesting that a Casimir type behaviour in gauge theories is in fact quite generic, rather than a peculiar feature of our choice of system.

4.3 Topological Sectors and the Casimir Correction in QCD

In this section we want to present few generic arguments suggesting that the emergence of a Casimir-like behaviour is not an accident, and not a computational peculiarity. Rather, the effect has a deep theoretical roots as argued in [103]. We review these arguments starting with analogy with the well known Aharonov-Casher effect as formulated in [63]. The relevant part of that work can be stated as follows. If one inserts an external charge

into superconductor wherein the electric field is exponentially suppressed $\sim \exp(-r/\lambda)$ with λ being the penetration depth, a neutral magnetic fluxon will be still sensitive to an inserted external charge at arbitrary large distance. The effect is purely topological and non-local in nature. The crucial point is that this phenomenon occurs, in spite of the fact that the system is gapped, due to the presence of different topological states in the system. We do not have a luxury of solving a similar problem in strongly coupled four dimensional QCD analytically. However, one can argue that the role of the "modular operator" of [63], which is the key element in the demonstration of long range order, is played by the large gauge transformation operator $\mathcal{T}$ in QCD, which also commutes with the Hamiltonian $[\mathcal{T}, H] = 0$, such that our system must be transparent to topologically nontrivial pure gauge configurations, similar to the transparency of the superconductor to the "modular electric field", see [103] for the details.

We interpret the computational results in a number of systems where Casimir like corrections have been established as a manifestation of the same physics which can be described in terms of the operator $\mathcal{T}$. We should mention that there are a few other systems, such as topological insulators, where a topological long range order emerges in spite of the presence of a gap in the system.

There are a number of simple systems in which the Casimir type behaviour $\Delta E \sim \mathbb{L}^{-1} + \mathcal{O}(\mathbb{L})^{-2}$ has been explicitly computed. In all known cases this behaviour emerges from non-dispersive contributions such that the dispersion relations do not dictate the scaling properties of this term.

The first example is an explicit computation [86] in exactly solvable two-dimensional QED defined in a box size $\mathbb{L}$. The model has all elements crucial for present work: non-dispersive contact term which emerges due to the topological sectors of the theory. This model is known to be a theory of a single physical massive field. Still, one can explicitly compute $\Delta E \sim \mathbb{L}^{-1}$ in contrast with naively expected exponential suppression, $\Delta E \sim e^{-\mathbb{L}}$. Another piece of support for a power like behaviour is an explicit computation in a simple case of Rindler space-time in four dimensional QCD [55, 100, 102] where Casimir like correction have been computed using the unphysical Veneziano ghost which effectively describes the dynamics of the topological sectors and the contact term when the background is slightly modified. Thus, power-like behaviour is not a specific feature of two dimensional physics.

Our next example is 2d CP^{N-1} model formulated on finite interval with size $\mathbb{L}$ [53]. In this case one can explicitly see emergence of $\Delta E \sim \mathbb{L}^{-1}$ in large N limit in close analogy to our case (4.18) where a theory has a

gap, but nevertheless, exhibits the power like corrections. The correction computed in [53] also comes from a non-dispersive contribution which can not be associated with any physical propagating degrees of freedom, similar to our case (4.18).

Power like behaviour $\Delta E \sim \mathbb{L}^{-1}$ is also supported by recent lattice results [36]. The approach advocated in [36] is based on physical Coulomb gauge, in which nontrivial topological structure of the gauge fields is represented by the so-called Gribov copies leading to a strong infrared singularity. Thus, the same Casimir-like scaling emerges in a different framework where the unphysical Veneziano ghost (used in [55, 100, 102]) is not even mentioned.

The very same conclusion also follows from the holographic description of the contact term presented in [103]. The key element for this conclusion follows from the fact that the contact term in holographic description is determined by massless Ramond-Ramond (RR) gauge field defined in the bulk of 5-dimensional space. Therefore, it is quite natural to expect that massless R-R field in holographic description leads to power like corrections when the background is slightly modified.

To avoid any confusion with terminology we follow [103] and call this effect as "Topological Casimir Effect" where no massless degrees of freedom are present in the system, but nevertheless, the system itself is sensitive to arbitrary large distances. It is very different from conventional Casimir effect where physical massless physical photons are responsible for power like behaviour. From the holographic viewpoint discussed in [103] the "Topological Casimir Effect" in our physical space-time can be thought as conventional Casimir effect in multidimensional space when massless propagating R-R field in the bulk is responsible for this type of behaviour, although this field is not a physical asymptotic state in our four dimensional world.

4.4 Comments

We tested a sensitivity of the deformed gauge theory model with non-trivial topological features to arbitrary large distances. A naive expectation based on dispersion relations dictates that a sensitivity to very large distances must be exponentially suppressed (4.3) when a mass gap is present in the system. However, we argued that along with conventional dispersive contribution there exists a non-dispersive contribution, not related to any physical propagating degrees of freedom. This non-dispersive (contact) term with the "wrong sign" emerges as a result of topologically nontrivial sectors, and can

be explicitly computed in our model. The variation of this contact term with variation of the background leads to a power like "Topological Casimir Effect" (4.4) in accordance with the arguments presented in Section 4.3 and in contrast with the naively expected exponential suppression (4.3).

The Topological Casimir Effect in QCD, if confirmed by future analytical and numerical studies, may have profound consequences for understanding of the expanding FLRW universe we live in. We already mentioned in Section 4.1 that the observed cosmological dark energy (4.1) may is fact be just a manifestation of this Topological Casimir Effect without adjusting any parameters. In the adiabatic approximation the universe expansion can be modeled as a slow process in which the size of the system adiabatically depends on time $\mathbb{L}(t)$ which leads to extra energy as equations (4.4) and (4.18) suggest. Such a model is obviously consistent with observations if $\mathbb{L}(t)$ is sufficiently large [87]. We do not insist that this is the model of our universe. Rather, we claim that if the effect persists in strongly coupled QCD, the energy density which can not be identified with any physical propagating degrees of freedom, is sensitive to arbitrary large distances as a result of nontrivial topological features of QCD. Different geometries (such as an FLRW universe) obviously would lead to different coefficients. Nonetheless, the important message from these computations in our simplified model is that the energy density in the bulk is sensitive to arbitrary large distances comparable with the visible size of the universe, and that this sensitivity comes not from any new physics but simply from the proper treatment of the topological structure of QCD.

We should mention, also, that with regard to extending from imposed boundaries in flat space, as we considered here, to effective boundary conditions due to curvature, the nontrivial holonomy along the compact (S^1) dimension is an important aspect of this model that warrants consideration. Mainly, there is no contradiction with the conventional argument that only a curvature $R \sim H^2$ should enter the bulk energy density in such an analysis on a curved (FLRW) manifold. This is because $\oint A_\mu dx^\mu$ around the compact dimension is an invariant characteristic of the system which cannot be reduced to the curvature, similar to the Aharonov-Bohm effect, where the relevant phenomenon is expressed in terms of the potential A_μ rather than the field strength $F_{\mu\nu}$. Essentially, this is just the statement that the effect is due to topological properties not local field configurations. For more on the topic of nontrivial holonomy and calculations in curved space see [107].

Finally, we add that a comprehensive phenomenological analysis based on this idea has been recently performed in [12] where comparison with

current observational data including SnIa, BAO, CMB, BBN has been presented, see also [13, 27, 55, 65, 66, 71] with related discussions. The conclusion was that the model (4.1) is consistent with all presently available data, and we refer to these papers on analysis of the observational data.

Chapter 5

Long Range Order and Domain Walls

This chapter reproduces the work presented in [81]. We consider the interaction between extended two dimensional domain walls and localised point-like topological monopoles. The domain walls considered here are topological defects that interpolate between the vacuum state and itself, essentially just a winding.

5.1 Motivation

The main motivation for the work presented in this chapter is the recent Monte Carlo studies in pure glue gauge theory which have revealed some very unusual features. To be more specific, the relevant gauge configurations display a laminar structure in the vacuum consisting of extended, thin, coherent, locally low-dimensional sheets of topological charge embedded in 4d space, with opposite sign sheets interleaved, see the original lattice QCD results [3, 37–39]. A similar structure has been also observed in lattice QCD by different groups [10, 11, 40, 41, 49] and also in a two dimensional CP^{N-1} model [1]. Furthermore, the studies of localisation properties of Dirac eigenmodes have also shown evidence for the delocalisation of low-lying modes on effectively low-dimensional surfaces. The following is a list of the key properties of these gauge configurations which we wish to study:

1) The tension of the "low dimensional objects" vanishes below the critical temperature and these objects percolate through the vacuum, forming a kind of a vacuum condensate;

2) These "objects" do not percolate through the whole 4d volume, but rather, lie on low dimensional surfaces $1 \leq d < 4$ which organise a coherent double layer structure;

3) The total area of the surfaces is dominated by a single percolating cluster of "low dimensional object";

4) The contribution of the percolating objects to the topological susceptibility has the same sign compared to its total value;

5) The width of the percolating objects apparently vanishes in the continuum limit;

6) The density of well localised 4d objects (such as small size instantons) apparently vanishes in the continuum limit.

It is very difficult to understand the above properties using conventional quantum field theory analysis. Indeed, the QCD lattice results [3, 10, 37–41, 49] imply that the topological density distribution is not localised in any finite size configurations such as instantons; rather the topological density is spread out on the surface of low-dimensional sheets. Such a structure can not be immediately seen in gluodynamics, at least not at the semiclassical level. At the same time, these Monte Carlo results could be interpreted very nicely with a conjecture that the observed structure is identified with the extended D2 branes in a holographic description[30, 31, 103].

One of the key elements of this conjecture is assumption that the tension of the D2 branes vanishes below the QCD phase transition $T < T_c$ such that an arbitrarily large number of these objects can be formed. The second key element in identification of the structure observed on the lattice [3, 10, 37–41, 49] with the holographic description in terms of the D branes is the assumption that the topological density distribution which is originally localised in well defined D0 branes (instantons), somehow spreads out along extended D2 branes as a result of the interaction between D0-D2 branes, leading to their binding. Such a picture was basically motivated, as mentioned in [31, 103], by the structure which emerges in supersymmetric field theories [20] where the relevant dynamics can be indeed formulated in terms of the strongly bound D0-D2 configurations.

In this chapter, we investigate precisely the second idea above in the framework of the "deformed gauge theory" developed in [85] and discussed in Chapter 2. The deformation allows us to bring the gauge theory into a weakly coupled regime wherein calculations can be performed in theoretically controllable manner. In spite of the great deal of analytic control provided, the deformed theory preserves many of the relevant structures present in strongly coupled QCD including confinement, degeneracy of topological sectors, and the correct nontrivial θ dependence. Furthermore, it seems, there is no order parameter differentiating the weakly coupled deformed regime from the strongly coupled regime, which reproduces undeformed QCD [85], so that the qualitative behaviour of the two theories may be quite similar.

In particular, the deformed theory exhibits two important structures of

note: first, the topological charge in this model is carried by the fractionally charged monopoles with topological charges $Q = \pm 1/N$; and second, there are domain walls present in the system as a result of a generic 2π periodicity of the effective low energy Lagrangian governing the dynamics. Given these ingredients, we would like to test the following two ideas which are apparently related to the configurations observed in the lattice simulations [3, 10, 37–41, 49]:

1) the domain walls form precisely a double layer structure with opposite sign sheets of the topological charge density interleaved;

2) the monopoles and domain walls attract each other and the topological charge originally localised on monopoles spreads out along the domain walls.

If the second occurs, there will be few well-localised finite sized sources carrying the topological charge. Instead, the topological charge density will be spread over extended domain walls, which is precisely the pattern that has been observed in simulations [3, 10, 37–41, 49]. For other discussions related to long range order in this model see [4, 106].

We note that a similar picture of attraction between monopoles and domain walls was originally discussed in a cosmological context [23], see also the related papers [2, 22, 24] and references therein. The basic idea there is that if physical monopoles and domain walls are present in the system, there will be an attractive force between them. Then, if these objects collide, the monopole's winding number (monopole charge) spreads out on the surface of the domain wall, and will be eventually pushed to the boundaries at infinity. This effect was suggested as a solution of the so-called "cosmological monopole problem". In our context we do not have real physical monopoles and real physical domain walls in Minkowski space, but rather Euclidean monopoles and domain walls which must be interpreted as configurations describing the tunnelling processes in physical Minkowski space, see [103] for a detailed discussion of this point. Nevertheless, the formal structure of the problem and relevant features (such as attraction between the objects and spreading the magnetic charge over the surface) are very much the same.

The structure of our presentation is as follows. In Section 5.2, we construct the domain walls and explicitly demonstrate the double layer structure apparently observed on the lattices. Then, in Section 5.3 we study the interaction of the domain walls and monopoles. And, finally, in Section 5.4 we comment on the important aspects of these results.

5.2 Domain Walls in Deformed Gauge Theory

In the deformed theory there is a discrete set of degenerate vacuum states as a result of the 2π periodicity of the effective Lagrangian (2.36) for the $\boldsymbol{\sigma}$ fields, and thus there exist domain wall configurations interpolating between these states. The corresponding configurations are not however conventional domain walls similar to the well known ferromagnetic domain walls in condensed matter physics which interpolate between physically distinct vacuum states. Here, instead, the corresponding configuration interpolates between topologically different but physically equivalent winding states $|n\rangle$, which are connected to each other by a large gauge transformation. Therefore, the corresponding domain wall configurations in Euclidean space are interpreted as configurations describing tunnelling processes in Minkowski space, similar to Euclidean monopoles which also interpolate between topologically different, but physically identical states. This interpretation should be contrasted with the conventional interpretation of static domain walls defined in Minkowski space when the corresponding solution interpolates between physically distinct states.

In fact, a similar domain wall which has an analogous interpretation is known to exist in QCD at high temperature (in the weak coupling regime) where it can be described in terms of classical equations of motion. These are the so-called Z_N domain walls which separate domains characterised by a different value for the Polyakov loop at high temperature. As is known, see the review papers [29, 75] and references therein, these Z_N domain walls interpolate between topologically different but physically identical states connected by large gauge transformations similar to our case. These objects can be described in terms of classical equation of motion and have finite tension $\sim T^3$ such that their contribution to path integral is strongly suppressed. While the corresponding topological sectors are still present in the system at low temperature (though they are realised in a different way) it is not known how to describe the fate of these Z_N walls in QCD in the strong coupling regime where the semiclassical approximation breaks down.

The domain walls to be discussed below in the deformed model are very much the same as Z_N domain walls at high temperature and their contribution to path integral is also strongly suppressed as their tension is finite in the weak coupling regime. Nevertheless, one can study the structure of these domain walls, as well as their interaction with dynamical magnetic monopoles. Furthermore, as we discussed in Section 5.1 the domain wall structure is apparently observed in the lattice simulations, which imply that

they may have effectively vanishing tension at low temperature. We conjecture that the domain walls we describe below in the weak coupling regime in the deformed model slowly become the objects (with effectively vanishing tension) which are observed in lattice simulations [3, 10, 37–41, 49] in the strong coupling regime, as we adiabatically increase the coupling constant without hitting the phase transition as argued in [85]. This portion of the theory can not be tested in the deformed model in the semiclassical approximation, but hopefully this portion of strongly coupled dynamics can be understood in the future using different techniques, such as the dual holographic description as advocated in the present context in [103].

5.2.1 Domain Wall Solution

There are a few different types of domain walls supported by the system (2.36) which have different physical meanings. Here we focus on the discrete symmetry of the effective Lagrangian (2.36)

$$S_{\rm dual} \to \int_{\mathbb{R}^3} \left[\frac{1}{2L} \left(\frac{g}{2\pi} \right)^2 (\nabla \boldsymbol{\sigma})^2 - \zeta \sum_{a=1}^{N} \cos \left(\alpha_a \cdot \boldsymbol{\sigma} + \frac{\theta}{N} \right) \right].$$

given by the 2π shift, $\sigma_a \to \sigma_a + 2\pi$, where any component of $\boldsymbol{\sigma}$ field can be shifted by 2π independently. To simplify analysis, we consider a single specific non-vanishing component for the $\boldsymbol{\sigma}$ field sitting at $a-$th position,

$$\boldsymbol{\sigma} = \Big(0, 0, \sigma^{(a)}, 0, \ldots, 0\Big) \quad a = 1, ...N. \tag{5.1}$$

This component describes a specific diagonal element of the original non-Abelian field strength. For example, $\chi^{(1)}$ corresponds to the following structure in conventional matrix notations

$$\mathbf{B}^{(1)} = \frac{g}{2\pi L} \nabla \sigma^{(1)} \cdot \begin{pmatrix} 1 & 0 & ... & 0 \\ 0 & -1 & ... & 0 \\ ... & ... & ... & 0 \\ 0 & 0 & 0 & 0 \end{pmatrix}. \tag{5.2}$$

There are N different domain wall types similar to the monopole case since classification of our system is based on $\alpha_i \in \Delta_{\rm aff}$. We emphasise that there are only $(N-1)$ physical propagating photons in the system as one scalar singlet field, though it remains massless, completely decouples from the system, and does not interact with other components at all, as we saw in Chapter 2. As a result of this structure, a configuration with N different types of

magnetic monopoles will carry zero magnetic charge and one unit of the topological charge $Q = 1$ as each monopole carries $Q = 1/N$ topological charge. The corresponding configuration can be identified with a conventional instanton with $Q = 1$ which is made of N constituents. A similar comment also applies to the domain wall structure: a configuration with N different types of domain walls on top of each other will produce a trivial vacuum configuration as the Abelian components of the magnetic field will cancel each other, similar to the magnetic monopole construction. Thus, although there are N different types of the domain walls in our construction, only $(N-1)$ of them are independent exactly as with the monopoles.

In what follows, without loss of generality, we consider the $N = 2$ case. In this case there is only one physical field $\chi = (\sigma_1 - \sigma_2)$ which corresponds to a single diagonal component from the original $SU(2)$ gauge group. The orthogonal combination $(\sigma_1 + \sigma_2)$ decouples from the system as explained in the original paper [85] and can be seen immediately in this situation. The action (2.36) becomes,

$$S_\chi = \int_{\mathbb{R}^3} d^3x \frac{1}{4L} \left(\frac{g}{2\pi}\right)^2 (\nabla\chi)^2 - \zeta \int_{\mathbb{R}^3} d^3x \left[\cos\left(\chi + \frac{\theta}{2}\right) + \cos\left(-\chi + \frac{\theta}{2}\right)\right]. \quad (5.3)$$

In terms of the χ field, the classical equation of motion which follows from (5.3) and which determines the profile of the domain wall has the form

$$\nabla^2\chi - m_\chi^2 \sin\chi = 0, \quad (5.4)$$

where we take $\theta = 0$ for simplicity, and the mass of χ field $m_\chi = 2m_\sigma$ is related to the Debye correlation length (2.41). The solution of this sine-Gordon equation which interpolates in one direction centered at the origin between $\chi(z = -\infty) = 0$ and $\chi(z = +\infty) = 2\pi$, and which is centered at $z_0 = 0$ being independent of x, y coordinates is well known

$$\chi(z) = 4 \arctan\left[\exp(m_\chi z)\right]. \quad (5.5)$$

We are now in position to explain the physical meaning of this solution. As we mentioned before, this domain wall solution (5.5) does not describe a physical domain wall which interpolates between physically distinct vacuum states, but rather interpolates between topologically different but physically identical states. We remark that a similar construction has been considered previously in relation to the so-called $N = 1$ axion model [33, 92], more

recently in the QCD context in [28], and in high density QCD in [76]. In the previously considered cases [28, 33, 76, 92] as well as in present case (5.5) there is a single physical unique vacuum state, and interpolation (5.5) corresponds to the transition from one to the same physical state. Therefore, such domain walls are not stable objects, but will decay quantum mechanically, see Appendix A for corresponding estimates. Nevertheless, if life time of the configuration (5.5) is sufficiently large, it can be treated as stable classical background, and it can be used to study the interaction of domain walls with monopoles, which is one of the main objectives of present work, see Figure 5.1 depicting the transition between two topologically different paths corresponding to the decay of some domain wall state to a domain wall free ground state. The path wrapping the peg represents a state with some domain walls, while the path that does not denotes a state with no domain walls. We can deform the domain wall path by lifting it over the obstacle so that we can unwind it and deform it into the domain wall free path. If the path describes domain walls with some weight, then it would require some energy to lift over the obstacle. If this energy is not available, then classically, the configurations that wind around the peg are stable. Quantum mechanically, however, the domain wall could still tunnel through the peg, and so the configurations are unstable quantum mechanically, see the estimate for this probability in Appendix A.

One can view these "additional" vacuum states, which are physically identical states and which have extra 2π phase in operator (2.39), as an analog to the Aharonov-Bohm effect with integer magnetic fluxes where electrons do not distinguish integer fluxes from identically zero flux. Our domain wall solution (5.5) describes interpolation between these two physically identical states. Finally, we should also comment that, formally, a similar soliton-like solution which follows from the action (5.3) appears in the computation of the string tension in Polyakov's 3d model [58, 85]. The solution considered there emerges as a result of the insertion of external sources in a course of computing the vacuum expectation of the Wilson loop. In contrast, in our case, the solution (5.5) is an internal part of the system without any external sources. Furthermore, the physical meaning of these solutions are fundamentally different. In our case the interpretation of the solution (5.5) is similar to an instanton describing the tunnelling processes in Minkowski space, while in the computations [58, 85] it was an auxiliary object which appears in the computation of the string tension.

The width of the domain wall is determined by m_χ^{-1}, while the domain

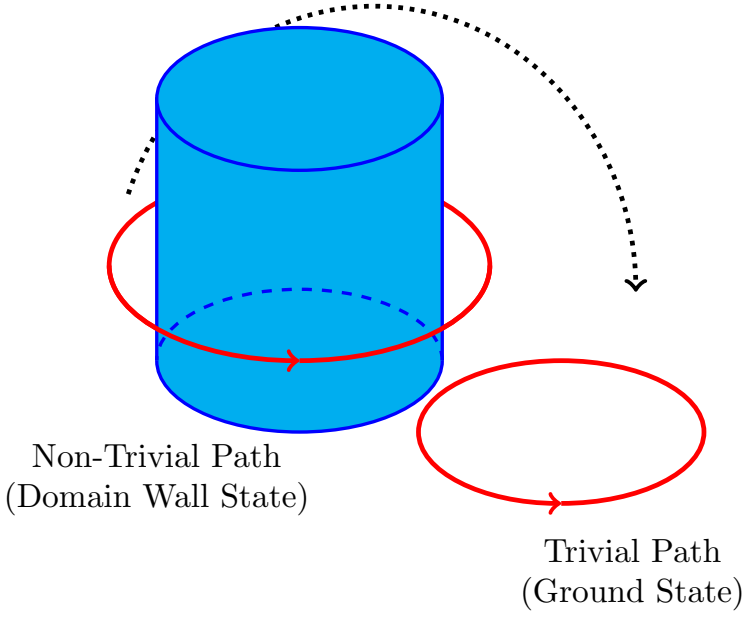

Figure 5.1: Picture depicting the transition between paths corresponding to the decay of some domain wall state to a domain wall free ground state. Inspired by a similar picture in [28].

wall tension σ for the profile (5.5) can be computed and is given by

$$\begin{aligned} \sigma &= 2 \cdot \int_{-\infty}^{+\infty} dz \frac{1}{4L^2} \left(\frac{g}{2\pi}\right)^2 (\nabla\chi)^2 \\ &= \frac{m_\chi}{L^2} \left(\frac{g}{2\pi}\right)^2 \sim \sqrt{\frac{\zeta}{L^3}}. \end{aligned} \tag{5.6}$$

In the deformed model, the topological charge density distribution (2.11)

can be written as

$$\begin{aligned} q(\mathbf{x}) &= \frac{1}{16\pi^2}\mathrm{tr}\left[F_{\mu\nu}\tilde{F}^{\mu\nu}\right] = \frac{-1}{8\pi^2}\epsilon^{ijk4}\sum_{a=1}^{N} F_{jk}^{(a)}F_{i4}^{(a)} \\ &= \frac{g}{4\pi^2}\sum_{a=1}^{N}\left\langle A_4^{(a)}\right\rangle\left[\nabla\cdot\mathbf{B}^{(a)}(\mathbf{x})\right], \end{aligned} \tag{5.7}$$

where the $U(1)^N$ magnetic field, $B^i = \epsilon^{ijk4}F_{jk}/2g$ is expressed in terms of the scalar magnetic potential as

$$F_{ij}^{(a)} = \frac{g^2}{2\pi L}\epsilon_{ijk}\partial^k\sigma^{(a)}, \qquad \mathbf{B}^{(a)} = \frac{g}{2\pi L}\nabla\sigma^{(a)}. \tag{5.8}$$

In the last step of (5.7) we have replaced the field in the compact direction by it's vacuum expectation value since we are considering a semiclassical approximation.

With the explicit solution at hand (5.5), the magnetic field distribution (5.8) for the domain wall is given by

$$B_z = \left(\frac{g}{4\pi L}\right)\frac{4m_\chi}{(e^{m_\chi z}+e^{-m_\chi z})}, \tag{5.9}$$

and the topological density can then be computed using formula (5.7) with the following result

$$q(z) = \frac{\zeta}{L}\sin\chi = \frac{4\zeta}{L}\frac{(e^{m_\chi z}-e^{-m_\chi z})}{(e^{m_\chi z}+e^{-m_\chi z})^2}. \tag{5.10}$$

From equation (5.10), we see that the net topological charge $Q \sim \int dz\, q(z)$ on the domain wall vanishes. However, the charge density has an interesting distribution; it is organised in a double layer structure, which is precisely what apparently has been measured in the lattice simulations mentioned earlier [3, 37–39]. For a graphical depiction see Figure 5.2 which is a 3d rendering of the domain wall solution (5.5). The same double layer structure can be seen by computing the magnetic charge density ρ_M which is defined as

$$\begin{aligned} \rho_M^{(a)} &\equiv \left[\nabla\cdot\mathbf{B}^{(a)}(\mathbf{x})\right] = \left(\frac{g}{4\pi L}\right)\frac{\partial^2\chi}{\partial z^2} \\ &= 4\zeta\cdot\left(\frac{4\pi}{g}\right)\frac{(e^{m_\sigma z}-e^{-m_\sigma z})}{(e^{m_\sigma z}+e^{-m_\sigma z})^2}. \end{aligned} \tag{5.11}$$

Thus, the relation between the topological charge density (5.10) and magnetic charge density (5.11) holds for the domain wall

$$q(z) = \left(\frac{g}{2\pi}\right) \cdot \left(\frac{1}{LN}\right) \cdot \rho_M(z) \tag{5.12}$$

in agreement with the general expression (5.7).

From eqs. (5.10), (5.11), we see that an average density of magnetic monopoles filling the interior of domain wall is expressed in terms of the same parameter ζ which characterises the average monopole's density in the system (2.36). One can interpret this relation as a hint that the topological charge sources have a tendency to reside in vicinity of the domain walls rather than being uniformly distributed. We further elaborate on this matter in Section 5.3.

It is interesting to note that the domain walls in the deformed model are very similar (algebraically) to well known domain walls studied previously in some SUSY models, see the review article [82]. Of course, there are fundamental differences between the two: in SUSY models the domain walls interpolate between physically distinct vacuum states, in contrast with our domain walls which correspond to interpolation between topologically different but physically identical states. Therefore, the interpretation in these two cases is fundamentally different: in SUSY models the domain walls are real physical objects, while in our deformed model they should be interpreted similar to instantons, objects which describe the tunnelling processes, see [103] for more comments on this interpretation. Furthermore, the classification of the domain walls in SUSY models is based on the flavour group symmetry breaking $SU(N_F) \to U(1)^{N_F-1}$, in contrast with colour symmetry breaking we consider here. However, the formal classification of the domain walls in SUSY models based on simple roots from the flavour group is very much the same as classification in our case based on $SU(N) \to U(1)^{N-1}$ breaking pattern, see equations (2.9) and (2.10). These similarities include, in particular, highly nontrivial properties such as ordering of the domain walls or their passing through each other. However, these questions will not be elaborated on in the present work.

The most important lesson from this analysis is that the double layer structure naturally emerges in the construction of the domain walls in the weak coupling regime in deformed gauge theory. As claimed in [85] the transition from the high temperature weak coupling regime to the low temperature strong coupling regime should be smooth without encountering any phase transitions on the way. Therefore, it seems reasonable to identify the

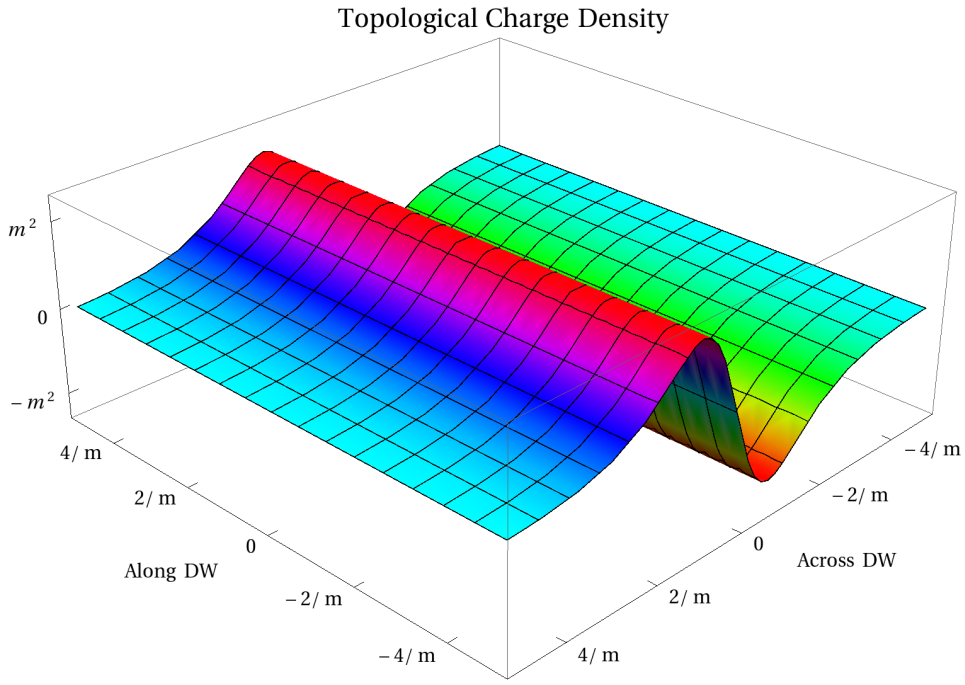

Figure 5.2: Graph showing the two layer structure of the topological charge density plotted against one direction across the Domain Wall and the other one of the two dimensions along it.

double layer structure found in this work (5.10) with the double layer structure from lattice measurements [3, 37–39] when one slowly moves along a smooth path from the weak coupling to the strong coupling regime.

5.3 Domain Wall - Monopole Interaction

From expressions (2.39) and (5.1) one can infer that the interaction, or to be more precise, the algebraic structure, of the domain wall with monopoles is very similar to monopole - monopole/antimonopole interactions. Since our domain walls are not dynamical configurations of the system, but rather, should be treated as a background classical fields, we can not address some hard fundamentally quantum issues such as: what the density of domain

wall configurations looks like, or why the topological charge density is mostly spread out in the domain walls rather than in localised objects, similar to the pattern lattice simulations suggest [3, 37–39]. Rather we can formulate a different question which can be addressed in the weak coupling regime. What happens to the monopoles if they are formed in the presence of the domain walls? As the number of different types of domain walls, N, is equal to the number of different types of monopoles, one could assume that a specific monopole type "a" will find a corresponding most attractive domain wall. Therefore, we concentrate below on analysis of a specific configuration containing two relevant elements: a domain wall of type (5.2) and a nearby anti-monopole with magnetic charge $-\alpha_1$ and topological charge $Q = -1/N$.

We now consider the domain wall configurations discussed in the previous section interacting with monopole configurations. In these computations the domain walls are treated as classical background fields, and as such we do not consider fundamentally quantum questions, such as the density of domain walls. Instead, we consider some questions which can be answered in the semiclassical context. We focus on the interaction between a monopole and domain wall, each acting as magnetic sources, and compute the energy of the configuration as a function of separation distance between the two. Therefore, the question we are addressing is where would a point charge prefer to sit in the presence of our domain wall? As stated in Section 5.1, this question is motivated by lattice simulations [3, 37–39] which suggest that the density of well localised 4d objects (such as small size 4d instantons) apparently vanishes. We should emphasise that our domain walls should not be thought of as empty objects, but should instead be thought of as already filled by magnetic monopoles with density determined by (5.10). Indeed, as discussed back in Section 2.3, the sigma fields are a dual description for a monopole gas model, so any configuration of sigma fields can be thought of as some distribution of monopoles.

Again, we consider the simplified scenario of $SU(2)$, which corresponds to considering the interaction between a single type of domain wall, a, and a monopole of the same type, or to be more precise an antimonopole so that the magnetic charge is $-\alpha_a$. The domain wall is defined as previously, (5.5), but centered at a distance z_0 from the origin, so that the magnetic scalar potential is given by (letting $m = m_\chi$)

$$\chi_{z_0}(\mathbf{x}) = 4 \arctan\left[e^{m(z-z_0)}\right]. \tag{5.13}$$

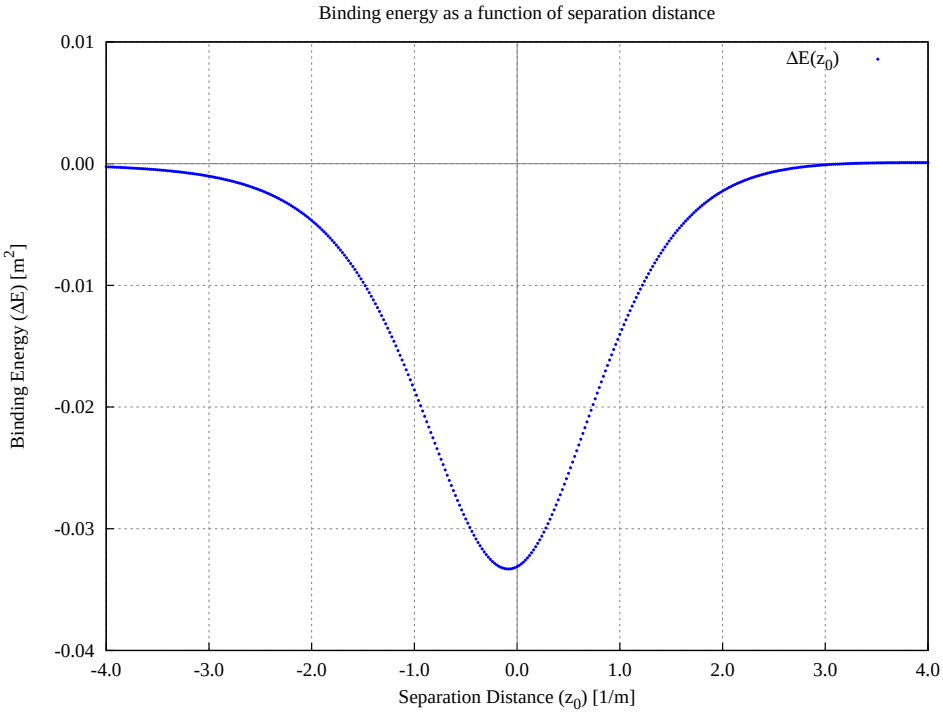

Figure 5.3: Plot of the numerical result for the binding energy at various separation distances between domain wall and monopole. Notice that for $z_0 < 0$, the monopole to the right of the domain wall, there is an "attractive" potential with a minimum near $z_0 = 0$.

The monopole is defined such that it is a point source solution to the Klein-Gordon equation,

$$\nabla_x^2 \varphi(\mathbf{x}) - m^2 \varphi(\mathbf{x}) = \delta(\mathbf{x}), \tag{5.14}$$

centered at the origin ($\mathbf{x}_0 = 0$), and is thus an approximate solution to the sine-Gordon equation, (5.4), away from the origin. The magnetic potential of the monopole is then given by the well known Yukawa potential,

$$\varphi(\mathbf{x}) = -\frac{e^{-m|\mathbf{x}|}}{4\pi m|\mathbf{x}|}. \tag{5.15}$$

We then consider the configuration of monopole and domain wall separated by a distance z_0 and would like to compute the magnetostatic energy

(Euclidean action) as a function of z_0. The energy associated with just a domain wall alone is proportional to the area of the domain wall, which is infinite in this case, so we compute instead the difference between the energy of the two together and the energy of the two independently,

$$\Delta E\left(z_0\right) = S\left[\chi_{z_0} + \varphi\right] - S\left[\chi_{z_0}\right] - S\left[\varphi\right], \tag{5.16}$$

where S is given by (axes have been rescaled relative to (5.3))

$$S\left[\chi\right] = \int_{\mathbb{R}^3} d^3x \left[\frac{1}{2}\left(\nabla\chi\right)^2 - m^2\cos\chi\right]. \tag{5.17}$$

The quantity ΔE defines a "binding energy" and is finite. We cannot however compute it analytically, and so we compute above integrals numerically instead, for z_0 varying near the domain wall. Some technical details of the computation are as follows. We work in a cylindrical volume oriented across the domain wall such that it respects the symmetries of the physical geometry. The cylinder is defined around the origin with radius $10/m$ and length $30/m$, so that we neglect the space outside of this region. It is valid to do so since the monopole potential is exponentially suppressed with length constant m and we are considering a binding energy. We were forced to remove a small volume around the origin when computing the potential energy term because the structure is that of the cosine of a divergent quantity, which is highly oscillatory. The potential energy due to the removed piece is bounded by the volume removed since it is a cosine so that we can make it arbitrarily small. These two approximations make up the bulk of the numerical uncertainty, which is $\sim m^2/10^6$.

Performing the numerical integration results in the plot given in Figure 5.3. There is an attractive potential between the monopole and domain wall with the monopole on one side ($z_0 < 0$), and a slightly repulsive one for the other side ($z_0 > 0$). The small barrier for $z_0 > 0$ is difficult to see in Figure 5.3 but obvious in Figure 5.5 which is just a plot of only points beyond $z_0 > 3$ with a much finer vertical scale. Also, there is a minimum at $z_0 \sim 1/10m$ (see Figure 5.4), while the peak of the domain wall charge distribution is $\sim 1/m$. Thus the monopole would prefer to sit "inside" the domain wall, between the center and the peak of the sheet with the same charge density. It is interesting that the monopole (with charge $-\alpha$) is attracted to the domain wall sheet with the same charge ($-\alpha$) rather than the sheet of opposing charge (α), but the theory is non-linear so it is not altogether unexpected. It also suggests a dynamical stability (at least at the classical level) of the domain wall in addition to the topological stability.

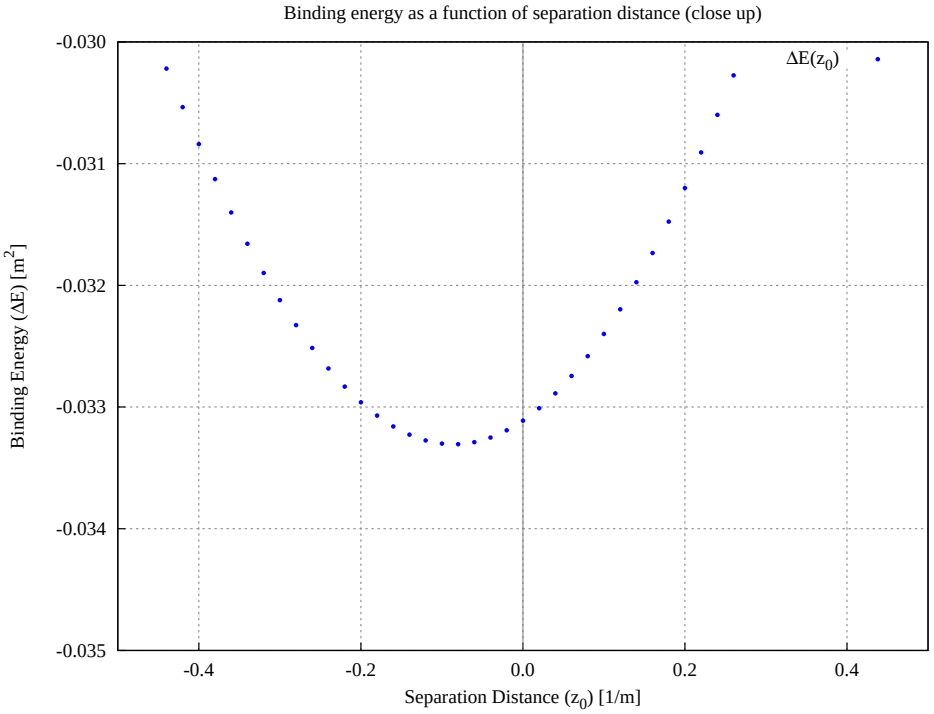

Figure 5.4: Close up plot of the points near the minimum in Figure 5.3 showing that the minimum is to the $z_0 < 0$ side of the center.

Figure 5.3 is not the complete story since we have not considered possible changes in the magnetic flux distribution coming from the monopole. Basically, the monopole shape could deform in response to the interaction with the domain wall, so as to become less spherically symmetric. In order to properly treat this problem, we should allow the spherical distribution of the monopole to vary to some superposition of solutions to the Klein-Gordon equation (5.14). This described further calculation is beyond the scope of this work, but we conjecture that the magnetic field will prefer to orient itself along the domain wall, so that the magnetic flux will be pushed out to the edge of the domain wall at the boundary of space, similar to arguments presented in refs. [2, 22, 24] in cosmological context. In this way, we have a picture in which any point-like magnetic monopoles become bound to extended domain walls with any magnetic flux being pushed along the domain walls to infinity. Apparently, this is precisely the picture discovered

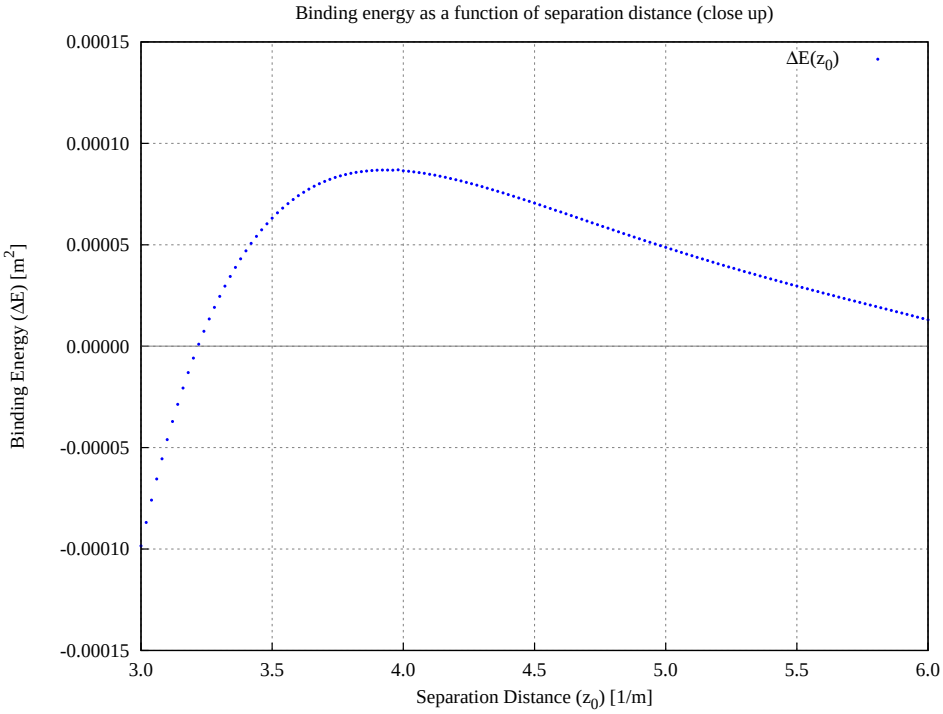

Figure 5.5: Close up plot of the points to the right in Figure 5.3 showing the small barrier present on the $z_0 > 0$ side. Notice the much finer vertical scale.

in lattice simulations [3, 37–39] wherein very few localised 4d objects are observed in the system.

As a preliminary toward calculating the angular dependence if we allow the angular distribution to vary, we write a more general expression for a monopole-like solution to the Klein-Gordon equation (5.14), which depends on the angular coordinates:

$$\varphi_n^m(\mathbf{x}) \sim H_n^{(1)}(imr)Y_n^m(\theta,\phi), \tag{5.18}$$

where $H_n^{(1)}$ are the spherical Hankel functions of the first kind and the Y_n^m are the spherical harmonics. Assuming the azimuthal axis is oriented across the domain wall, the problem is azimuthally symmetric and the spherical harmonics reduce to Legendre polynomials of $\cos(\theta)$.

When we attempt to calculate the binding energy as defined above for

φ_n it is negative and divergent for $n \geq 2$. It thus appears that the system is very sensitive to angular changes. Furthermore, the divergence in ΔE seems to come from the core (near the divergence in φ) since it is highly sensitive to the amount of the core we remove when performing the numerical calculations. This however is also the region in which this approximation by Klein-Gordon monopoles is not really justified, and in fact the whole low-energy effective theory is suspect. We therefore conclude that some other more sophisticated techniques will be required to address this problem of angular distribution, and as such it is well beyond the scope of this work. Nevertheless, we do conjecture that the flux will have a tendency to spread along domain wall, but unfortunately cannot make a more quantitative claim.

5.4 Comments

There are two important results of this work. Firstly, a double layer structure similar to that which is observed in lattice simulations [3, 37–39] naturally emerges in the construction of the domain walls in the weak coupling regime in the deformed gauge model. Secondly, monopole configurations characterised by well localised topological (and magnetic) charge interact with domain walls in such a way that there is an attraction between the two, and the monopole favors a position inside the domain wall. We introduced these domain walls as external background fields, while they are expected to be dynamical configurations with effectively vanishing tension in the strong coupling regime. We further suggest a tendancy that the magnetic field due a monopole in the presence of a domain will tend to align with the domain wall, such that the flux is pushed to the boundary of the domain wall. If this effect persists in strongly coupled regime, it could be an explanation for the observation in lattice simulations [3, 37–39] that there are no well localised objects with finite size which would carry the topological charge.

In weak coupling the domain wall solution is a nicely behaved smooth function, but what happens when we transition slowly to the strong coupling regime? The holographic picture suggests that the effective domain wall tension vanishes and so they can be formed easily in vacuum. It is possible that the domain walls become "clumpy" with a large number of folders. Such fluctuations would then increase the entropy of the domain wall, which eventually could overcome the intrinsic tension. If this happens, the domain walls would look like very crumpled and wrinkled objects with large number of folds, and as such, the domain walls may loose their natural

dimensionality, and become characterised by a Hausdorff dimension as some recent lattice simulations suggest [11]. Nevertheless, the topological charge distribution on larger scales after averaging over a large number of these foldings should be sufficiently smooth so that the double layer structure would not disappear because the transition from weak to strong coupling should be sufficiently smooth as argued in [85]. Therefore, we identify the double layer structure found in this work (5.10) with the double layer structure from the lattice measurements [3, 37–39]. These particularities of the transition from weak to strong coupling are also interesting future questions, which will require an analysis beyond the semi-classical level.

Chapter 6

Metastable Vacuum Decay

This chapter reproduces the work presented in [7]. We demonstrate the presence of metastable vacuum states and calculate the decay rate from such states to the true ground state in the context of the deformed model discussed in Chapter 2.

6.1 Motivation

A study of the QCD vacuum state in the strong coupling regime is the prerogative of numerical Monte Carlo lattice computations. However, a number of very deep and fundamental questions about the QCD vacuum structure can be addressed and, more importantly, answered using some simplified versions of QCD. Here, we study a set of questions related to metastable vacuum states and their decay to the true vacuum state using the deformed gauge theory model wherein we can work analytically. This model describes a weakly coupled gauge theory, which however preserves many essential elements expected for true QCD, such as confinement, degenerate topological sectors, proper θ dependence, and so on, as we have seen in previous chapters. This allows us to study difficult and nontrivial features, particularly related to vacuum structure, in an analytically tractable manner.

The fact that some high energy metastable vacuum states must be present in a gauge theory system in the large N limit has been known for quite some time [94]. A similar conclusion also follows from the holographic description of QCD as originally discussed in [96]. Furthermore, the decay rate of these excited vacua in the large N limit in strongly coupled pure gauge theory can be estimated as $\Gamma \sim \exp(-N^4)$ [73].

The fundamental observation on the emergence of these excited vacuum states was made in a course of studies related to the resolution of the $U(1)_A$ problem in QCD in the large N limit [90, 91, 93]. In the present work we do not introduce quarks (which play an essential role in the formulation of the $U(1)_A$ problem) into the system, but rather, study pure gluodynamics, and the metastable vacuum states which occur there. Nevertheless, the key object relevant for the resolution of the $U(1)_A$ problem, the so-called

topological susceptibility χ, still emerges in our discussions in pure gluodynamics because it plays an important role in understanding the spectrum of the ground state and multiple metastable states. Indeed, the topological susceptibility is defined as $\chi(\theta) = \frac{\partial^2 E_{\rm vac}(\theta)}{\partial\theta^2}$. Therefore, the information about the ground (or in general metastable) states $E_{\rm vac}(\theta)$ is related to the θ behaviour of the system formulated in terms of the topological susceptibility $\chi(\theta)$.

When some deep questions are studied in a simplified version of a theory, there is always a risk that some effects which emerge in the simplified version of the theory could be just artifacts of the approximation, rather than genuine consequences of the original underlying theory. Our study using this deformed theory as a toy model is not free from this potential difficulty with potential misinterpretation of artifacts as inherent features underlying QCD. Nevertheless, there are few strong arguments suggesting that we indeed study some intrinsic features of the system rather than some artificial effects. The first argument is discussed in the original paper on "centre-stablised Yang-Mills" [85], which we have been calling the "deformed gauge theory model", where it has been claimed that this model describes a smooth interpolation between a strongly coupled gauge theory and the weakly coupled deformed model without any phase transition by combining a smooth deformation and an apparently smooth transition to small compactification. In addition, there are a few more arguments based on our previous experience with the this model, which also suggest that we indeed study some intrinsic features of QCD rather than some artifact of the deformation.

Our arguments are based on the computations presented in Chapter 3 (published in [80]) of the contact term in the deformed theory, see also [84] for some related discussions. The key point is that this contact term with a positive sign (in the Euclidean formulation) in the topological susceptibility χ is required for the resolution of the $U(1)_A$ problem [90, 91, 93]. At the same time, any physical propagating degrees of freedom must contribute with a negative sign. In [93] this positive contact term has been simply postulated while in [90, 91] an unphysical Veneziano ghost was introduced into the system to saturate this term with the "wrong" sign in the topological susceptibility. This entire non-trivial picture has been successfully confirmed by numerical lattice computations. More importantly for the present studies, this picture has been supported by our analytical computations in which all the nontrivial crucial elements for the resolution of the $U(1)_A$ problem emerge.

Indeed, the non-dispersive contact term in the topological susceptibility

can be explicitly computed in this model and is given by [80]

$$\chi_{\text{contact}} = \int d^4x \langle q(x), q(0) \rangle \sim \int d^3x \left[\delta(\mathbf{x}) \right], \tag{6.1}$$

where $q(x)$ is the topological density operator. It has the required "wrong" sign as this contribution is not related to any physical propagating degrees of freedom, but is rather related to the topological structure of the theory, and has a $\delta(\mathbf{x})$ function structure as it should. In this model χ is saturated by fractionally charged weakly interacting monopoles describing the tunnelling transitions between topologically distinct, but physically equivalent topological winding sectors as discussed previously. Furthermore, the $\delta(\mathbf{x})$ function in (6.1) should be understood as a total divergence related to the infrared (IR) physics, rather than to ultraviolet (UV) behaviour as explained in [80]

$$\chi_{\text{contact}} \sim \int \delta(\mathbf{x}) \, \mathrm{d}^3x = \int \mathrm{d}^3x \; \partial_\mu \left(\frac{x^\mu}{4\pi x^3} \right). \tag{6.2}$$

The singular behaviour of the contact term has been confirmed by lattice computations where it has been found that the singular behaviour at $x \to 0$ is an inherent IR feature of the underlying QCD rather than some lattice size effect [10, 38, 40, 41].

In addition, one can explicitly see how the Veneziano ghost postulated in [90, 91] is explicitly expressed in terms of auxiliary topological fields which saturate the contact term (6.1) in this model as was shown in [106]. In other words, the η' field in this model generates its mass (which is precisely the formulation of the $U(1)_A$ problem) as a result of a mixture of the Goldstone field with the topological auxiliary field governed by a Chern-Simons like action, see [106] for the details.

All these features related to the θ dependence which are known to be present in the strongly coupled regime also emerge in the weakly coupled deformed toy model. Therefore, we interpret such behaviour as a strong argument supporting our assumption that the deformed model properly describes, at least qualitatively, the features related to the θ dependence and vacuum structure of QCD, including the presence of metastable states which is main subject of the present work.

The specific computations we perform related to the metastable vacuum states have never been performed using numerical lattice (or any other) methods. Therefore, we do not have the same luxury present in our previous studies of the contact term [80] in which our results were supported by numerous lattice computations. Nevertheless, as the specific questions about the metastable states are closely related to much more generic studies of the

θ dependence in the system, as reviewed above, we are still confident that our results presented below, based on the deformed model, are inherent qualitative properties of QCD rather than some artificial effects which may occur due to the deformation.

Our presentation is organised as follows. In Section 6.2 we explicitly demonstrate the presence of metastable states in the deformed gauge model. In Section 6.3 we review the general strategy to compute a decay of metastable vacuum states to the true vacuum in the path integral formulation. In Section 6.4 we present our numerical analysis on the life time of the metastable states as a function of a "semi-classicality" which is a parameter determining the region of validity of our semiclassical computations. Finally, we conclude in Section 6.5 with speculations on possible consequences and manifestations of our results for physics of heavy ion collisions where a metastable state might be formed as a result of collision, and the system, which is order the size of a nuclei, might be locked in this state for sufficiently long period of time ~ 10 fm/c.

6.2 Metastable Vacuum States

Here we concentrate on the Euclidean potential density for the σ fields at $\theta = 0$,

$$U(\boldsymbol{\sigma}) = \sum_{n=1}^{N} \left[1 - \cos\left(\sigma_n - \sigma_{n+1}\right)\right], \tag{6.3}$$

where again σ_{N+1} is identified with σ_1. To simplify notations we skip a large common factor $\mathcal{N}$ in our discussions which follow. We restore this factor in our final formula. Also, we have added a constant (N) so that the potential is positive semi-definite. The lowest energy state, denoted by $\boldsymbol{\sigma}^{(-)}$, is the state with all σ fields sitting at the same value $(\sigma_n = \sigma_{n+1})$ and has zero energy. This is clearly the true ground state of the system, but there are also potentially some higher energy metastable states. For an extremal state we must have

$$\frac{\partial U}{\partial \sigma_n} = 0 \tag{6.4}$$

for all n, which immediately gives

$$\sin\left(\sigma_n - \sigma_{n+1}\right) = \sin\left(\sigma_{n-1} - \sigma_n\right). \tag{6.5}$$

A necessary condition for a higher energy minimum of the potential is thus that the σ fields are evenly spaced around the unit circle or (up to a total

rotation),

$$\sigma_n = m\frac{2\pi n}{N}, \tag{6.6}$$

where m is an integer. A sufficient condition is then

$$\frac{\partial^2 U}{\partial \sigma_n^2} > 0, \tag{6.7}$$

again for all n. This gives us

$$\cos\left(\sigma_n - \sigma_{n+1}\right) + \cos\left(\sigma_{n-1} - \sigma_n\right) > 0, \tag{6.8}$$

which using (6.6) gives

$$\cos\left(m\frac{2\pi}{N}\right) > 0. \tag{6.9}$$

So, we get a constraint on m in the form of (6.9), and also on N. From (6.9) it is quite obvious that metastable states always exist for sufficiently large N, which is definitely consistent with old generic arguments [94]. In our simplified version of the theory one can explicitly see how these metastable states emerge in the system, and how they are classified in terms of the scalar magnetic potential fields $\boldsymbol{\sigma}(\mathbf{x})$.

We should also remark here that a non-trivial solution with $m \neq 0$ in (6.9) does not exist[9] in this simplified model for the lowest $N = 2, 3, 4$. Therefore, in our study we always assume $N \geq 5$.

Looking back at the potential (6.3), the lowest energy of the possibilities are given by $m = \pm 1$, so that the lowest energy metastable states, denoted by $\boldsymbol{\sigma}^{(+)}$, are given by (again up to a constant rotation)

$$\sigma_n^{(+)} = \pm\frac{2\pi n}{N}. \tag{6.10}$$

To understand the physical meaning of the solutions describing the non-trivial metastable vacuum states, we recall that the operator $e^{i\alpha_a \cdot \boldsymbol{\sigma}(\mathbf{x})}$ is the creation operator for a monopole of type a at point $\mathbf{x}$, as it was explicitly demonstrated in [80],

$$\mathcal{M}_a(\mathbf{x}) = e^{i\alpha_a \cdot \boldsymbol{\sigma}(\mathbf{x})}. \tag{6.11}$$

Therefore, the vacuum expectation value $\langle \mathcal{M}_a(\mathbf{x}) \rangle$ describes the magnetisation of a given metastable ground state classified by the parameter m.

[9] $N = 4$ deserves a special consideration as at $m = \pm 1$ the second derivative (6.7) vanishes. It may imply a presence of the massless particles in the spectrum for these excited vacuum states. It may also correspond to a saddle point in configuration space. We shall not elaborate on this matter in the present work.

As one can see from (6.6), the corresponding vacuum expectation value $\langle \mathcal{M}_a(\mathbf{x})\rangle$ always assumes the element from the centre of the $SU(N)$ gauge group. Specifically, for the lowest metastable vacuum states given by (6.10), the magnetisation is given by

$$\langle \mathcal{M}_a(\mathbf{x})\rangle = \exp\left[\pm i\frac{2\pi}{N}\right]. \tag{6.12}$$

The fact that the confinement in this model is due to the condensation of fractionally charged monopoles has been known since the original paper [85]. Now we understand the structure of the excited metastable states also; mainly, these metastable vacuum states can be also thought of as a condensate of the monopoles. However, the condensates of different monopole types, n from (6.10), are now shifted by a phase such that the corresponding magnetisation receives a non-trivial phase (6.12).

A different, but equivalent way to classify all these new metastable vacuum states is to compute the expectation values for the topological density operator for those states. By definition

$$\begin{aligned}\langle \frac{1}{16\pi^2}\mathrm{tr}\left[F_{\mu\nu}\tilde{F}^{\mu\nu}\right]\rangle_m &\equiv -i\frac{\partial S_{\mathrm{dual}}(\theta)}{\partial\theta}|_{\theta=0} \\ &= -i\frac{\zeta}{L}\langle \sin\left(\alpha_a\cdot\boldsymbol{\sigma}\right)\rangle_m = -i\frac{\zeta}{L}\sin\left(\frac{2\pi m}{N}\right).\end{aligned} \tag{6.13}$$

The imaginary i in this expression should not confuse the readers as we work in Euclidean space-time. In Minkowski space-time this expectation value is obviously a real number. A similar phenomenon is known to occur in the exactly solvable two dimensional Schwinger model wherein the expectation value for the electric field in the Euclidean space-time has an i, see [105] for discussions in present context. The expectation value (6.13) is the order parameter of a given metastable state.

A crucial point we want to make here is that a metastable vacuum state with $m \neq 0$ in general violates $\mathcal{P}$ and $\mathcal{CP}$ invariance since the topological density operator itself is not invariant under these symmetries. Precisely this observation inspires our suggestion, discussed in Section 6.5, that such metastable states could be the major source of the local $\mathcal{P}$ and $\mathcal{CP}$ violation observed in heavy ion collisions at the Relativistic Heavy Ion Collider (RHIC) at Brookhaven, and the Large Hadron Collider (LHC).

Now we come back to our discussions of the lowest metastable states (6.10). Putting the metastable configuration back into the potential (6.3) we find that the energy density separation between the true ground state

and the lowest metastable states (6.10) is given by[10]

$$\epsilon \equiv \left(E^{(+)} - E^{(-)}\right) = N\left[1 - \cos\left(\frac{2\pi}{N}\right)\right]. \tag{6.14}$$

The choice of sign in (6.10) is irrelevant for the purposes of calculating the vacuum decay since the two states $m = \pm 1$ are degenerate in terms of energy and so have the same energy splitting with respect to the ground state. These states, however, are physically distinct as the expectation value of the gauge invariant operator (6.13) has opposite signs for these two metastable vacuum states. This implies that all $\mathcal{P}$ and $\mathcal{CP}$ effects will have the opposite signs for these two states, while the probability to form these two metastable states is identical, as is the decay rate. So, while our fundamental Lagrangian is invariant under these symmetries, the metastable vacuum states, if formed, may spontaneously break that symmetry.

6.3 Metastable Vacuum Decay

In this section we briefly review the general theory and framework for calculating metastable vacuum decay rates in Quantum Field Theory, restating the important results for the three dimensional model discussed above. For a more thorough discussion see Appendix B or the original papers [14, 15, 47]. There is also a great, and fairly extensive, discussion on this topic in Chapter 7 of [72]. The process for the decay of a metastable vacuum state to the true vacuum state is analogous to a bubble nucleation process in statistical physics. Considering a fluid phase around the vaporisation point, thermal fluctuations will cause bubbles of vapor to form. If the system is heated beyond the vaporisation point, the vapor phase becomes the true ground state for the system. Then, the energy gained by the bulk of a bubble transitioning to the vapor phase goes like a volume while the energy cost for forming a surface (basically a domain wall) goes like an area. Thus, there

[10] We should comment here that the vacuum energy of the ground state $E^{(\pm)} \sim N$ in this model scales as N in contrast with conventional N^2 scaling in strongly coupled QCD. However, the ratio $\epsilon/E^{(\pm)} \sim N^{-2}$ shows the same scaling as in strongly coupled QCD. The difference in behaviour in large N limit between weakly coupled "deformed QCD" and strongly coupled QCD obviously implies that we should anticipate a different asymptotic scaling for the decay rate in the large N limit in our simplified model in comparison with result [73]. As we discuss in Sections 6.4.2 and 6.4.3 this is indeed the case. Furthermore, the region of validity in this model shrinks to a point in the limit $N \to \infty$ as discussed in [85]. Therefore, the asymptotic behaviour at $N \to \infty$ should be considered with great caution.

is some critical size such that smaller bubbles represent a net cost in energy and will collapse while larger bubbles represent a net gain in energy. Once a bubble forms which is larger than the critical size it will grow to consume the entire volume and transition the whole of the sample to the vapor phase. To understand the lifetime of such a 'superheated' liquid state, the important calculation is, therefore, the rate of nucleation of critical bubbles per unit time per unit volume (Γ/V). Similarly, we aim to calculate this decay rate for our system from the metastable state $\boldsymbol{\sigma}^{(+)}$ to the ground state $\boldsymbol{\sigma}^{(-)}$, though through quantum rather than thermal fluctuations. Classically, a system in the configuration $\boldsymbol{\sigma}^{(+)}$ is stable, but quantum mechanically the system is rendered unstable through barrier penetration (tunneling).

The semiclassical expression for the tunneling rate per unit volume is given by [14, 15, 47]

$$\frac{\Gamma}{V} = Ae^{-S_E(\boldsymbol{\sigma}_b)/\hbar}\left[1 + O\left(\hbar\right)\right] \tag{6.15}$$

where S_E is the Euclidean action (3.11) and is evaluated in the field configuration called the "Euclidean bounce" which we have denoted $\boldsymbol{\sigma}_b$. The Euclidean bounce is a finite action, spherically symmetric configuration which solves the classical equations of motion and interpolates from the metastable state to a configuration "near" the ground state and back.

In the limit of small separation energy ϵ the bounce approaches $\boldsymbol{\sigma}^{(-)}$ more closely and spends longer in the region nearby, so that the bounce configuration resembles a bubble with the interior at $\boldsymbol{\sigma}^{(-)}$, the exterior at $\boldsymbol{\sigma}^{(+)}$, and a domain wall surface interpolating between the two[11]. If the bubble is very large, corresponding to very small ϵ, then the curvature at the interpolating surface is small and the surface appears flat.

Therefore, if the separation energy, ϵ, between the two states is small, we need only solve for the one dimensional soliton interpolating between $\boldsymbol{\sigma}^{(+)}$ and $\boldsymbol{\sigma}^{(-)}$ which solves

$$S_1 = \int dx \sum_{n=1}^{N}\left[\frac{1}{2}\left(\frac{d\sigma_n}{dx}\right)^2 + 1 - \cos\left(\sigma_n - \sigma_{n+1}\right)\right]. \tag{6.16}$$

This is called the thin-wall approximation, and is the framework in which we will work. In the deformed model, as discussed in the previous section,

[11] One should comment here that this model also exhibits very different types of the domain walls, mainly those considered in Chapter 5 (and [81]). The objects discussed there are fundamentally different from solutions in the present work as they essentially describe the tunnelling events between different topological sectors, while in here the domain wall-like objects play the auxiliary role in order to evaluate the life time of a metastable state.

the separation $\epsilon \sim 1/N$, so that the thin-wall approximation coincides with the large N approximation.

For the thin wall approximation the full action reduces to

$$S_3 = 4\pi R^2 S_1 - \frac{4}{3}\pi R^3 \epsilon = \frac{16}{3}\pi \frac{S_1^3}{\epsilon^2}, \tag{6.17}$$

where the last step is computed by using variational analysis to get $R = 2S_1/\epsilon$. Notice again the similarity to a bubble nucleation problem. This extremal action with respect to the bubble size is in fact a maximum, and as such the action increases with R for smaller size and decreases with R for larger. Hence, the bounce configuration which saturates the decay rate is essentially a bubble of critical size as discussed when making this analogy to bubble nucleation.

The condition for the validity of the thin wall approximation is essentially that the interior of the bubble is very near the true ground state $\boldsymbol{\sigma}^{(-)}$ so that it is nearly stable and stays near $\boldsymbol{\sigma}^{(-)}$ for large ρ. We want $R\mu \gg 1$, where $\mu^2 = \partial^2 U/\partial\sigma_n^2(\boldsymbol{\sigma}^{(-)})$ is the curvature of the potential at the ground state; here $\mu = \sqrt{2}$. Thus, we need

$$2\sqrt{2}S_1 \gg \epsilon, \tag{6.18}$$

where ϵ is given by (6.14).

We now have everything required to calculate the exponent for the vacuum decay (B.1) assuming we can solve for a classical path associated with the one dimensional action (6.16) interpolating between the two states $\boldsymbol{\sigma}^{(+)}$ and $\boldsymbol{\sigma}^{(-)}$. We have not discussed the coefficient A, and indeed it is a much more complicated problem related to the functional determinant of the full differential operator, $\delta^2 S/\delta\sigma^2$. This calculation is beyond the scope of this work for the deformed model as it does not change the basic physical picture advocating in this work. We want to see that the leading factor in the decay rate is indeed exponentially small, and our computations are justified as long as our semiclassical parameter (3.25) is sufficiently large, $\mathcal{N} \gg 1$. Furthermore, we anticipate that the dependence on N in the exponent is much more important than the N dependence in pre exponential factor $\sim \delta^2 S/\delta\sigma^2$. The only power -like corrections which may emerge from the determinant is through a factor of $\sqrt{S_E/2\pi}$ for each zero mode [15], and we can safely neglect these corrections in comparison with much more profound exponential behaviour in N, see Sections 6.4.2 and 6.4.3.

6.4 Computations

We now proceed to solve the equations of motion

$$\frac{d^2\sigma_n}{dx^2} = \sin\left(\sigma_n - \sigma_{n+1}\right) - \sin\left(\sigma_{n-1} - \sigma_n\right), \tag{6.19}$$

with σ_{N+1} identified with σ_1, derived from the action (6.16) subject to the boundary conditions

$$\sigma_n\left(x \to -\infty\right) = 0, \tag{6.20}$$

and

$$\sigma_n\left(x \to +\infty\right) = \frac{2\pi}{N} n + \varphi. \tag{6.21}$$

The φ in (6.21) is a relative rotation angle between the two boundaries, since each of the two states are only defined up to a rotation. The angle is determined by demanding a minimal action interpolation. That is, we should minimise the action with respect to the interpolating field configuration and also with respect to this angle φ. The final solution thus obtained will then be defined only up to an arbitrary total rotation which will be important later. Additionally, we expect the solution to be a soliton (instanton-like) in the sense that it should be well contained with only exponential tails away from the center so that the interpolation occurs in an exponentially small region. The characteristic size of this region, we expect, is given by m_σ^{-1} in the original model, or just 1 in dimensionless notations used here. Then, we can calculate the vacuum decay rate as

$$\frac{\Gamma}{V} \sim \left(\frac{S_3}{2\pi}\right)^3 e^{-S_3}, \tag{6.22}$$

where we have put in the part of the coefficient that we can calculate related to the zero modes in the system. There are six zero modes: three translations, two spacial rotations, and the one global σ-rotation discussed earlier. We now discuss in Section 6.4.1 the numerical technique employed to solve this problem, and in Section 6.4.2 the results of these numerical calculations.

6.4.1 Numerical Technique

The sine-Gordon equation for a single field, $u'' = \sin(u)$, has a soliton solution given by

$$u\left(x\right) = 4\arctan\left(e^x\right), \tag{6.23}$$

interpolating between 0 and 2π, which seems like good starting point. As such, we choose a similar form for the initial guess at the solution for the coupled equations, and hence define our initial guess to be of the form

$$\sigma_n = \left(\frac{n}{N} + \frac{\varphi}{2\pi}\right) 4 \arctan\left(e^x\right). \tag{6.24}$$

This initial guess has two important properties; it satisfies the boundary conditions (6.20) and (6.21), and tails off toward those boundaries as decaying exponentials for $x \to \pm\infty$, which is the type of behaviour expected, as discussed previously.

The equations of motion (6.19) are on an infinite domain and must be truncated to be solved numerically. We want to truncate the domain to a region beyond which changes in the $\sigma_i(r)$ are numerically insignificant. Given that the tails of the $\sigma_n(r)$ (and we expect the final solution) are decaying exponentials, choosing the domain $[-16, 16]$ means that the boundary values are within $\sim 10^{-7}$ of their final values and is suitable for our purpose.

In order to promote numerical stability particularly around the boundary values we employ Chebyshev spectral methods for integrals and derivatives, as described in [9][83], using an unevenly spaced Chebyshev grid given by

$$x_i = cos\left(\frac{\pi i}{N_p}\right), \ \ \forall \ \ 0 \leq i \leq N_p \tag{6.25}$$

where N_p is the number of grid points. Notice that the Chebyshev grid defines a domain $[-1, 1]$ and so we scale $x \to \ \frac{x}{16}$ in order to express functions with the chosen domain on the spectral grid.

From now on, we will use the following notation: σ_n^i denotes the i^{th} grid point of the n^{th} field, where N is the total number of fields while N_p is the number of grid points. The differentiation matrix $(N_p \times N_p)$ is given by [9] (page 570) as

$$D_{ij} = \begin{cases} \frac{2N_p^2+1}{6} & i = j = 0 \\ -\frac{2N_p^2+1}{6} & i = j = N_p \\ -\frac{x_j}{2\left(1-x_j^2\right)} & 0 < i = j < N_p \\ \frac{(-1)^{i+j} p_i}{p_j (x_i - x_j)} & i \neq j \end{cases} \tag{6.26}$$

where,

$$p_j = \begin{cases} 2 & j = 0 \, or \, N \\ 1 & otherwise. \end{cases}$$

Any higher derivative is then given by repeated multiplication by D. This differentiation matrix (6.26) is basically just the linear operator describing interpolating a function on the grid points by an N_p^{th} order polynomial and differentiating that polynomial. Since it uses knowledge of the entire function rather than just the few nearby points like a finite difference, the accuracy of the derivative is generally much better than any small order finite difference. Furthermore, using a grid spaced in this way provides much more numerical stability, counteracting the so called Runge phenomenon [83], which leads to large oscillations near boundaries of uniform grids.

The algorithm we employ to minimise the action with respect to the field configuration is a gradient descent method, which is to treat the action as a potential over the configuration space formed by each σ field at each grid point, then to take steps in the negative gradient direction. Essentially, iterating the expression

$$\begin{aligned} \sigma_n^i \to \sigma_n^i &- \delta \frac{dS_1}{d\sigma_n^i} \\ \sigma_n^i \to \sigma_n^i &+ \delta \left(D^2 \sigma_n\right)^i - \delta \sin\left(\sigma_n^i - \sigma_{n+1}^i\right) \\ &+ \delta \sin\left(\sigma_{n-1}^i - \sigma_n^i\right) \end{aligned} \tag{6.27}$$

where δ is a chosen step size, which we start as $\delta = 1$. At each iteration, we enforce the boundary conditions and check if the action (6.16) applied to the new configuration is in fact smaller than the old configuration. If so, we move to the new configuration. If not, the step was too large and we have overstepped the section of the potential with a downward slope, so we go back to the old configuration and reduce the step size by $\delta \to \delta/2$ and iterate this procedure until we find a good step or reduce the step size below our desired precision. We then reset $\delta = 1$ and continue until we cannot find a good step within our desired precision. Once reaching a position from which no step reduces the action, we are within the defined precision of a minimum of the action. In order to probe more of the configuration space we took a Monte-Carlo-like approach wherein we adjusted our initial guess by adding some Gaussian noise in an envelope, $(1-|x|)^2$. We chose an envelope of this form because we expect that the solution has the sort of exponential tails of our initial guess (6.24), while we do not know the form of the core of the domain wall. Thus, it is sensible to probe more of the configuration space related to the specific details of the core.

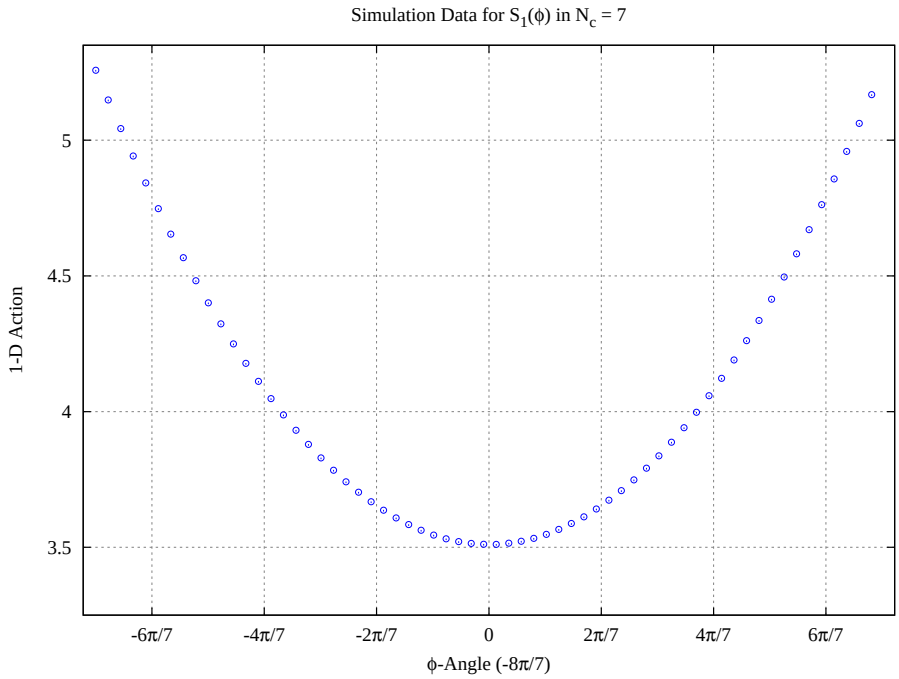

Figure 6.1: Plot of some simulation data for the one dimensional action (6.16) as a function of the angle φ between the boundary conditions done for $N = 7$.

6.4.2 Results

The first issue we address is the question about the favoured angle, φ, between the two boundaries, (6.20) and (6.21). In order to find the angle we chose (arbitrarily) $N = 7$ and varied the angle in the range $[-\pi, \pi] - 8\pi/7$, and look at the action S_1 as a function of φ. The results of that simulation are plotted in figure 6.1. The center point on the plot, $-8\pi/7$, may seem odd, but it is the value for φ which leads to a maximally symmetric solution, so it is very believable minimum for the potential, and indeed this is what we see. The solution for the minimal σ field configuration corresponding to $\varphi = -8\pi/7$ is shown in figure 6.2 across the domain wall. Extending these

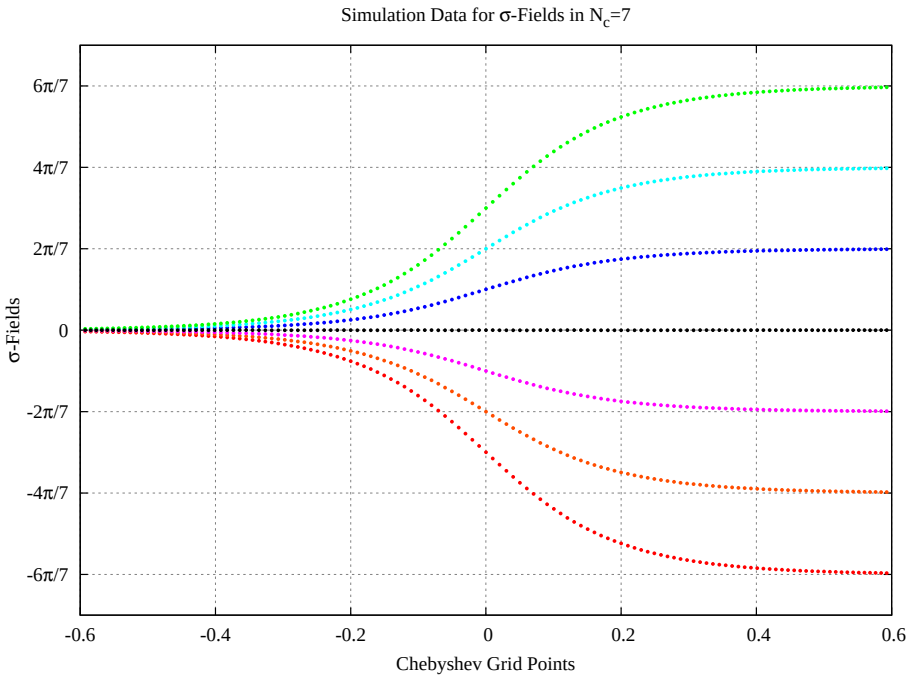

Figure 6.2: Plot of some simulation data for the σ field configuration plotted across the domain wall done for $N = 7$ and $\phi = -8\pi/7$.

results to arbitrary N we set

$$\varphi = -\pi \left(\frac{N+1}{N} \right), \tag{6.28}$$

which just ensures that the solution we look for is maximally symmetric in the same sense as the fields in figure 6.2, basically that $\sigma_n = -\sigma_{N+1-n}$. We have checked that this choice of φ, (6.28), does in fact lead to the lowest action configuration for $N = 20$ and $N = 35$ with results much like those shown in figure 6.1 for $N = 7$, so we are comfortable with our assumption.

Next, we are expecting a non-perturbative function of the form $\Gamma/V \sim \exp\left[-F\left(N\right)\right]$ [73, 94], so running simulations for $\Gamma/V\left(N\right)$ we plot the results in the form $F\left(N\right)$. This plot is given in figure 6.3 where the points and error bars given are the mean and standard deviation for 25 trials of our simulation at each N between 15 and 75 using 312 Chebyshev grid points; it is shown

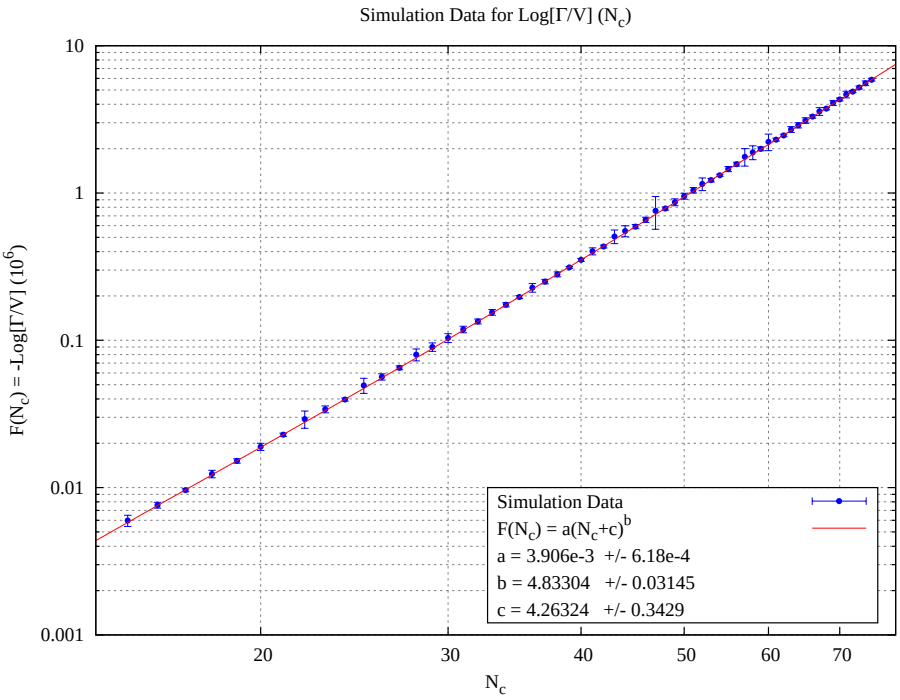

Figure 6.3: Plot of some simulation data for the decay exponent $F(N)$ plotted for N in the range 15 to 75.

on a log-log scale to emphasise the power law behaviour of $F(N)$.

The particular fit parameters are given for completeness but should not be regarded as terribly important. In fact, the most important result for the present analysis is that the computations are performed in a theoretically controllable manner where every single step is justified in the semi-classical limit (3.25) governed by the parameter $\mathcal{N} \gg 1$. We are after all working in a toy model, and as such should expect a good qualitative picture but not take the numerical details too seriously. It is however interesting that the final form for the decay rate is given as, putting the parameter $\mathcal{N}$ back in,

$$\frac{\Gamma}{V} \sim \exp\left\{-\mathcal{N}\left(aN^b\right)\right\} \tag{6.29}$$

with both a and b positive. Thus, the decay rate does drop off exponentially in N and our other semiclassical parameter $\mathcal{N}$, and indeed faster than any perturbation term would describe as previously conjectured. It is a semi-classical calculation, but the behaviour is fundamentally non-perturbative, and it is only parametrically justified when $\mathcal{N} \gg 1$.

A few comments are in order. First, our numerical estimates (6.29) can be only trusted for finite $N > 5$, but not for parametrically large $N \to \infty$ where the region of validity of the model shrinks to a point. Furthermore, if the external parameter N were allowed to vary in a very large region it may lead (and, in fact, it does) to a systematic error in our numerical simulations. This is because in our numerical simulations we assume that all our variables are order of unity, rather than having some functional dependence on N, which may not be the case when the external parameter N is allowed to vary in wide region of parameter space. Finally, one should not expect that our formula (6.29) would reproduce the asymptotic behaviour [73] due to the differences in large N scaling between the deformed model and strongly coupled QCD. As mentioned previously, the main goal of our computations is to support the qualitative, rather than quantitative picture of metastable vacua and their decay, conjectured in [94, 96] in a simplified model where calculations are parametrically justified at $\mathcal{N} \gg 1$ and finite N. Nevertheless, there is room to improve our numerical simulations in a much wider range of N as a result of a recent analysis [51] in which the asymptotic expression at $N \to \infty$ has been analytically computed. These improvements are discussed in the next section.

6.4.3 Improved Results

Recently, an analytical analysis of the asymptotic behaviour of this calculation, inspired by the above numerical results, has been carried out [51] with

the asymptotic expression for the decay rate per unit volume given by

$$\frac{\Gamma}{V} \sim \exp\left[-\mathcal{N}\frac{256N^{7/2}}{9\sqrt{3}\pi\left(\pi-\theta\right)^2}\right]. \tag{6.30}$$

We briefly reproduce these results in Appendix C. The asymptotic expression (6.30) gives us a hint about how to produce a better estimate for the decay rate for very large $N \gg 1$ in comparison with our naive numerical results presented in Section 6.4.2 above, wherein we assumed that parameter N is not allowed to vary in an extended region of parameter space.

Indeed, the analysis in [51] suggests the specific reason for the disparity between the asymptotic expression and the numerical results shown in figure 6.3 for large N. Mainly, the asymptotic guess solution is given by

$$\sigma_n\left(x\right) = \left(\frac{4n}{N}-2\right)\arctan\left[\exp\left(-2\sqrt{\frac{3}{N}}x\right)\right], \tag{6.31}$$

which has a size $\sim\sqrt{N}$ changing with the parameter N. Our guess solution (6.24) does not scale with N and so becomes an increasingly bad guess at asymptotically larger N, such that our numerical solver becomes increasingly likely to find some other local minimum of the action. Furthermore, our integration domain was fixed for all N as we did not even attempt to consider any large variations with N in our analysis in Section 6.4.2. When we allow the external parameter N to become large, the true minimal action interpolating trajectory eventually will not fit in the finite size numerical grid which we fixed for all N. Essentially, forcing boundary conditions on too small a domain also forces a higher action local minimum as N increases. This is precisely the mechanism by which a systematic error is introduced into the numerical simulations as a result of large variation in the external parameter N, as suggested in the previous section.

Fortunately, the analytical expression (6.31) which is valid for asymptotically large N suggests a simple fix to improve our numerical solution at higher N by explicitly taking into account the variation of the trajectory size with this parameter. Technically, we can allow the integration domain to scale $\sim\sqrt{N}$, and start with the asymptotic guess (6.31) in which the large parameter N explicitly enters, as the initial guess for the "improved" numerical algorithm. Again, we added some Gaussian noise to get an ensemble of 25 initial guesses for each N and relaxed them as described in Section 6.4.1 to arrive at a minimum of the action. These improved results are shown in figure 6.4 plotted along with the asymptotic expression for the decay rate

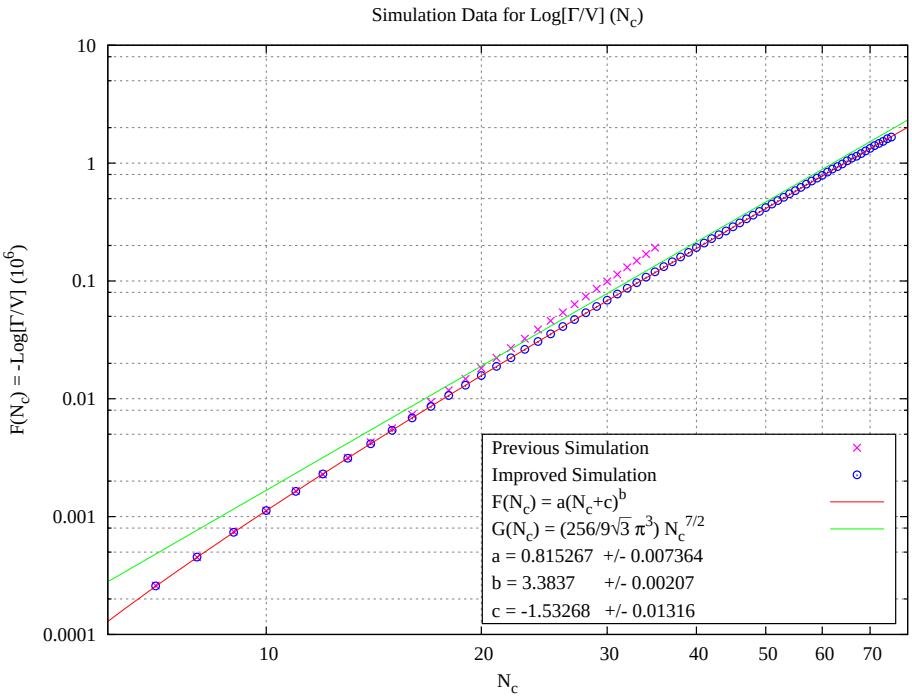

Figure 6.4: Plot of the improved simulation data for the decay exponent $F(N)$ plotted for N in the range 7 to 75.

and the first few points from the original simulations in Section 6.4.2. They reproduce the previous results for finite $N \leq 15$ and approach the asymptotic result (6.30) given in [51] from below for large N. Numerically, the asymptotic expression (6.30), which is formally valid at $N \to \infty$, describes our improved simulation data sufficiently well (with accuracy better than 10%) only at large $N \geq 35$.

6.5 Comments

Our comments here can be separated into two different parts: solid theoretical results within the deformed model; and some speculations related to strongly coupled QCD realised in nature.

We start with the first part of the conclusion in which our basic result

is as follows. We have demonstrated that the deformed model shows (once again) that some qualitative features expected to occur in the strongly coupled regime in the large N limit as argued in [94] do emerge in the simplified version of the theory as well. We demonstrated the existence of metastable vacuum states with energy density higher than the ground state by $\epsilon \sim 1/N$, and have shown that the lifetime of the metastable states is exponentially suppressed in this model with respect to the semi-classicality parameter $\mathcal{N}$. The suppression increases even further with increasing number of colours N for a fixed $\mathcal{N}$, and it is given by (6.29).

In this simplified system one can explicitly see these metastable states, how they are classified, and the microscopic dynamics which govern the corresponding physics. The $\mathcal{P}$ and $\mathcal{CP}$ invariance is generally violated in these metastable vacuum states as the expectation value for the topological density (6.13) explicitly shows. We believe that this feature of spontaneous breaking of the $\mathcal{P}$ and $\mathcal{CP}$ invariance in metastable states is quite a generic feature which is shared by strongly coupled pure gauge theories (for sufficiently large N). Precisely this feature of the metastable states plays a crucial role in our speculative portion of the conclusion.

Therefore, we now speculate that precisely this spontaneous symmetry breaking effect is responsible for the asymmetries in event by event studies observed at the RHIC (Relativistic Heavy Ion Collider) and the LHC (Large Hadron Collider). To be more specific, the violation of local $\mathcal{P}$ and $\mathcal{CP}$ symmetries has been the subject of intense studies for the last couple of years as a result of very interesting ongoing experiments at RHIC [16, 26] and, more recently, at the LHC [17, 18, 25, 70], see [44] for a recent review and introduction to the subject with a large number of references to original papers.

The main idea for explaining the observed asymmetries is to assume [43, 44] that an effective $\theta(\vec{x}, t)_{ind} \neq 0$ is induced in the process of cooling of the system representing the high temperature quark-gluon plasma. In other words, the system in the process of cooling may spontaneously choose one or another state which is not the absolute minimum of the system corresponding to the $\theta = 0$, but rather, some excited state, similar to the old idea when the disoriented chiral condensate can be formed as a result of heavy ion collisions. The key assumption is that this induced $\theta(\vec{x}, t)_{ind} \neq 0$ is coherent on a relatively large scale, of order the size of nuclei ~ 10 fm. If a state with $\langle \theta(\vec{x}, t)_{ind} \rangle \neq 0$ is indeed induced, it implies a violation of the local $\mathcal{P}$ and $\mathcal{CP}$ symmetries on the same scales where $\theta(\vec{x}, t)_{ind} \neq 0$ is correlated. It may then generate a number of $\mathcal{P}$ and $\mathcal{CP}$ violating effects, such as Charge/Chiral Separation (CSE) and Chiral Magnetic (CME) Effects, see

[44] for a recent review.

One of the critical questions for the applications of the CME to heavy ion collisions is a correlation length of the induced $\langle\theta(\vec{x},t)_{ind}\rangle \neq 0$. Why are these $\mathcal{P}$ odd domains large?

We suggest that the system being originally formed at high temperature might be locked in one of these metastable states during the cooling stage[12]. If this happens one should obviously expect a number of $\mathcal{P}$ and $\mathcal{CP}$ effects to occur coherently in the entire system characterised by a large scale of order the size of nuclei $\mathbb{L} \gg \Lambda_{\rm QCD}^{-1}$. We therefore identify $\theta(\vec{x},t)_{ind} \neq 0$ from [43] with the effective theta parameter $2\pi/N$ which enters (6.13) and which manifests a spontaneous violation of the $\mathcal{P}$ and $\mathcal{CP}$ symmetries in the system.

The presence of such long range order (which itself is a consequence of a spontaneous selection of a metastable vacuum state in the entire system during the cooling process) may explain why the CME is operational in this system and how the asymmetry can be coherently accumulated. This identification would justify the effective Lagrangian approach advocated in [43, 104] wherein $\theta(\vec{x},t)_{ind}$ is treated as a slow background field with correlation length much larger than any conventional QCD fluctuations, $\mathbb{L} \gg \Lambda_{\rm QCD}^{-1}$. It is important to emphasise that the $\mathcal{P}$ and $\mathcal{CP}$ symmetries are good symmetries of the fundamental QCD. As mentioned in footnote 12, the asymmetries can only be observed in heavy ion collisions in event by event analyses when the system might be locked, for sufficiently long period of time $\tau \sim \mathbb{L}/c \gg \Lambda_{\rm QCD}^{-1}$, in a metastable state in one collision with one specific sign for the topological density (6.13). Because the metastable states with opposite signs for the topological density operator (6.13) have the same energy, which state is chosen for a particular event is random and evenly distributed. Thus, it is clear that if one averages over a large number of events, the asymmetry will be washed out as the probability to form these metastable states is identical and the lifetime for the two is the same as we mentioned in Section 6.2. However, in the event by event studies the asymmetry will be evident in the system. Apparently, this is precisely what has been observed. The $\mathcal{P}$ and $\mathcal{CP}$ violation is seen in collider events only on an event by event basis but averages to zero over many events, see the

[12] The $\mathcal{P}$ and $\mathcal{CP}$ symmetries, of course, are good symmetries in QCD. The probability to produce the $m = +1$ state from equation (6.9) is identical to that to produce the $m = -1$ state. Therefore, there will not be any $\mathcal{P}$ and $\mathcal{CP}$ violating effects if one averages over a large number of events. However, one should expect some asymmetries if one analyses the system on an event by event basis, which is precisely the procedure used at RHIC and the LHC, see [44] for a recent review.

recent review paper [44] for details.

Chapter 7

Conclusion

We examined some interesting aspects of the modified deformed gauge theory developed by Lawrence Yaffe and Mithat Ünsal [85] in a confined phase in an theoretically controllable manner, which is impossible with current methods in real strongly coupled QCD. This model, as discussed in Chapter 2, is constructed by taking a standard Yang-Mills Lagrangian and putting in an extra potential by hand that penalises an expectation value for the Wilson line in the compact direction. The Wilson line acts as an order parameter for a center symmetry breaking that characterises the deconfinement phase transition, so that the extra potential, if chosen to be strong enough, forces a confined phase. Thus, we have a system at weak coupling (small compactification scales) that is nonetheless confined and gapped, for which the low energy effective dynamics is given by two dual descriptions: a multi-species Coulomb gas; or a coupled sine-Gordon model.

In Chapter 3 we calculated the topological susceptibility analytically in both dual descriptions, demonstrating the presence of a nondispersive contact term with the sign opposite that of the contribution from any physical propagating degrees of freedom. We discussed the necessity of such a term in the resolution of the $U(1)_A$ problem in QCD, which provides the physical mass for the η' meson, and explained how such a term has previously been postulated either directly or via an extra unphysical ghost field. In the deformed model however, the contact term emerges naturally and can be seen in both descriptions.

Next, in Chapter 4, we considered the Coulomb gas description for the deformed model, and performed an analysis of the zero modes for the collective coordinates of a monopole, following a similar analysis performed by Gerard 't Hooft [77] in his classic paper on four dimensional instantons. We calculated the corrections to these zero mode contributions to the measure due to a finite size of the manifold. The results of this analysis are that the monopole fugacity, and so also the bulk energy density, receives some Casimir-like power law corrections based on the size of the manifold. This is in contrast to the naive expectation that in a gapped system with only massive degrees of freedom should only have a weaker exponentially suppressed

dependence on the boundary. We further argued that, if such an effect persists in strongly coupled undeformed QCD, it provides a natural solution to the cosmological dark energy problem, with a rough prediction for the magnitude, $H\Lambda_{QCD}^3 \sim (10^{-3}\mathrm{e}V)^4$, that is of the correct order of magnitude. Furthermore, this explanation requires no new physics, coming merely from long distance "nondispersive" effects in the QCD sector interacting with a finite sized manifold.

Then, in Chapter 5, performed a numerical analysis of the interaction between a point-like topological monopole and an extended topological domain wall in the sine-Gordon description. The domain wall solution in the sine-Gordon picture is qualitatively similar to relevant gauge configurations discussed in the context of some Lattice QCD simulations [3, 10, 37–41, 49], which suggest that extended topological objects are more relevant than the point-like instantons that have been discussed traditionally. We found that the lowest energy configuration involves the monopole sitting within the domain wall toward the side with the same topological charge as the monopole. This result suggests a dynamical reason for the absence of instanton-like configurations in lattice simulations, and perhaps a dynamical stability for the domain walls also, above and beyond the classical topological stability.

Finally, in Chapter 6, we demonstrated the presence of metastable vacuum states with energy greater than the true ground state in the deformed gauge model, and calculated the decay rate from the lowest energy of such states to the ground state following the procedure developed by Sidney Coleman [14, 15]. We solved for configurations interpolating between the true vacuum state and the higher energy metastable state numerically, then used these to find the decay rate as a function of N_c, the number of colours defined by the gauge group $SU(N)$ for the model, confirming the predicted behaviour predicted by Edward Witten for undeformed gauge theory at large N_c [95]. As expected, the result is given as $\Gamma/V \sim \exp[aN^b]$, for some coefficients a and b which we computed, confirming a nonperturbative origin for such behaviour since this dependence cannot arise at any order of perturbation expansion.

The deformed gauge theory model is an extremely useful toy model for studying ideas in true undeformed gauge theory, especially topological properties, in a confined phase. It allows for semiclassical analysis of a topologically nontrivial, confined theory with a mass gap at weak coupling, which is smoothly connected parametrically to undeformed strongly coupled Yang-Mills gauge theory. As shown, we can calculate quantities that are impossible to compute in undeformed strongly coupled QCD, and test ideas that have only been postulated in true QCD.

Bibliography

[1] S. Ahmad, J. T. Lenaghan, and H. B. Thacker. Coherent topological charge structure in CP(N-1) models and QCD. *Phys. Rev. D*, 72:114511, 2005, arXiv:hep-lat/0509066.

[2] S. Alexander, R. H. Brandenberger, and R. Easther. Attractive forces between global monopoles and domain walls. 2000, arXiv:hep-ph/0008014.

[3] A. Alexandru, I. Horvath, and J. B. Zhang. The reality of the fundamental topological structure in the QCD vacuum. *Phys. Rev. D*, 72:034506, 2005, arXiv:hep-lat/0506018.

[4] M. M. Anber, E. Poppitz, and M. Ünsal. 2d affine XY-spin model/4d gauge theory duality and deconfinement. *JHEP*, 4:40, 2012, arXiv:1112.6389 [hep-th].

[5] T. Banks, C. Bender, , and T. Wu. Coupled anharmonic oscillators I: Equal-mass case. *Phys. Rev. D*, 8:3346, 1973.

[6] F. Belgiorno and S. Liberati. Black hole thermodynamics, Casimir effect and induced gravity. *Gen. Rel. Grav.*, 29:1181, 1997, arXiv:gr-qc/9612024.

[7] A. Bhoonah, E. C. Thomas, and A. R. Zhitnitsky. Metastable vacuum decay and θ dependence in gauge theory. Deformed QCD as a toy model. *Nucl. Phys. B*, 890:30, 2015, arXiv:1407.5121 [hep-ph].

[8] N. D. Birrell and P. C. W. Davies. *Quantum Fields In Curved Space*. Cambridge University Press, Cambridge, 1982.

[9] J. Boyd. *Chebyshev and Fourier Spectral Methods*. General Publishing Company, Toronto, 2001.

[10] F. Bruckmann, F. Gruber, N. Cundy, A. Schafer, and T. Lippert. Topology of dynamical lattice configurations including results

from dynamical overlap fermions. *Phys. Lett. B*, 707:278, 2012, arXiv:1107.0897 [hep-lat].

[11] P. V. Buividovich, T. Kalaydzhyan, and M. I. Polikarpov. Fractal dimension of the topological charge density distribution in SU(2) lattice gluodynamics. *Phys. Rev. D*, 86:074511, 2012, arXiv:1111.6733 [hep-lat].

[12] R. G. Cai, Q. Su, Z. L. Tuo, and H. B. Zhang. Notes on ghost dark energy. *Phys. Rev. D*, 84:123501, 2011, arXiv:1011.3212 [astro-ph.CO].

[13] R. G. Cai, Z. L. Tuo, Y. B. Wu, and Y. Y. Zhao. More on QCD ghost dark energy. *Phys. Rev. D*, 86:023511, 2012, arXiv:1201.2494 [astro-ph.CO].

[14] C. G. Callan and S. Coleman. Fate of the false vacuum II: First quantum corrections. *Phys. Rev. D*, 16:1762, 1977.

[15] S. Coleman. Fate of the false vacuum: Semiclassical theory. *Phys. Rev. D*, 15:2929, 1977.

[16] G. Wang [STAR Collaboration]. Search for chiral magnetic effects in high-energy nuclear collisions. *Nucl. Phys. A*, 904:248, 2013, arXiv:1210.5498 [nucl-ex].

[17] I. Selyuzhenkov [ALICE Collaboration]. Alice probes of local parity violation with charge dependent azimuthal correlations in Pb-Pb collisions. *PoS WPCF*, 2011:044, 2011, arXiv:1203.5230 [nucl-ex].

[18] S. A. Voloshin [ALICE Collaboration]. Results on flow from the ALICE collaboration. *Nucl. Phys. A*, 904:90, 2013, arXiv:1211.5680 [nucl-ex].

[19] N. M. Davies, T. J. Hollowood, and V. V. Khoze. Monopoles, affine algebras and the gluino condensate. *J. Math. Phys.*, 44:3640, 2003, arXiv:hep-th/0006011.

[20] N. M. Davies, T. J. Hollowood, V. V. Khoze, and M. P. Mattis. Gluino condensate and magnetic monopoles in supersymmetric gluodynamics. *Nucl. Phys. B*, 559:123, 1999, arXiv:hep-th/9905015.

[21] N. Dorey, V. V. Khoze, M. P. Mattis, D. Tong, and S. Vandoren. Instantons, three-dimensional gauge theory, and the Atiyah-Hitchin manifold. *Nucl. Phys. B*, 502:59, 1997, arXiv:hep-th/9703228.

[22] G. Dvali and A. Vilenkin. Solitonic D-branes and brane annihilation. *Phys. Rev. D*, 67:046002, 2003, arXiv:hep-th/0209217.

[23] G. R. Dvali, H. Liu, and T. Vachaspati. Sweeping away the monopole problem. *Phys. Rev. Lett.*, 80:2281, 1998, arXiv:hep-ph/9710301.

[24] G. R. Dvali and M. A. Shifman. Domain walls in strongly coupled theories. *Phys. Lett. B*, 396:64, 1997, arXiv:hep-th/9612128.

[25] B. Abelev *et al.* [ALICE Collaboration]. Charge separation relative to the reaction plane in Pb-Pb collisions at $\sqrt{s_{NN}} = 2.76$ TeV. *Phys. Rev. Lett.*, 110:012301, 2013, arXiv:1207.0900 [nucl-ex].

[26] B. I. Abelev *et al.* [STAR Collaboration]. Observation of charge-dependent azimuthal correlations and possible local strong parity violation in heavy ion collisions. *Phys. Rev. C*, 81:054908, 2010, arXiv:0909.1717 [nucl-ex].

[27] C. J. Feng, X. Z. Li, and P. Xi. Global behavior of cosmological dynamics with interacting Veneziano ghost. *JHEP*, 05:046, 2012, arXiv:1204.4055 [astro-ph.CO].

[28] M. M. Forbes and A. R. Zhitnitsky. Domain walls in QCD. *JHEP*, 0110:013, 2001, arXiv:hep-ph/0008315.

[29] K. Fukushima. QCD matter in extreme environments. *J. Phys. G*, 39:013101, 2012, arXiv:1108.2939 [hep-ph].

[30] A. Gorsky and V. Zakharov. Magnetic strings in lattice QCD as non-abelian vortices. *Phys. Rev. D*, 77:045017, 2008, arXiv:0707.1284 [hep-th].

[31] A. S. Gorsky, V. I. Zakharov, and A. R. Zhitnitsky. On classification of QCD defects via holography. *Phys. Rev. D*, 79:106003, 2009, arXiv:0902.1842 [hep-ph].

[32] D. J. Gross, R. D. Pisarki, and L. G. Yaffe. QCD and instantons at finite temperature. *Rev. Mod. Phys.*, 53:43, 1981.

[33] C. Hagmann, S. Chang, and P. Sikivie. Axion radiation from strings. *Phys. Rev. D*, 63:125018, 2001, arXiv:hep-ph/0012361.

[34] I. E. Halperin and A. Zhitnitsky. Can theta / N dependence for gluodynamics be compatible with 2 pi periodicity in theta? *Phys. Rev. D*, 58:054016, 1998, arXiv:hep-ph/9711398.

[35] S. W. Hawking and G. T. Horowitz. The gravitational Hamiltonian, action, entropy and surface terms. *Class. Quant. Grav.*, 13:1487, 1996, arXiv:gr-qc/9501014.

[36] B. Holdom. From confinement to dark energy. *Phys. Lett. B*, 697:351–356, 2011, arXiv:1012.0551 [hep-ph].

[37] I. Horvath, A. Alexandru, J. B. Zhang, Y. Chen, S. J. Dong, T. Draper, F. X. Lee, and K. F. Liu *et al.* Inherently global nature of topological charge fluctuations in QCD. *Phys. Lett. B*, 612:21–28, 2005, arXiv:hep-lat/0501025.

[38] I. Horvath, A. Alexandru, J. B. Zhang, Y. Chen, S. J. Dong, T. Draper, K. F. Liu, and N. Mathur *et al.* The negativity of the overlap-based topological charge density correlator in pure-glue QCD and the non-integrable nature of its contact part. *Phys. Lett. B*, 617:49–59, 2005, arXiv:hep-lat/0504005.

[39] I. Horvath, S. J. Dong, T. Draper, F. X. Lee, K. F. Liu, N. Mathur, H. B. Thacker, and J. B. Zhang. Low dimensional long range topological charge structure in the QCD vacuum. *Phys. Rev. D*, 68:114505, 2003, arXiv:hep-lat/0302009.

[40] E. M. Ilgenfritz, K. Koller, Y. Koma, G. Schierholz, T. Streuer, and V. Weinberg. Exploring the structure of the quenched QCD vacuum with overlap fermions. *Phys. Rev. D*, 76:034506, 2007, arXiv:0705.0018 [hep-lat].

[41] E. M. Ilgenfritz, D. Leinweber, P. Moran, K. Koller, G. Schierholz, and V. Weinberg. Vacuum structure revealed by over-improved stout-link smearing compared with the overlap analysis for quenched QCD. *Phys. Rev. D*, 77:074502, 2008, arXiv:0801.1725 [hep-lat].

[42] K. Kawarabayashi and N. Ohta. The problem of eta in the large N limit: Effective Lagrangian approach. *Nucl. Phys. B*, 175:477, 1980.

[43] D. Kharzeev and A. Zhitnitsky. Charge separation induced by P-odd bubbles in QCD matter. *Nucl. Phys. A*, 797:67, 2007, arXiv:0706.1026 [hep-ph].

[44] D. E. Kharzeev. The chiral magnetic effect and anomaly-induced transport. *Prog. Part. Nucl. Phys.*, 75:133, 2014, arXiv:1312.3348 [hep-ph].

[45] F. R. Klinkhamer and G. E. Volovik. Self-tuning vacuum variable and cosmological constant. *Phys. Rev. D*, 77:085015, 2008, arXiv:0711.3170 [gr-qc].

[46] F. R. Klinkhamer and G. E. Volovik. Gluonic vacuum, Q-theory, and the cosmological constant. *Phys. Rev. D*, 79:063527, 2009, arXiv:0811.4347 [gr-qc].

[47] I. Y. Kobzarev, L. B. Okun, and M. B. Voloshin. Bubbles in metastable vacuum. *Sov. J. Nucl. Phys.*, 20:644, 1975.

[48] J. B. Kogut and L. Susskind. How to solve the eta $\rightarrow$ 3 pi problem by seizing the vacuum. *Phys. Rev. D*, 11:3594, 1975.

[49] A. V. Kovalenko, M. I. Polikarpov, S. N. Syritsyn, and V. I. Zakharov. Three dimensional vacuum domains in four dimensional SU(2) gluodynamics. *Phys. Lett. B*, 613:52, 2005, arXiv:hep-lat/0408014.

[50] D. Krotov and A. M. Polyakov. Infrared sensitivity of unstable vacua. *Nucl. Phys. B*, 849:410–432, 2011, arXiv:1012.2107 [hep-th].

[51] X. Li and M. B. Voloshin. Metastable vacuum decay in center-stabilized Yang-Mills theory at large N. *Phys. Rev. D*, 90:105028, 2014, arXiv:1408.3054 [hep-th].

[52] M. Maggiore. Zero-point quantum fluctuations and dark energy. *Phys. Rev. D*, 83:063514, 2011, arXiv:1004.1782 [astro-ph.CO].

[53] A. Milekhin. CP(N-1) model on a finite interval in the large N limit. *Phys. Rev. D*, 86:105002, 2012, arXiv:1207.0417 [hep-th].

[54] P. Nath and R. L. Arnowitt. The U(1) problem: Current algebra and the theta vacuum. *Phys. Rev. D*, 23:473, 1981.

[55] N. Ohta. Dark energy and QCD ghost. *Phys. Lett. B*, 695:41, 2011, arXiv:1010.1339 [astro-ph.CO].

[56] A. Parnachev and A. R. Zhitnitsky. Phase transitions, theta behavior and instantons in QCD and its holographic model. *Phys. Rev. D*, 78:125002, 2008, arXiv:0806.1736 [hep-ph].

[57] G. Plunien, B. Muller, and W. Greiner. The Casimir effect. *Phys. Rep.*, 134:87, 1986.

[58] A. M. Polyakov. Quark confinement and topology of gauge theories. *Nucl. Phys. B*, 120:429, 1977.

[59] A. M. Polyakov. Decay of vacuum energy. *Nucl. Phys. B*, 834:316–329, 2010, arXiv:0912.5503 [hep-th].

[60] E. Poppitz, T. Schäfer, and journal = JHEP volume = 03 year = 2013 pages = 087 eprint = arXiv:1212.1238 [hep-th] M. Ünsal", title = Universal mechanism of (semi-classical) deconfinement and theta-dependence for all simple groups.

[61] E. Poppitz, T. Schäfer, and M. Ünsal. Continuity, deconfinement, and (super) Yang-Mills theory. *JHEP*, 10:115, 2012, arXiv:1205.0290 [hep-th].

[62] E. Poppitz and M. Ünsal. Seiberg-Witten and Polyakov-like magnetic bion confinements are continuously connected. *JHEP*, 2011(7), 2012, arXiv:1105.3969 [hep-th].

[63] B. Reznik and Y. Aharonov. Question of the nonlocality of the Aharonov-Casher effect. *Phys. Rev. D*, 40:4178–4183, 1989.

[64] C. Rosenzweig, J. Schechter, and C. G. Trahern. Is the effective Lagrangian for QCD a sigma model? *Phys. Rev. D*, 21:3388, 1980.

[65] A. Rozas-Fernandez. Kinetic K-essence ghost dark energy model. *Phys. Lett. B*, 709:313–321, 2012, arXiv:1106.0056 [astro-ph.CO].

[66] K. Saaidi, A. Aghamohammadi, and B. Sabet. Ghost dark energy in $f(r)$ model of gravity. *Int. J. Mod. Phys. D*, 21:1250057, 2012, arXiv:1203.4518 [physics.gen-ph].

[67] I. Sachs and A. Wipf. Finite temperature Schwinger model. *Helv. Phys. Acta*, 65:652, 1992, arXiv:1005.1822 [hep-th].

[68] I. Sachs and A. Wipf. Generalized Thirring models. *Ann. Phys.*, 249:380, 1996, arXiv:hep-th/9508142.

[69] R. Schutzhold. Small cosmological constant from the QCD trace anomaly? *Phys. Rev. Lett.*, 89:081302, 2002.

[70] I. Selyuzhenkov. Azimuthal correlations and collective effects in a heavy-ion collisions at the LHC energies. *Jour. of Phys. Con. Ser.*, 426:012002, 2013, arXiv:1212.5489 [nucl-ex].

[71] A. Sheykhi and M. S. Movahed. Interacting ghost dark energy in non-flat universe. *Gen. Rel. Grav.*, 44:449–465, 2012, arXiv:1104.4713 [hep-th].

[72] M. Shifman. *Advanced Topics in Quantum Field Theory: A Lecture Course*. Cambridge University Press, 2012.

[73] M. A. Shifman. Domain walls and decay rate of the excited vacua in the large N Yang-Mills theory. *Phys. Rev. D*, 59:021501, 1999, arXiv:hep-th/9809184.

[74] E. V. Shuryak and J. J. M. Verbaarschot. Screening of the topological charge in a correlated instanton vacuum. *Phys. Rev. D*, 52:295, 1995, arXiv:hep-lat/9409020.

[75] A. V. Smilga. Physics of thermal QCD. *Phys. Rep.*, 291:1–106, 1997.

[76] D. T. Son, M. A. Stephanov, and A. R. Zhitnitsky. Domain walls of high density QCD. *Phys. Rev. Lett.*, 86:3955, 2001, arXiv:hep-ph/0012041.

[77] G. 't Hooft. Computation of the quantum effects due to a four-dimensional pseudoparticle. *Phys. Rev. D*, 14:3432, 1976.

[78] E. C. Thomas, F. R. Urban, and A. R. Zhitnitsky. The cosmological constant as a manifestation of the conformal anomaly? *JHEP*, 0908:043, 2009, arXiv:0904.3779 [gr-qc].

[79] E. C. Thomas and A. R. Zhitnitsky. Casimir scaling in gauge theories with a gap: Deformed QCD as a toy model. *Phys. Rev. D*, 86:065029, 2012, arXiv:1203.6073 [hep-ph].

[80] E. C. Thomas and A. R. Zhitnitsky. Topological susceptibility and contact term in QCD: A toy model. *Phys. Rev. D*, 85:044039, 2012, arXiv:1109.2608 [hep-th].

[81] E. C. Thomas and A. R. Zhitnitsky. Long range order in gauge theories: Deformed QCD as a toy model. *Phys. Rev. D*, 87:085027, 2013, arXiv:1208.2030 [hep-ph].

[82] D. Tong. TASI Lectures on solitons: Instantons, monopoles, vortices and kinks. 2005, arXiv:hep-th/0509216.

[83] L. Trefethen. *Spectral Methods in Matlab*. Society for Industrial and Applied Mathematics, Philadelphia, 2000.

[84] M. Ünsal. Theta dependence, sign problems and topological interference. *Phys. Rev. D*, 86:105012, 2012, arXiv:1201.6426 [hep-th].

[85] M. Ünsal and L. G. Yaffe. Center-stablized Yang-Mills theory: Confinement and large N volume independence. *Phys. Rev. D*, 78:065035, 2008, arXiv:0803.0344 [hep-th].

[86] F. R. Urban and A. R. Zhitnitsky. The cosmological constant from the ghost: A toy model. *Phys. Rev. D*, 80:063001, 2009, arXiv:0906.2165 [hep-th].

[87] F. R. Urban and A. R. Zhitnitsky. Cosmological constant, violation of cosmological isotropy and CMB. *JCAP*, 0909:018, 2009, arXiv:0906.3546 [astro-ph.CO].

[88] F. R. Urban and A. R. Zhitnitsky. The cosmological constant from the QCD Veneziano ghost. *Phys. Lett. B*, 688:9, 2010, arXiv:0906.2162 [gr-qc].

[89] F. R. Urban and A. R. Zhitnitsky. The QCD nature of dark energy. *Nucl. Phys. B*, 835:135, 2010, arXiv:0909.2684 [astro-ph.CO].

[90] P. Di Vecchia and G. Veneziano. Chiral dynamics in the large N limit. *Nucl. Phys. B*, 171:253, 1980.

[91] G. Veneziano. U(1) without instantons. *Nucl. Phys. B*, 159:213, 1979.

[92] A. Vilenkin and A. E. Everett. Cosmic strings and domain walls in models with Goldstone and pseudoGoldstone bosons. *Phys. Rev. Lett.*, 48:1867, 1982.

[93] E. Witten. Current algebra theorems for the U(1) Goldstone boson. *Nucl. Phys. B*, 156:269, 1979.

[94] E. Witten. Large N chiral dynamics. *Ann. Phys.*, 128:363, 1980.

[95] E. Witten. Large n chiral dynamics. *Ann. Phys.*, 128:363, 1980.

[96] E. Witten. Theta dependence in the large N limit of four-dimensional gauge theories. *Phys. Rev. Lett.*, 81:2862, 1998, arXiv:hep-th/9807109.

[97] Y. B. Zeldovich. Cosmological constant and elementary particles. *JETP Lett.*, 6:316, 1967.

[98] Y. B. Zeldovich and J. Bjorken. Emergent gauge bosons. 1967, arXiv:hep-th/0111196.

[99] A. R. Zhitnitsky. Confinement- deconfinement phase transition and fractional instanton quarks in dense matter. 2006, arXiv:hep-ph/0601057.

[100] A. R. Zhitnitsky. The gauge fields and ghosts in Rindler space. *Phys. Rev. D*, 82:103520, 2010, arXiv:1004.2040 [gr-qc].

[101] A. R. Zhitnitsky. Entropy, contact interaction with horizon and dark energy. *Phys. Rev. D*, 84:124008, 2011, arXiv:1105.6088 [hep-th].

[102] A. R. Zhitnitsky. P and CP violation and new thermalization scenario in heavy ion collisions. *Nucl. Phys. A*, 853:135–163, 2011, arXiv:1008.3598 [nucl-th].

[103] A. R. Zhitnitsky. Contact term, its holographic description in QCD and dark energy. *Phys. Rev. D*, 86:045026, 2012, arXiv:1112.3365 [hep-ph].

[104] A. R. Zhitnitsky. Local p violation effects and thermalization in QCD: Views from quantum field theory and holography. *Nucl. Phys. A*, 886:17, 2012, arXiv:1201.2665 [hep-ph].

[105] A. R. Zhitnitsky. Maxwell theory on a compact manifold as a topologically ordered system. *Phys. Rev. D*, 88:105029, 2013, arXiv:1308.1960 [hep-th].

[106] A. R. Zhitnitsky. QCD as topologically ordered system. *Ann. Phys.*, 336:462–481, 2013, arXiv:1301.7072 [hep-ph].

[107] A. R. Zhitnitsky. Dynamical de Sitter phase and nontrivial holonomy in strongly coupled gauge theories in an expanding universe. *Phys. Rev. D*, 92:043512, 2015, arXiv:1505.05151 [hep-ph].

Appendix A

Domain Wall Decay

Here we briefly discuss the decay of domain walls between physically equivalent domains by hole formation. The decay mechanism for a domain wall is a tunnelling process which creates a hole in the domain wall that connects the $\chi = 0$ domain on one side of the wall to the $\chi = 2\pi$ domain on the other, see (5.5). Because the ground state on the two sides is physically identical, it is possible for the fields to remain in the ground state as they pass through the hole. That is, there is no interpolation (winding) as they pass through the hole. This lowers the energy of the configuration over that where the hole was filled by the domain wall transition by an amount proportional to R^2 where R is the radius of the hole. The hole, however, must be surrounded by a string-like field configuration which interpolates between an unwound configuration and a wound one. This string represents an excitation in the heavy degrees of freedom and thus costs energy, however, this energy scales linearly as R. Thus, if a large enough hole can form, it will be stable and the hole will expand and consume the wall. This process is commonly called quantum nucleation and is similar to the decay of a metastable wall bounded by strings; therefore, we use a similar technique to estimate the tunnelling probability. The idea of the calculation was suggested in [92] to estimate the decay rate in the so-called $N = 1$ axion model. In a QCD context similar estimates have been discussed for the η' domain wall in large N QCD in [28] and for the η' domain wall in high density QCD in [76].

If the radius of the nucleating hole is much greater than the wall thickness, we can use the thin-string and thin-wall approximation. This approximation is justified, as we shall see, when we calculate the critical radius R_c. In this case, the action for the string and for the wall are proportional to the corresponding worldsheet areas

$$S_0\left(\mathbb{R}^3 \times \mathbb{S}^1\right) = 2\pi RL\alpha - \pi R^2 L\sigma. \tag{A.1}$$

The first term is the energy cost of forming a string, where α is the string tension and $2\pi RL$ is its worldsheet area. The second term is the energy gain by forming the hole over keeping the domain wall, in which σ is the wall tension and $\pi R^2 L$ is its worldsheet volume. We should note that formula

(A.1) replaces the following more familiar expression for the classical action, which was used in previous similar computations [28, 76]

$$S_0(\mathbb{R}^4) = 4\pi R^2\alpha - \frac{4\pi}{3}R^3\sigma. \tag{A.2}$$

Minimizing (A.1) with respect to R we find the critical radius R_c and the action S_0,

$$R_c = \frac{\alpha}{\sigma}, \quad S_0\left(\mathbb{R}^3\times\mathbb{S}^1\right) = \frac{\pi\alpha^2 L}{\sigma}, \tag{A.3}$$

which replace the more familiar expressions for the critical radius $R_c = \frac{2\alpha}{\sigma}$ and classical action $S_0(\mathbb{R}^4) = \frac{16\pi\alpha^3}{3\sigma^2}$ from [28, 76].

Therefore, the semiclassical probability of this process is proportional to

$$\Gamma \sim \exp\left(-\frac{\pi\alpha^2 L}{\sigma}\right) \tag{A.4}$$

where σ is the DW tension determined by (5.6), while α is the tension of the vortex line in the limit when the interaction term $\sim\zeta$ due to the monopole's interaction in the low energy description (2.36) is neglected and the $U(1)$ symmetry is restored. In this case the vortex line is a global string with logarithmically divergent tension

$$\alpha \sim 2\pi\frac{1}{4L^2}\left(\frac{g}{2\pi}\right)^2 \ln\frac{R}{R_{core}} \tag{A.5}$$

where $R\sim m_\chi^{-1}$ is a long-distance cutoff which is determined by the width of the domain wall, while $R_{core}\sim L$ where the low energy description breaks down. The vortex tension is dominated by the region outside the core, so our estimates for computing α to the logarithmic accuracy are justified. Furthermore, the critical radius can be estimated as

$$R_c = \frac{\alpha}{\sigma} \sim \frac{\pi}{2m_\chi}\ln\left(\frac{1}{m_\chi L}\right), \tag{A.6}$$

which shows that the nucleating hole $\sim R_c$ is marginally greater than the wall thickness $\sim m_\chi^{-1}$ as the logarithmic factor $\ln(\frac{1}{m_\chi L}) \sim \ln\mathcal{N} \gg 1$ when $\mathcal{N}\gg 1$ is the large parameter of the model, see (3.25). Therefore, our thin-string and thin-wall approximation is marginally justified.

As a result of our estimates (A.4), (5.6), (A.5) the final expression for the decay rate of the domain wall is proportional to

$$\begin{aligned}\Gamma &\sim \exp\left(-\tfrac{\pi\alpha^2 L}{\sigma}\right) \sim \exp\left(-\pi^3\left(\tfrac{g}{4\pi}\right)^3\frac{\ln^2(\frac{1}{m_\chi L})}{\sqrt{L^3\zeta}}\right)\\ &\sim \exp\left(-\gamma\cdot\mathcal{N}\ln^2\mathcal{N}\right)\ll 1,\end{aligned} \tag{A.7}$$

with γ being some numerical coefficient. The estimate (A.7) supports our claim that in the deformed gauge theory model, with a weak coupling regime enforced and $\mathcal{N} \gg 1$, our treatment of the domain walls as stable objects is justified.

Appendix B

Metastable Vacuum Decay

In this appendix we briefly review the general theory and framework for calculating metastable vacuum decay rates in Quantum Field Theory. For a more thorough discussion see [14, 15]. The process for the decay of a metastable vacuum state to the true vacuum state is analogous to a bubble nucleation process in statistical physics. Considering a fluid phase around the vaporisation point, thermal fluctuations will cause bubbles of vapor to form. If the system is heated beyond the vaporisation point, the vapor phase becomes the true ground state for the system. Then, the energy gained by the bulk of a bubble transitioning to the vapor phase goes like a volume while the energy cost for forming a surface (basically a domain wall) goes like an area. Thus, there is some critical size such that smaller bubbles represent a net cost in energy and will collapse while larger bubbles represent a net gain in energy. Once a bubble forms which is larger than the critical size it will grow to consume the entire volume and transition the whole of the sample to the vapor phase. To understand the lifetime of such a 'superheated' liquid state, the important calculation is, therefore, the rate of nucleation of critical bubbles per unit time per unit volume (Γ/V). Similarly, we aim to calculate this decay rate for our system with from the metastable state $\boldsymbol{\sigma}^{(+)}$ to the ground state $\boldsymbol{\sigma}^{(-)}$, though through quantum rather than thermal fluctuations.

Consider a general system with a ground state field configuration, $\phi^{(-)}$, and metastable field configuration, $\phi^{(+)}$, with an energy density difference between the two given by ϵ. Qualitatively the potential for the system should be understood as something like Figure B.1. Classically, a system in the configuration $\phi^{(-)}$ is stable, but quantum mechanically the system is rendered unstable through barrier penetration (tunneling).

The semiclassical expression for the tunneling rate per unit volume is given by [15]

$$\frac{\Gamma}{V} = Ae^{-S_E(\phi_b)/\hbar}\left[1 + O\left(\hbar\right)\right] \tag{B.1}$$

where the Euclidean action, S_E, is the action upon analytically continuing

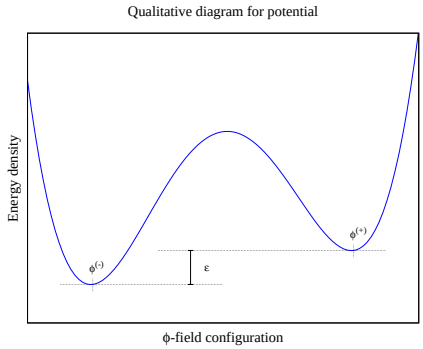

Figure B.1: Qualitative picture for the potential of a general system with a global ground state, $\phi^{(-)}$, and a higher energy metastable state, $\phi^{(+)}$, with an energy splitting between the two given by ϵ.

to imaginary time and is given by

$$S_E = \int d^4x \left[\frac{1}{2} \left(\partial_t \phi \right)^2 + \frac{1}{2} \left(\nabla \phi \right)^2 + U \left(\phi \right) \right]. \tag{B.2}$$

We have explicitly left $\hbar$ in (B.1) to emphasise the semiclassical expansion. The action, (B.2), in the exponent of (B.1) is evaluated in the field configuration called the "Euclidean bounce" which we have denoted ϕ_b. The Euclidean bounce is a finite action configuration which solves the classical equations of motion and interpolates, in Euclidean time, from the metastable state to a configuration "near" the ground state and back. Making reference to the potential depicted in Figure B.1, continuing to Euclidean time essentially describes a system with the sign of the potential flipped. As such, the bounce describes a path starting at the now local maximum $\phi^{(+)}$ at $t \to -\infty$ rolling down into the valley and up to the classical tuning point near the higher peak $\phi^{(-)}$, then reversing and traveling back to $\phi^{(+)}$ at $t \to +\infty$. In order for the action to be finite the bounce must also tend to $\phi^{(+)}$ as the spacial coordinates go to infinity in any direction.

Additionally, we have glossed over one technicality by representing ϕ as a single dimension while in fact it is not. In principle there is a classical turning surface, call it Σ, rather than a single point and so there may be many paths from the peak at $\phi^{(+)}$ to the surface Σ. The resolution however is straightforward. Each such path contributes as (B.1) and so the path of minimal action is the dominant path. For details see [5]. Furthermore,

the minimal action path is spherically symmetric so that the action can be written in terms on a single radial dimension,

$$S_E = \int_0^\infty \left(2\pi^2\rho^3\right) d\rho \left[\frac{1}{2}\left(\frac{d\phi}{d\rho}\right)^2 + U\left(\phi\right)\right]. \tag{B.3}$$

Thus, the bounce we should find is the minimal action configuration which solves the equation of motion,

$$\frac{d^2\phi}{d\rho^2} + \frac{3}{\rho}\frac{d\phi}{d\rho} = U'\left(\phi\right), \tag{B.4}$$

subject to the boundary conditions $\phi \to \phi^{(+)}$ as $\rho \to \infty$ and $d\phi/d\rho \to 0$ as $t \to 0$.

In the limit of small separation energy ϵ the bounce approaches the peak $\phi^{(-)}$ more closely and spends longer in the region around the peak, so that the bounce configuration resembles a bubble with the interior at $\phi^{(-)}$, the exterior at $\phi^{(+)}$, and a domain wall surface interpolating between the two. If the bubble is very large, corresponding to very small ϵ, then the curvature at the interpolating surface is small and the surface appears flat. Alternately, simply note that the second term in (B.4) goes like $1/\rho$, so if the fields only change appreciably around a thin surface at large ρ, the second term can be neglected and the equation of motion reduces further to the much simpler form

$$\frac{d^2\phi}{d\rho^2} = U'\left(\phi\right). \tag{B.5}$$

Therefore, if the separation energy, ϵ, between the two states is small, we need only solve for the one dimensional soliton interpolating between $\phi^{(+)}$ and $\phi^{(-)}$ which solves (B.5). This is called the thin-wall approximation, and is the framework in which we work in Chapter 6. In the deformed model discussed in Chapter 2, the separation $\epsilon \sim 1/N^2$, so that the thin-wall approximation coincides with the large N approximation.

For the thin wall approximation the full action reduces to

$$S_E \approx -\frac{1}{2}\pi^2 R^4 \epsilon + 2\pi^2 R^3 S_1 \tag{B.6}$$

where S_1 is the one dimensional action across the domain wall given by

$$S_1 = \int dx \left[\frac{1}{2}\left(\frac{d\phi}{dx}\right)^2 + U\left(\phi\right)\right]. \tag{B.7}$$

What remains then is to determine the size of the bubble, R. The stipulation that the bounce configuration describes a classical path implies that it extremises the action (B.6). Thus, by variation,

$$\frac{dS_E}{dR} = 0 = -2\pi^2 R^3 \epsilon + 6\pi^2 R^2 S_1, \tag{B.8}$$

which yields $R = 3S_1/\epsilon$. Notice again the similarity to a bubble nucleation problem. This extremal action with respect to the bubble size is in fact a maximum, and as such the action increases with R for smaller size and decreases with R for larger. Hence, the bounce configuration which saturates the decay rate is essentially a bubble of critical size as discussed when making this analogy to bubble nucleation.

Appendix C

Asymptotic Vacuum Decay

Here we briefly reproduce the large N_c asymptotic calculation for the metastable vacuum decay rate performed in [51]. Starting with the action (2.24),

$$S = \frac{1}{L}\left(\frac{g}{2\pi}\right)^2 \int_{\mathbb{R}^3} d^3x \sum_{n=1}^{N} \left[\frac{1}{2}\left(\nabla\sigma_n\right)^2 - m_\sigma^2 \cos\left(\sigma_n - \sigma_{n+1} + \frac{\theta}{N}\right)\right], \quad \text{(C.1)}$$

with $m_\sigma = \zeta L\left(2\pi/g\right)^2$, adding the constant shift and rescaling $x \to x/m_\sigma$ we have the action used for our calculations in Chapter 6,

$$S = \mathcal{N} \int_{\mathbb{R}^3} d^3x \sum_{n=1}^{N} \left[\frac{1}{2}\left(\nabla\sigma_n\right)^2 + 1 - \cos\left(\sigma_n - \sigma_{n+1} + \frac{\theta}{N}\right)\right], \quad \text{(C.2)}$$

where

$$\mathcal{N} = \frac{1}{m_\sigma L}\left(\frac{g}{2\pi}\right)^2$$

is our semi-classicality parameter. Then, considering the same two vacuum states ($\sigma_n = 0$ and $\sigma_n = 2\pi n/N$) with the energy difference $\epsilon = 2\pi(\pi-\theta)/N$, we introduce the "centre of gravity" (Σ) and "distance" (σ) as

$$\Sigma = \frac{1}{N}\sum_{n=1}^{N} \sigma_n \,, \qquad \sigma = \sigma_N - \sigma_1 \,, \quad \text{(C.3)}$$

in terms of which the vacuums are given by

$$\sigma_n = \Sigma + \left(\frac{n-1}{N-1} - \frac{1}{2}\right)\sigma \xrightarrow[N\gg 1]{} \left(\frac{n}{N} - \frac{1}{2}\right)\sigma \,, \quad \text{(C.4)}$$

for $\sigma = 0$ and $\sigma = 2\pi$, with $\Sigma = 0$ being equivalent to our previously discussed choice of ϕ, (6.28). In terms of those redefinitions, we have the action

$$S \to \mathcal{N} \int d^3x \left[\frac{N}{24}\left(\nabla\sigma\right)^2 + 1 - \cos\sigma + \frac{\sigma^2}{2N}\right], \quad \text{(C.5)}$$

which immediately gives (ignoring the last term which is small for large N) the kink solution,

$$\sigma(x) = 4\arctan\left[\exp\left(-2\sqrt{\frac{3}{N}}x\right)\right], \tag{C.6}$$

and the $1d$ action

$$S_1 = 4\sqrt{\frac{N}{3}} \tag{C.7}$$

as claimed.